

Color Screening in Quantum Chromodynamics

Alexei Bazavov, Johannes H. Weber

Department of
Computational Mathematics, Science and Engineering and
Department of Physics and Astronomy,
Michigan State University, East Lansing, MI 48824, USA

January 8, 2022

Abstract

We review lattice studies of the color screening in the quark-gluon plasma. We put the phenomena related to the color screening into the context of similar aspects of other physical systems (electromagnetic plasma or cold nuclear matter). We discuss the onset of the color screening and its signature and significance in the QCD transition region, and elucidate at which temperature and to which extent the weak-coupling picture based on hard thermal loop expansion, potential nonrelativistic QCD, or dimensionally-reduced QCD quantitatively captures the key properties of the color screening. We discuss the different regimes pertaining to the color screening and thermal dissociation of the static quarks in depth for various spatial correlation functions that are studied on the lattice, and clarify the status of their asymptotic screening masses. We finally discuss the screening correlation functions of dynamical mesons with a wide range of flavor and spin content, and how they conform with expectations for low- and high-temperature behavior.

Contents

1	Introduction	3
2	Field theoretical foundations	7
2.1	Partition function and Lagrangian	7
2.2	Finite temperature field theory	11
2.3	Lattice regularization	14
2.4	Renormalization and weak coupling	17
2.5	Light quarks	19
2.6	Heavy quarks	21
2.7	Implementation of QCD on the lattice	23
3	Screening of static charges	25
3.1	The Polyakov loop and related quantities	26
3.1.1	Wilson line and the Polyakov loop	26
3.1.2	The static quark potential and the renormalized Polyakov loop	29
3.1.3	Static quark free energy and entropy	31
3.2	Polyakov loop correlators	36
3.2.1	Singlet and octet free energies	38
3.2.2	Vacuum-like regime and vacuum physics	41
3.2.3	Thermal dissociation and the free energy	45
3.2.4	Chromoelectric screening	45
3.2.5	Asymptotic screening	48
3.2.6	Screening in different representations	56
3.2.7	Screening at finite chemical potential	57
3.2.8	Screening in external magnetic fields	59
4	Interplay between screening and dissociation	61
4.1	Euclidean correlation functions and spectral functions	61
4.1.1	Temporal correlation functions	62
4.1.2	Spatial correlation functions	63
4.2	The complex static energy	64
4.3	Meson screening masses for heavy and heavy-light mesons	71
4.4	Meson screening masses for light mesons	76
5	Summary	79

1 Introduction

Whenever the interactions of particulate matter are described in terms of a field theoretical approach, these interactions can be understood as the exchange of one or more excitations of the fields mediating these interactions. The contribution to the potential from the exchange of n field excitations with mass m is $V \sim (e^{-mr}/r)^n$. If the leading contribution is due to the exchange of a single massless, classical field excitation, then the dominant contribution takes the form of the classical Coulomb potential, i.e. $V_C \sim 1/r$ and the force is $F_C \sim 1/r^2$. If the leading contribution is due to the exchange of a single massive, classical field excitation, then the dominant contribution takes the form of the famous Yukawa potential [1], i.e. $V_Y \sim e^{-mr}/r$, and the force is $F_Y \sim (e^{-mr} + mr)/r^2 = F_C (1 + \mathcal{O}(rm)^2)$. The Yukawa potential is the textbook example of a screened interaction with the Debye-Hückel or screening length $\lambda = 1/m$ [2]. The basic features of the Coulomb or Yukawa forces are present in the classical limit of all known fundamental gauge forces of the Standard Model of Particle Physics, they are present in the classical field theory of gravitation, and they are present in most of the many-body effective field theories, too, e.g. in the chiral effective theory that describes the formation of nuclei from individual nucleons, or in many condensed matter applications.

We generally speak of *screening* whenever the presence of mobile charges is the cause for the falloff of the leading contribution to a potential being larger than the power law $V \sim 1/r^n$ that would be expected for the exchange of n massless, classical field excitations. This applies to the case of the quantum corrections due to the vacuum polarization, and it applies to the case of the thermal screening inside of a plasma. We take a first look at the more simple case of the electromagnetism and contrast it later with the more complicated case of the strong interactions.

Electromagnetism is an Abelian U(1) gauge theory. For this reason the electromagnetic fields themselves carry no electromagnetic charge, and they couple to each other only indirectly by coupling to the same electromagnetically charged matter. The Coulomb potential $V \sim \alpha_{\text{em}}/r$ in (classical) electromagnetism is a long-range interaction. Nevertheless, at large but still finite distances the electromagnetic potential exhibits in many systems a dominant power-law behavior $1/r^n$, where $n \geq 2$. This may be understood in a many-body picture by applying Gauss's law to a case where multiple

opposite charges reside in the same local volume. They compensate each other when summed up to the total charge, which may exactly cancel the leading Coulomb contributions to the force felt by another observing charge distribution at a far distance. However, subleading contributions due to the higher moments of this local charge distribution are associated with higher powers $1/r^n$, and are still relevant at large distances, if the observing charge distribution may accommodate higher moments of the same kind. We think of the multipole expansion and the dipole radiation as well-known classical examples of such a scenario. Since the dominant contribution exhibits a clean power-law falloff in such scenarios, this is not an example of screening.

In a quantum field theory such as Quantum Electrodynamics (QED), the leading contribution to the Coulomb force between an electron-positron pair at rest is mediated by the exchange of a single *electric* A_0 *photon*. However, an effect reminiscent to the aforementioned many-body picture plays out through the vacuum polarization, where each individual electron (or positron) creates a polarized charge distribution of virtual electron-positron pairs from the quantum fluctuations of the vacuum [3, 4]. These lead to a larger charge $\alpha_{\text{em}}(1/r)$ being felt by an observer at smaller distances r , where less quantum fluctuations can contribute to the total charge [5]. The dependence of $\alpha_{\text{em}}(1/r)$ is logarithmic at distances much smaller than the electron's Compton wave length $\lambda_e = 1/m_e$, such that the QED potential behaves as $V \sim \alpha_{\text{em}}(1/r)/r \sim \log(r)/r$ for $r \ll \lambda_e$, i.e. V does not exhibit the power-law falloff of the classical Coulomb force! The same effect applies also to exchanges mediated by the emission of multiple (electric or magnetic) photons. Although this effect of the QED vacuum polarization is a screening mechanism, it is quite different from the mechanisms of the thermal screening inside of an electromagnetic plasma.

A surrounding electromagnetic plasma breaks the Poincaré symmetry of the local interactions and the energies of all of the thermally equilibrated fields are discretized. On the one hand, the *electric* A_0 *photons* are subject to the thermal modification and acquire an effective thermal mass – the Debye mass – that amounts to $m = eT/\sqrt{3}$ (for a theory with only one massless fermion with charge $e = \sqrt{4\pi\alpha_{\text{em}}}$) at leading order [6]. Hence, inside the plasma the electric fields are screened with the screening length $\lambda = 1/m$. On the other hand, the magnetic fields are not screened at all, and the *electric* A_0 *photons* can couple to magnetic photons through fermion loops. Hence, at large enough distances $r \gg \lambda$, the leading contribution to the potential

between two electromagnetic charges is not of the (screened) Coulomb form $V \sim \alpha_{\text{em}} e^{-mr}/r$ anymore, but instead it is dominated by the exchange of multiple *magnetic photons*, i.e. it is of the form $V \sim \alpha_{\text{em}}^6/r^6$ for the magnetic van-der-Waals interaction. Due to the smallness of the electromagnetic coupling α_{em} , there is an intermediate range, where the dominant contribution to the electromagnetic potential is still of the form $V \sim \alpha_{\text{em}} e^{-mr}/r$, such that the electromagnetic Debye mass m can be determined straightforwardly. However, at larger distances the van-der-Waals contribution from the exchange of two *magnetic photons* is dominant, and thus the electromagnetic potential inside a plasma exhibits the power-law behavior at large enough distances, see e.g. Ref. [7].

Regarding the strong interaction, the picture is very different. In the many-body field theoretical description of nuclei and hypernuclei, the excitation and exchange of a single pion, kaon or eta meson is mediating the leading contribution to the potential between the octet baryons $V \sim e^{-mr}/r$. Given the pion, kaon and eta masses of $m_\pi = 135$ MeV, $m_K = 496$ MeV, and $m_\eta = 548$ MeV the screening lengths are different for different processes and are of the order of $\lambda \sim 1/m_\eta \sim 0.36$ fm to $1/m_\pi \sim 1.5$ fm, which is about twice the charge radius of a charged octet baryon. The existence of different screening lengths in different interaction channels is a feature of QCD that is also found for the screening inside of a quark-gluon plasma.

At much shorter distances this picture of baryons and mesons is not appropriate, and the strong interactions have to be described in terms of quarks and gluons in the Quantum Chromodynamics (QCD), which is a non-Abelian SU(3) gauge theory. Due to the asymptotic freedom, the leading contribution to the force between two color charges at short enough distances is again the exchange of a single massless gluon, and the potential has the Coulomb form $V \sim \alpha_s/r$ (with quantum corrections). In contrast to the QED, each individual quark or gluon creates a polarized charge distribution of virtual quark-antiquark pairs and virtual gluons from quantum fluctuations of the vacuum. While the former have a screening effect as in the QED, the latter have an even stronger anti-screening effect [8, 9]. These lead to a larger charge $\alpha_s(1/r)$ being felt by an observer at larger distances r , where more quantum fluctuations contribute to the total charge. The dependence of $\alpha_s(1/r)$ is logarithmic such that the QCD potential behaves as $V \sim \alpha_s(1/r)/r \sim 1/(r \log(r))$, i.e. V does not exhibit the classical power-law falloff [10].

At distances $r \sim 1/\Lambda_{\overline{\text{MS}}}$, where $\Lambda_{\overline{\text{MS}}}$ is the intrinsic scale of the QCD (in the $\overline{\text{MS}}$ scheme), the charge $\alpha_s(1/r)$ would actually diverge, indicating the breakdown of a description in terms of individual quarks and gluons. At such distances the force approaches a constant, the QCD string tension, and the energy of this QCD string grows linearly with the distance. This is the color confinement of the QCD [11]. Due to the presence of sea quarks this string eventually breaks apart at a string-breaking distance λ_{sb} , where the total energy $E(\lambda_{\text{sb}})$ of the QCD string becomes sufficiently large for creating a quark-antiquark pair $q'\bar{q}'$ from the vacuum, see e.g. Refs. [12, 13]. Two separate bound states with masses $m_{q\bar{q}'} = m_{q'\bar{q}} \sim m_q + 1/\lambda_{\text{sb}}$ are formed by consuming this pair. For distances not too different from λ_{sb} the energy of the quark-antiquark pair exhibits some characteristic features of the exponential screening of color charges, although the underlying unscreened QCD potential includes the contribution from the QCD string as well.

Neither of these two screening mechanisms is the one of the color screening in the quark-gluon plasma at high temperatures. As in the case of the electromagnetic plasma, the surrounding quark-gluon plasma breaks the Poincaré symmetry of the local interactions and the energies of all of the thermally equilibrated fields are discretized. On the one hand, inside such a quark-gluon plasma the *electric* A_0 *gluons* are subject to the thermal modification and acquire a Debye mass – that amounts to $m_D \sim gT$ at leading order, where $g = \sqrt{4\pi\alpha_s}$. Hence, inside the quark-gluon plasma the *electric fields* are screened with the screening length $\lambda = 1/m_D$. However, in contrast to the QED, one has to deal in the definition of the Debye mass with subtleties due to the gauge dependence of the vacuum polarization [14]. On the other hand, the *magnetic fields* that are not screened at all are subject to the confining three-dimensional Yang-Mills theory. Hence, the nonperturbative interactions among the *magnetic gluons* or with the *electric* A_0 *gluons* lead to bound states with masses at the associated confining scale g^2T [7, 15], which can be related to various inverse screening lengths of in-medium correlation functions in the corresponding channels. Moreover, since the *electric* A_0 *gluons* can couple directly to the magnetic gluons due to the nontrivial structure of the gauge group SU(3), the dominant contribution from the magnetic gluons is larger than in QED and does not require the presence of fermion loops at all [14].

At this point it is already evident that there are fundamental differences between the mechanisms of *electric screening* in electromagnetic or *color*

screening in quark-gluon plasma. The key aspects of the *color screening* can be understood only within a proper quantum field theoretical framework. We give a brief overview of the quantum field theoretical foundations of QCD and of the related thermal field theory in Section 2. In Section 3 we discuss the screening of the static charges and of bound states of static charges in QCD. Later on, in Section 4 we discuss the interplay between screening and dissociation for static and non-static mesons in QCD. Finally, we conclude with a concise summary in Section 5.

2 Field theoretical foundations

2.1 Partition function and Lagrangian

Nuclear matter and the strong interactions are realized on the fundamental level in the Standard Model in terms of the Quantum Chromodynamics (QCD). The hadron spectrum, hadron structure and hadron reactions are – up to effects from the electroweak sector – completely described by the QCD partition function (in any finite or infinite volume V)

$$Z(V) = \int \prod_{\mu} \mathcal{D}A_{\mu} \prod_f \mathcal{D}\bar{\psi}_f \mathcal{D}\psi_f e^{i \int_{-\infty}^{+\infty} dt \int_V d^{d-1}x \mathcal{L}[A_{\mu}, \bar{\psi}_f, \psi_f]}, \quad (1)$$

which can be expressed in terms of a path integral over the N_f quark (and antiquark) fields $(\bar{\psi}_f, \psi_f)$ with $f = u, d, s, c, b, t$ (up, down, strange, charm, bottom, and top) and the gluon fields A_{μ} . This partition function implicitly depends on the strong coupling g (or equivalently $\alpha_s = \frac{g^2}{4\pi}$) and the masses $\mathbf{m} = (m_u, m_d, m_s, \dots)$ of the quark flavors, which are the only parameters of the classical QCD Lagrangian $\mathcal{L}[A_{\mu}, \bar{\psi}_f, \psi_f]$. Since the top quark mass m_t is significantly larger than the electroweak scale M_W , it decouples in most respects from nuclear matter at any lower scales and will be omitted in the following. Observables can be calculated in QCD by expressing them through the fundamental fields and evaluating the path integral

$$\langle O \rangle = \frac{1}{Z} \int \prod_{\mu} \mathcal{D}A_{\mu} \prod_f \mathcal{D}\bar{\psi}_f \mathcal{D}\psi_f O[A_{\mu}, \bar{\psi}_f, \psi_f] e^{iS[A_{\mu}, \bar{\psi}_f, \psi_f]}, \quad (2)$$

where we use the QCD action $S = \int d^d x \mathcal{L}$ and omit any explicit reference to the volume.

All interactions among these fundamental fields are encoded into the monomials of the QCD Lagrangian, which satisfies a local symmetry under the gauge group $SU(N_c)$, where $N_c = 3$ for QCD. Namely, the quark flavors $(\bar{\psi}_f^a, \psi_f^a)$ exist in N_c copies (color indices $a = 1, \dots, N_c$) that transform in the fundamental representation of the gauge group, and the gluons

$$A_\mu^c \equiv A_\mu^{ab} t_{ab}^c, \quad (3)$$

in $N_c^2 - 1$ copies (color indices $c = 1, \dots, (N_c^2 - 1)$, $a, b = 1, \dots, N_c$) that transform in the adjoint representation of the gauge group. Here, t_{ab}^c are the generators of the Lie algebra $\mathfrak{su}(N_c)$ normalized as $\text{tr}(t^c t^d) = \frac{1}{2} \delta^{cd}$. The classical QCD Lagrangian has a gauge part and a matter part,

$$\mathcal{L}[A_\mu, \bar{\psi}_f, \psi_f] = \mathcal{L}_{\text{gauge}}[A_\mu] + \mathcal{L}_{\text{matter}}[A_\mu, \bar{\psi}_f, \psi_f] \quad (4)$$

$$= -\frac{1}{4g_0^2} F_c^{\mu\nu}(x) F_{\mu\nu}^c(x) - \sum_f \bar{\psi}_f^{\alpha a}(x) \left\{ i \not{D}_{\alpha\beta}^{ab} - m_{0f} \delta_{\alpha\beta} \delta_{ab} \right\} \psi_f^{\beta b}, \quad (5)$$

where all indices are understood to be summed over. The Dirac or spin indices $\alpha = 1, \dots, d$ are indicated with greek characters. In the notation used in the following, color, flavor, and spin indices, and the space-time arguments x will be generally omitted whenever this is appropriate. The matter part is restricted to the N_f quark flavors that are considered as dynamical degrees of freedom. As such, the QCD Lagrangian explicitly depends on the bare gauge coupling g_0 , the number N_f of dynamical quark flavors, and the N_f respective bare quark masses m_{0f} as its only parameters.

The massless Dirac operator $\not{D}_{\alpha\beta}^{ab}$ is given in terms of the covariant derivative D_μ^{ab} as

$$\not{D}_{\alpha\beta}^{ab} = \sum_\mu \gamma_\mu^{\alpha\beta} D_\mu^{ab}, \quad D_\mu^{ab} = i(\delta^{ab} \partial_\mu - i t_c^{ab} A_\mu^c). \quad (6)$$

The matter part of the QCD Lagrangian is locally gauge invariant under a transform

$$\begin{aligned} \psi(x) &\rightarrow \Omega(x) \psi(x), & \bar{\psi}(x) &\rightarrow \bar{\psi}(x) \Omega^\dagger(x), \\ A_\mu(x) &\rightarrow \Omega(x) \{ A_\mu(x) + i \Omega^\dagger(x) \partial_\mu \Omega(x) \} \Omega^\dagger(x) \end{aligned} \quad (7)$$

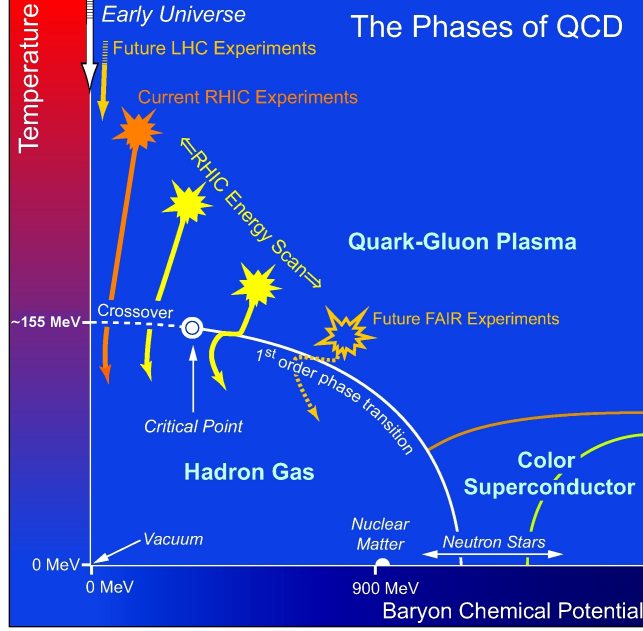


Figure 1: The conjectured QCD phase diagram in the plane of two external parameters: temperature and the baryon chemical potential. Possible reach of the current and future heavy-ion collision experiments is indicated with orange and yellow arrows and symbols.

for any $\Omega(x) \in \text{SU}(N_c)$. The field strength tensor $F_{\mu\nu}^a(x)$ can be expressed in terms of the structure constants f_{abc} of the Lie algebra $\mathfrak{su}(N_c)$, or in terms of commutators of A_μ or of covariant derivatives D_μ ,

$$\begin{aligned} F_{\mu\nu}^c(x) &= \partial_\mu A_\nu^c - \partial_\nu A_\mu^c + f_{abc} A_\mu^a A_\nu^b \\ &= t_{ab}^c \{ \partial_\mu A_\nu^{ab} - \partial_\nu A_\mu^{ab} - i[A_\mu, A_\nu]^{ab} \} = -it_{ab}^c [D_\mu, D_\nu]^{ab}. \end{aligned} \quad (8)$$

The invariance of the gauge part follows immediately from Eq. (7). The gauge part on its own is also referred to as the Yang-Mills or pure gauge Lagrangian. For mostly technical reasons this is still of particular relevance to lattice gauge theory as will be explicitly addressed later on.

QCD has multiple inherently nonperturbative aspects such as the confinement, the spontaneous chiral symmetry breaking, and the axial anomaly, all of which are directly reflected in the low-energy hadron spectrum and control the key properties of nuclear matter. These key properties change quite dramatically as the external parameters such as the temperature T ,

the volume V , or the quark flavor chemical potentials $\boldsymbol{\mu} = (\mu_u, \mu_d, \mu_s, \dots)$ are modified. Quark flavor chemical potentials can be introduced by adding a source term

$$\mathcal{L}_{\boldsymbol{\mu}\boldsymbol{n}} = \boldsymbol{\mu} \cdot \mathcal{N}[\bar{\psi}_f, \psi_f] = \sum_f \mu_f \bar{\psi}_f \gamma_0 \psi_f, \quad (9)$$

to the QCD Lagrangian of Eq. (4), where $\mathcal{N}_f = \bar{\psi}_f \gamma_0 \psi_f$ is the quark number density. A finite temperature can be introduced through a compact imaginary time direction with periodic boundary conditions for the bosons (gluons) and antiperiodic boundary conditions for the fermions (quarks). In practice this can be achieved by replacing the Minkowski space-time through a Wick rotation $t \rightarrow -i\tau$ with a Euclidean space-time with (anti-)periodic boundaries (in time). Thermally equilibrated strongly interacting matter is then described by the grand canonical QCD partition function $Z(T, V, \boldsymbol{\mu})$,

$$Z(T, V, \boldsymbol{\mu}) = \int \prod_{\mu} \mathcal{D}A_{\mu} \prod_f \mathcal{D}\bar{\psi}_f \mathcal{D}\psi_f e^{-\int_0^{\frac{1}{T}} d\tau \int_V d^{d-1}x \mathcal{L}_E[A_{\mu}, \bar{\psi}_f, \psi_f]}, \quad (10)$$

where \mathcal{L}_E is the classical QCD Lagrangian in Euclidean space-time. The definition of observables in a background of thermally equilibrated nuclear matter follows from applying the same steps to Eq. (2). Since the matter part of the QCD Lagrangian in Eqs. (4) and (9) is bilinear in the quark and antiquark fields, the quark degrees of freedom can be integrated out in the path integral to obtain

$$Z(T, V, \boldsymbol{\mu}) = \int \prod_{\mu} \mathcal{D}A_{\mu} \prod_f \det\{D[A_{\mu}](m_{0f}, \mu_f)\} e^{-\int_0^{\frac{1}{T}} d\tau \int_V d^{d-1}x \mathcal{L}_{\text{gauge}}[A_{\mu}]}. \quad (11)$$

Strongly interacting matter described by Eq. (10) has a rich phase structure, see Fig. 1, with many similarities to well-studied condensed matter systems. In particular, QCD has a well-established hadron gas phase for small values of the temperature T and the chemical potentials $\boldsymbol{\mu}$, and another well-established quark-gluon plasma phase for large values of the temperature T . In the limit of massless quarks and vanishing chemical potentials, there is a sharp chiral phase transition that takes place at the critical temperature $T_c^0 = 132_{-6}^{+3}$ MeV [16]. For small enough quark masses and

small enough chemical potentials μ , this transition is turned into a smooth crossover at a somewhat higher pseudo-critical temperature [17, 18, 19, 20], i.e. $T_c = 156.5(1.5)$ MeV for physical quark masses, while being still sensitive to the sharp phase transition. Recently, there have been hints [21] of a *stringy-fluid* phase with a spin-chiral symmetry at values of the temperature slightly above this transition, although not much is known about this state so far. For a long time, there have been speculations about a critical end-point and phase transition line for larger values of the chemical potentials, but these prove elusive despite major efforts in experimental or theoretical studies to date. For small temperatures and densities around the average nuclear matter density, one encounters the larger nuclei of the elements in the periodic table, and – for much larger densities – eventually neutron stars. While this regime is well-studied experimentally, theory calculations are still challenging due to a sign problem (i.e. breakdown of stochastic importance sampling and/or exponentially decreasing signal-to-noise ratio) in the partition function of Eq. (10).

2.2 Finite temperature field theory

The restriction of a quantum field theory to finite temperature has profound consequences that play out in QCD quite similar as in most other quantum field theories. The energies of all fields become quantized and are restricted to the Matsubara modes ω_n , which are fixed for any bosons as $\omega_n = 2n \pi T$ and for any fermions as $\omega_n = (2n + 1) \pi T$, where $n = 0, 1, \dots$. Hence, the lowest bosonic Matsubara mode $\omega_0 = 0$ is the *Matsubara zero mode* or *static Matsubara mode*, and is well-separated from all higher (bosonic or fermionic) Matsubara modes.

This scale separation entails an approximate decoupling of the *static modes* of the fields from their higher Matsubara modes. Namely, the interactions between these different modes take place at the temperature scale, and the coupling depends on the temperature. The most important interactions between the *static modes* and the higher Matsubara modes induce (in the massless limit divergent) contributions that modify the large-distance behavior of the *static modes*. Namely, the correlation lengths of the *static modes* may be temperature dependent and finite in the interacting theory, despite being infinite at the tree level. The inverse of such a screening length can be rephrased in terms of a screening mass that vanishes in the non-interacting

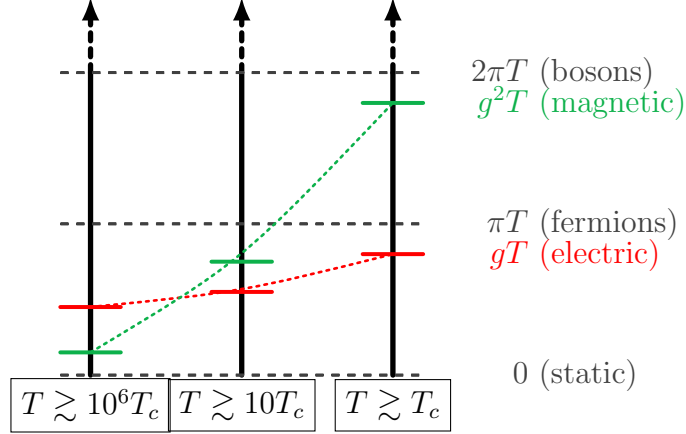


Figure 2: Thermal QCD hierarchies for very high temperatures (left), and high (center) or low (right) temperatures in the phenomenologically interesting range. The naive hierarchy $g^2T \ll gT$ between magnetic and electric scales is inverted for phenomenologically interesting temperatures. Eventually, it is not even clear if the magnetic or even electric scales can be distinguished from the lowest non-static scales at all, if the coupling $g(T)$ becomes too large.

or zero-temperature limits. While a similar screening mechanism affects the higher Matsubara modes as well, it is generally subleading compared to the non-zero Matsubara frequencies $\omega_n = (2n) \pi T$ for $n > 0$. Since the lowest fermionic Matsubara mode is $\omega_0 = \pi T$, contributions from fermions are generally suppressed similarly to the higher Matsubara modes, too.

In particular, the interactions of these *static modes* can be understood in terms of the three-dimensional effective field theory [22, 23], see [24] for a concise review. The higher Matsubara modes and the fermions are integrated out and are manifest in the Wilson coefficients of suppressed higher order operators. In the case of QCD, there are a few key differences between the vacuum field theory and the thermal field theory. First, the symmetry between the *magnetic gluons* and the *electric A_0 gluons* is broken in the thermal theory. Second, there are contributions at odd powers of the gauge coupling $g(T)$, which are due to the screening of the *electric A_0 gluons*. Third, perturbation theory has an infrared cutoff at order $\sim g^2T$, which leads to a complete breakdown of perturbation theory at order g^6T^4 for the thermodynamic potentials [25]. These scales – T (or rather $2\pi T$ or πT),

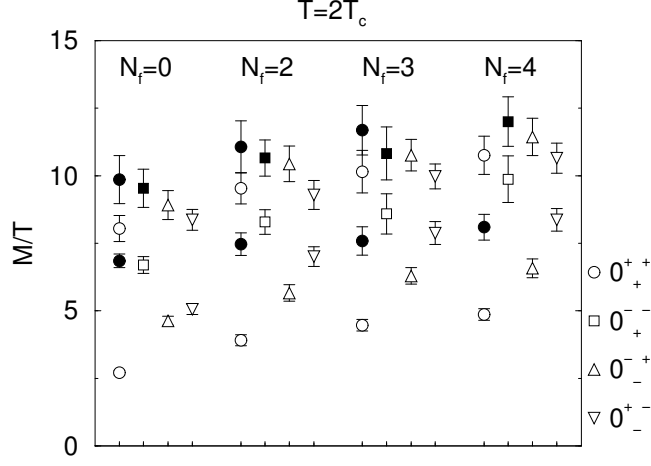


Figure 3: The spectrum of electrostatic QCD as obtained in nonperturbative lattice simulations [26]. Open symbols correspond to states containing *electric* A_0 gluons, filled symbols correspond to genuine magnetic glue-balls. The naive hierarchy is inverted in all channels. From Ref. [26].

$g(T)T$, and $g^2(T)T$ – are hierarchically ordered for very high temperatures. For phenomenologically interesting temperatures not too far above the QCD scale $\Lambda_{\overline{\text{MS}}}$, this hierarchy might not be realized at all in practice, since the coupling $g(T \gtrsim \Lambda_{\overline{\text{MS}}})$ is large, see Fig. 2. Under these circumstances, the predictive power of the weak-coupling approach may strongly vary between different quantities.

On the one hand, the interactions among the *magnetic gluons* can be described by a three-dimensional, i.e. confining $\text{SU}(N_c)$ pure gauge theory with the coupling $g_M^2 \sim g^2 T$ and the confinement radius $\sim 1/(g^2 T)$ [7]. This effective field theory is called the *magnetostatic QCD* (MQCD). The *magnetic gluons* themselves are not affected by the thermal screening, although they have finite correlation lengths due the confinement radius $\sim 1/(g^2 T)$ of the pure gauge theory. Accordingly, these *magnetic gluons* combine to the same glue-ball spectrum as in the three-dimensional Yang-Mills theory at zero temperature. The lowest-lying glue-ball masses $m \sim g^2 T$ correspond (for $m \ll 2\pi T$) to certain inverse correlation lengths of long-range correlations between the *static modes* of the thermal QCD medium. These *magnetostatic QCD* contributions to the correlation lengths in the thermal QCD medium cannot be determined using perturbation theory.

On the other hand, the large-distance correlations of the *electric* A_0 gluons are severely impacted by the thermal modifications. These modifications can be accounted for in terms of a thermal *Debye mass*, which is of the (leading) order $m_D \sim gT$ and affects only the *electric* A_0 gluons. To the leading order the *electric* A_0 gluons may be treated as a massive adjoint scalar field with A_0^4 self-interactions (with the coupling at the order $\lambda_E \sim g^4 T$), and with the minimal coupling to the *magnetic gluons* using the charge $g_E^2 \sim g^2 T$. This effective field theory is called the *electrostatic QCD* (EQCD). Its spectrum also contains nonperturbative bound states of multiple *electric* A_0 gluons or of *electric* A_0 gluons with *magnetic gluons*. These bound states, which are formed at the confinement scale $\sim g^2 T$ of the *magnetostatic QCD*, can be understood as a manifestation of the Linde problem [25]. Whether the lightest states with any given quantum numbers are purely magnetic glueballs or bound states involving *electric* A_0 gluons depends on the value of the coupling $g(T)$, and therefore on the temperature, see Fig. 3 for a glance on the spectrum of the *electrostatic QCD* [26].

In the weak-coupling approach a *Debye mass* can be defined order-by-order in terms of the pole position of the *static mode* of the thermal gluon propagator. The higher Matsubara modes or the fermions contribute order-by-order only at odd powers of the coupling, i.e. $m_D/T \sim c_1 g + c_2 g^3 + \dots$. However, while this pole position is gauge invariant order-by-order in perturbation theory, one cannot avoid using the gauge-dependent gluon propagator for its definition, and hence it is dependent on a gauge-fixed approach. Moreover, contributions from the *magnetic gluons* yield a nonperturbative contribution to m_D that is of order $\sim g^2 T$. This is yet another manifestation of the Linde problem [25]. The perturbative expansion breaks down as soon as scales of order $g^2 T$ contribute. For these reasons it is not obvious to which extent the weak-coupling approach may yield a physically meaningful description of the screening of the *electric* A_0 gluons at all [14]. Answers to this problem can be provided through the comparison between the results obtained in the weak-coupling approach or in a direct nonperturbative calculation. We return to this point in Section 3.2.

2.3 Lattice regularization

Quantum effects are inherent to the properties and interactions of strongly interacting matter. As such the classical QCD Lagrangian of Eq. (4) has

physical significance only through its role inside of the path integral definition of the partition function of Eqs. (1) or (10). Alas, this definition is not well-defined, but fraught with divergences. These are both of the infrared kind due to the propagation of massless (the gluons) or almost massless modes (some of the quark flavors), or of the ultraviolet kind due to the presence of quantum loops with infinite momenta. The former are only present in an infinite space-time volume and eventually regulated by the nonperturbative phenomena at the QCD scale $\Lambda_{\overline{\text{MS}}}$, the latter originate in the contributions from infinitesimally separated fields. Hence, Eqs. (10) only permits the calculation of QCD amplitudes if all of the divergences are regulated accordingly.

Any such regularization scheme introduces its particular variety of unphysical properties at intermediate stages of a calculation. Eventually, physical predictions for the strong interactions are recovered only after the removal of this regulator. A reformulation of QCD on a finite (hypercubic) lattice of $N_\sigma^{d-1} \times N_\tau$ sites with the lattice spacing a is such a regularization scheme that removes all of the divergences and explicitly enforces the local gauge symmetry. Here, N_τ is the number of points along the time axis and N_σ the number of points along each spatial axis. Usually, periodic boundary conditions are used for all axes (antiperiodic for fermions in the time direction), although use of open boundary conditions in one of the directions has become more common in recent years¹. The path integral in lattice gauge theory with (anti-)periodic boundary conditions in the time direction and a Euclidean metric automatically samples the partition function of thermally equilibrated matter at temperature $T = \frac{1}{aN_\tau}$. Yet as long as this temperature is significantly smaller than the most infrared scale, i.e. the pion mass, this partition function is practically indistinguishable from a true $T = 0$ result. These periodic boundaries of the spatial directions imply that the lattice is a finite volume regulator with the smallest nonzero spatial momentum being $k_\mu = \frac{\pi}{aN_\sigma}$. The finite lattice spacing enforces $k_\mu = \frac{\pi}{a}$ as the largest accessible four-momenta, and thus provides an ultraviolet cutoff.

Any lattice regularization entails (at least) the explicit breaking of the rotational symmetry from $O(d)$ to a discrete symmetry of lattice rotations (typically a hypercubic symmetry W_d). Since there is no derivative operator on a lattice, it has to be approximated through finite difference operators for

¹The reasons why open boundary conditions may be more beneficial are related to sampling of the topology of the gauge fields but are too technical to be discussed in this review.

any lattice regularization, i.e., in the simplest symmetric form

$$\begin{aligned}\partial_\mu &= \frac{\nabla_\mu + \nabla_\mu^*}{2} + \mathcal{O}(a^2), \\ \nabla_\mu \psi(x) &= \frac{\psi(x + a\hat{\mu}) - \psi(x)}{a}, \quad \nabla_\mu^* \psi(x) = \frac{\psi(x) - \psi(x - a\hat{\mu})}{a}.\end{aligned}\quad (12)$$

Here and in the following $a\hat{\mu}$ denotes the vector of one lattice spacing a in the μ direction. Due to this lack of an exact derivative operator, Eq. (7) cannot be realized on the lattice for arbitrary gauge transforms Ω . However, QCD can be rephrased on a (hypercubic) lattice by substituting the gauge fields $A_\mu(x)$, which are elements of the Lie algebra $\mathfrak{su}(N_c)$, with the gauge links

$$U_{\mu,x} = \exp[iaA_\mu(x + \frac{a}{2}\hat{\mu})], \quad U_{\mu,x} \rightarrow \Omega_x U_{\mu,x} \Omega_{x+a\hat{\mu}}^\dagger, \quad (13)$$

that transform as elements of the Lie group $SU(N_c)$. Whereas the quark and antiquark fields are defined on the sites of the lattice, the gauge fields on the lattice are placed on the links between the sites. Wilson lines are constructed by attaching the gauge links as path-ordered segments of a continuous path, and the gauge invariance of the trace of any closed contour follows from Eq. (13). There are two general classes of closed contours – the topologically trivial Wilson loops, which can be deformed into a point (i.e., do not wrap around a boundary) and the topologically nontrivial Wilson loops, which can be deformed into a line wrapping around the lattice. The smallest possible Wilson loop wrapping around one elementary square is called the plaquette.

The covariant derivative can be expressed with the gauge links

$$D_\mu \psi(x) = \frac{U_{\mu,x} \psi(x + a\hat{\mu}) - U_{\mu,x-a\hat{\mu}} \psi(x - a\hat{\mu})}{2} + \mathcal{O}(a^2). \quad (14)$$

From Eq. (14) the gauge invariance of the matter part of the QCD Lagrangian is evident, too. It follows that Wilson lines with a quark and an antiquark on their ends are also gauge invariant.

There are different possibilities for the discretization of the field monomials of the continuum QCD Lagrangian of Eqs. (4) and (9) that differ only in terms of the discretization errors, i.e., unphysical effects of order a , a^2 , ..., which vanish as the regulator is removed in the *continuum limit*. Various formulations of lattice QCD present different regularization schemes that are distinguished by the type and the magnitude of the unphysical effects that are introduced by the regulator. These effects can always be systematically diminished in so-called *improved actions*, but never fully eliminated without taking the continuum limit.

2.4 Renormalization and weak coupling

The fundamental charge $g(\nu) = \sqrt{4\pi\alpha_s(\nu)}$ associated with the local gauge symmetry explicitly depends on the scale ν , at which the respective interactions transpire. The evolution of the charge $\alpha_s(\nu)$ with the scale ν is controlled by the QCD beta function [8, 9]

$$\frac{d\alpha_s(\nu)}{d\ln\nu} = \alpha_s \beta(\alpha_s) = -\frac{\alpha_s^2}{2\pi} \sum_{n=0}^{\infty} \left(\frac{\alpha_s}{4\pi}\right)^n \beta_n = -2\alpha_s \left[\beta_0 \frac{\alpha_s}{4\pi} + \beta_1 \left(\frac{\alpha_s}{4\pi}\right)^2 + \dots \right], \quad (15)$$

Only its first two coefficients are universal (independent of the regularization scheme)

$$\beta_0 = \frac{11}{3}C_A - \frac{4}{3}T_F N_f, \quad \beta_1 = \frac{34}{3}C_A^2 - \frac{20}{3}C_A N_f T_F - 4C_F N_f T_F, \quad (16)$$

with the color factors being

$$C_F = \frac{N_c^2 - 1}{2N_c}, \quad C_A = N_c, \quad T_F = \frac{1}{2}, \quad (17)$$

where N_c is the number of colors. N_f has to be understood as the number of (approximately massless) quark flavors contributing up to the scale ν . As such, the multiplicative factor $1/g_0^2$ that scales the gauge Lagrangian $\mathcal{L}_{\text{gauge}}$ has to be understood as a bare gauge coupling that is related to the physical charge $g(\nu)$ at the scale ν through the QCD beta function of Eq. (15). In a similar way, the bare quark masses m_{0f} are related to renormalized quark masses $m_f(\nu)$ at the scale ν through the renormalization group flow.

In the lattice formulation, the lattice spacing is not an explicit input parameter. Instead it is related to the bare gauge coupling g_0 by the QCD beta function as

$$a\Lambda_{\text{lat}} = \left(\frac{1}{\beta_0 g_0^2} \right)^{\frac{\beta_1}{2\beta_0^2}} e^{-\frac{1}{2\beta_0 g_0^2}}, \quad (18)$$

where $\Lambda_{\text{lat}} \sim \Lambda_{\overline{\text{MS}}}$ (parametrically) is a representation of the QCD Lambda parameter that is specific to the details of each lattice regularization scheme. Any quantities with nontrivial mass dimension are given in units of the lattice spacing. Namely, the bare quark masses are given as am_{0f} . The lattice spacing is determined a posteriori by *setting the scale* using an observable

with nontrivial mass dimension that can be easily computed with high precision and has only a small sensitivity to the discretization errors, i.e. higher powers in a . Keeping physical observables constant while approaching the continuum limit requires that the bare gauge coupling g_0 as well as the bare quark masses am_{0f} are adjusted to smaller values along lines of constant physics.

Due to the adjoint charge of the gluons (A_μ^{ab}) the gauge Lagrangian $\mathcal{L}_{\text{gauge}}$ contains anti-screening self-interactions, which express themselves in the first, i.e., positive contributions to β_0 and β_1 . These self-interactions give rise to the emergent scale of QCD, $\Lambda_{\overline{\text{MS}}}$, at which Eq. (15) has a Landau pole, where the strong coupling $\alpha_s(\nu = \Lambda_{\overline{\text{MS}}})$ diverges. In fact, the confinement property of QCD at low values of the temperature implies that the energy density in strongly interacting matter grows linearly with the separation. Hence, fields in any nontrivial representation of the gauge group must be dressed in clouds of nuclear matter with typical energies $E \sim \Lambda_{\overline{\text{MS}}}$, and may only propagate over very small distances $r \ll 1/\Lambda_{\overline{\text{MS}}}$. On longer times scales $t \gtrsim 1/\Lambda_{\overline{\text{MS}}}$ these fields have to aggregate into bound states that transform in the trivial representation. For temperatures as high as $T \gtrsim \Lambda_{\overline{\text{MS}}}$, the confinement property is lifted due to the color screening of long-range forces in the quark-gluon plasma.

At much higher scales $\nu \gg \Lambda_{\overline{\text{MS}}}$ the strong coupling constant becomes small, and this asymptotic freedom explicitly permits a weak-coupling expansion of the strong interactions. In an equivalent scheme that is particularly convenient for a weak-coupling expansion the gauge fields are defined as $A_\mu = g_0 \mathcal{A}_\mu$, i.e., the bare gauge coupling g_0 explicitly multiplies all three-point functions and g_0^2 multiplies all four-point functions.

Processes at scales in the vicinity of $\Lambda_{\overline{\text{MS}}}$ are inherently nonperturbative, i.e. a perturbative expansion in powers of g (or α_s) cannot describe such interactions at all. The lattice formulation lends itself to a nonperturbative calculation of the QCD partition function. This is accomplished by performing a Wick rotation $t \rightarrow -i\tau$ that trades Minkowski space-time for Euclidean space-time and transforms the action as $iS_M \rightarrow -S_E$. Thus, the exponential factors in Eqs. (10) and (2) become real, and importance sampling can be applied for evaluating the path integral in a Markov Chain Monte Carlo simulation in practice. Under these conditions the weak-coupling expansion is not necessary anymore and the nonperturbative calculation is explicitly

feasible.

The different quark flavors can be generally grouped into the two subsets of *light* or *heavy* quark flavors, which are distinguished by the ordering of the respective quark masses m_f and $\Lambda_{\overline{\text{MS}}}$. Namely, the *light* quark flavors $f = u, d, s$ have $m_f \lesssim \Lambda_{\overline{\text{MS}}}$, while the *heavy* quark flavors $f = c, b$ have $m_h \equiv m_f \gg \Lambda_{\overline{\text{MS}}}$. These two different ordered hierarchies may permit the use of the effective field theory (EFT) approach for QCD. The low-energy limit of QCD is rephrased in terms of specific sets of low-energy degrees of freedom, and the high-energy modes above some matching scale ν are integrated out and absorbed into the Wilson coefficients of the EFT. Suitable EFT approaches for the *light* quark flavors are the chiral perturbation theory (for a review see, i.e. Refs. [27, 28]) and chiral effective field theory (for a review see, i.e. Refs. [29, 30]), whose convergence is restricted to $p \ll \Lambda_{\overline{\text{MS}}}$ for all external momenta. The corresponding Wilson coefficients are calculated at the scale $\nu \sim \Lambda_{\overline{\text{MS}}}$. Suitable EFT approaches for the *heavy* quark flavors take the nonrelativistic limit of QCD, whose convergence is restricted to $p \ll m_h$ for all external momenta. The corresponding Wilson coefficients are calculated at the scale $\nu \sim m_h$. Thus, whereas the interactions of the former necessitate nonperturbative approaches, the latter can be addressed by means of the weak-coupling expansion.

2.5 Light quarks

On the one hand, since $m_f/\Lambda_{\overline{\text{MS}}}$ is a small quantity for the *light* quark flavors, these behave as almost massless in QCD, and it is permissible to expand QCD amplitudes involving the *light* quark flavors in terms of $m_f/\Lambda_{\overline{\text{MS}}}$. This introduces a power counting even for large values of the coupling. The matter Lagrangian has an accidental, chiral symmetry in the massless limit. This chiral symmetry is in part broken by the axial anomaly of the fermion measure (flavor singlet chiral symmetry), and in part spontaneously broken for all states of the hadron spectrum due to the formation of a scalar quark-antiquark condensate (*chiral condensate*) at low temperatures (all flavor nonsinglet chiral symmetries), and, finally, explicitly broken by the nonzero *light* quark masses. As a consequence of the interplay between the nonzero *light* quark masses and the spontaneous breaking of the chiral symmetry the associated Pseudo-Goldstone bosons (pion, kaon, eta) acquire masses significantly below one unit of $\Lambda_{\overline{\text{MS}}}$ for each contributing quark (or antiquark). These are the

lightest modes that transform in the trivial representation, and thus propagate over large distances in the hadronic phase and induce the strongest sensitivity to effects of the finite spatial volume. A further consequence of the spontaneously broken chiral symmetry is the absence of parity doubling in the hadron spectrum.

If the temperature or the density of a nuclear matter system is increased beyond a certain delimiting region in the phase diagram, the description in terms of hadronic degrees of freedom breaks down. Instead, the bulk properties of the strongly interacting matter system have to be understood in terms of the partonic (quark and gluon) degrees of freedom, or in terms of a mix between hadronic and partonic degrees of freedom. The corresponding thermal expectation values undergo violent thermal fluctuations when the system changes between the low and high temperature phases. The details of these fluctuations and of the transition strongly depend on the number of *light* quark degrees of freedom and on the values of the parameters (*light* quark masses and *light* quark chemical potentials) in the QCD partition function of Eq. (10).

In the limit of pure gauge theory, where the matter part of Eq. (4) is absent (or, equivalently, where all quarks are infinitely heavy), the QCD partition function has a $Z(N_c)$ center symmetry that is manifest in the hadronic phase due to the frequent tunneling between the N_c different sectors of the $Z(N_c)$ center symmetry. In the quark-gluon plasma phase this $Z(N_c)$ center symmetry is broken spontaneously and the system becomes stuck in one of the N_c different sectors of the $Z(N_c)$ center symmetry for arbitrarily long times. For four-dimensional $SU(N_c)$ pure gauge theory with $N_c = 3$, the transition between the phases is of first order. The associated non-local *order parameter* is the Polyakov loop, namely, the most simplest case of a topologically nontrivial Wilson loop wrapping around the periodic Euclidean time direction, whose fluctuations diverge at the phase transition, see Section 3.1. Above the transition, the Polyakov loop assumes a non-zero expectation value (in the infinite volume limit) due to the color screening.

In full QCD with dynamical *light* quark flavors this $Z(N_c)$ center symmetry is explicitly broken by the presence of the *light* quark flavors. Namely, the associated *chiral condensate* couples to the Polyakov loop and acts as a $Z(N_c)$ center symmetry breaking field already in the vacuum. Therefore, the Polyakov loop does not play the role of an order parameter in full QCD with

dynamical *light* quark flavors and is not related to the critical behavior in the chiral limit. Instead, the *chiral condensate* is the order parameter of full QCD, and the partition function becomes singular at the *chiral phase transition* in the limit of vanishing masses of the *light* quark flavors. The role of the symmetry breaking field in full QCD is thus played by the finite masses of the *light* quark flavors. At higher temperatures, the thermal fluctuations of the *chiral condensate* eventually become too large, and the thermal expectation value of the *chiral condensate* drops to zero. Depending on the number of *light* quark flavors and their masses, the universality class and the details of the transition vary. For the physical values of the quark masses, there is no sharp phase transition, but a smooth crossover. Nevertheless, the physical *light* quark masses are small enough that the real world is quite sensitive to the *chiral phase transition*. The fluctuations of the *chiral condensate* diverge in the massless limit at the critical temperature $T_c^0 = 132_{-6}^{+3}$ MeV [16], and reach a pronounced maximum for physical *light* quark masses at the pseudo-critical temperature $T_c = 156.5(1.5)$ MeV [17, 18, 19].

In the quark-gluon plasma phase at temperatures sufficiently above the *chiral phase transition*, namely for temperatures at or above $T \gtrsim 2T_c \sim \Lambda_{\overline{\text{MS}}}$, the *chiral condensate* has already melted, all flavor nonsinglet chiral symmetries are restored, and there are no associated Pseudo-Goldstone bosons accordingly. The masses of the thermalized *light* quark flavors are much smaller than the lowest fermionic Matsubara frequency $\omega_0 = \pi T$. Hence, the bulk properties of the quark-gluon plasma depend only mildly on the details of the dynamical *light* quark flavors for such temperatures. Nevertheless, thermalized *heavy* quark flavors may become relevant at such high temperatures.

2.6 Heavy quarks

On the other hand, since $\Lambda_{\overline{\text{MS}}}/m_h$ is a small quantity for the *heavy* quark flavors, these behave as almost infinitely heavy in QCD, and it is permissible to expand QCD amplitudes for the *heavy* quark flavors in terms of $\Lambda_{\overline{\text{MS}}}/m_h$. In the static limit the *heavy* quark flavors are treated as infinitely heavy (*static quarks*) and do not propagate in space. Such immobile *static quarks* are test charges in the fundamental representation of $\text{SU}(N_c)$, and one is able to define a potential, or rather the quark-antiquark static energy E , which can be calculated on the lattice and in the weak-coupling approach, reaching

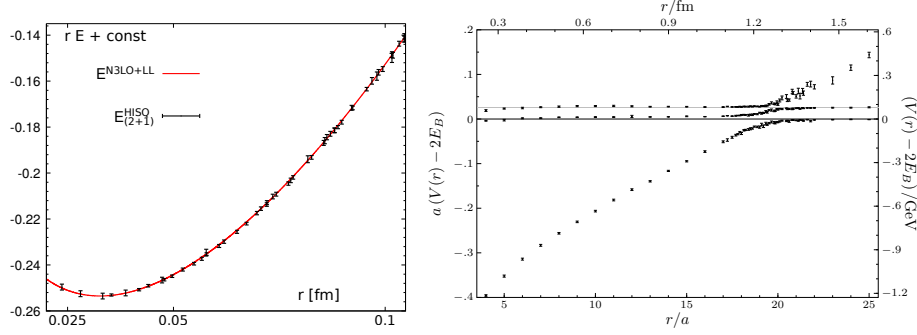


Figure 4: The static energy in (2+1)-flavor QCD on the lattice. (Left) After removing the discretization errors at small distances from the lattice result (with the HISQ action), the result is well-described by the N³LO result for $\alpha_s(M_Z) = 0.1167$ (with resummation of leading ultrasoft logarithms, LL) up to $r \sim 0.10$ fm [31]. (Right) In full QCD (with improved Wilson fermions) the string-breaking disrupts the QCD string [32]. There are two avoided level crossings due to the two non-degenerate quark masses of the sea, where the horizontal lines correspond to the twice static-light (lower) or static-strange (higher) meson masses. From Ref. [32].

good agreement at small distances, see Fig. 4 (left). The typical scale of the gluons that contribute to this energy is $p \sim 1/r$. Due to the asymptotic freedom this energy has a Coulombic core $E \sim \alpha_s/r$ at short distances $r \ll 1/\Lambda_{\overline{\text{MS}}}$. Due to the confinement the energy also exhibits a linearly rising contribution $E \sim \sigma r$ at larger distances $r \sim 1/\Lambda_{\overline{\text{MS}}}$, the QCD string or QCD flux tube, where $\sigma \sim \Lambda_{\overline{\text{MS}}}^2$. The most simple potential model that features these two aspects is the Cornell potential $V_{\text{Cornell}} = -\alpha/r + \sigma r$. At even larger distances, $r \sim 1/m_\pi$, the potential picture breaks down and the QCD string rips apart and a *light* quark-antiquark pair is generated from the vacuum for the formation of two *heavy-light* mesons, i.e. a pair of static D and D^* mesons, see Fig. 4 (right). This string-breaking process can occur only if *light* quark flavors are present in the sea, i.e., this mechanism is impossible with the pure gauge Lagrangian. Further terms (relativistic corrections, Darwin-term, spin-orbit or spin-spin coupling, etc.) are included in the sophisticated nonrelativistic quark models, which describe the spectra and transitions in *heavy-heavy* quark-antiquark bound states quite successfully.

Upon expansion about the static limit one obtains the nonrelativistic

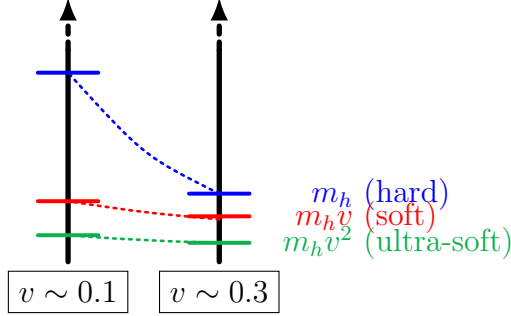


Figure 5: Nonrelativistic QCD hierarchies for the bottom quark (left), and the charm quark (right).

QCD (NRQCD) [33, 34] for the *heavy* quark flavors. The nonrelativistic *heavy* quarks and antiquarks decouple to leading order, namely, pair creation or annihilation are suppressed, since typical gluon momenta are $p \sim \Lambda_{\overline{\text{MS}}} \ll m_h$. The symmetry of the couplings between nonrelativistic quarks (and antiquarks) to chromoelectric and -magnetic gluons is broken by powers of $\Lambda_{\overline{\text{MS}}}/m_h$. Eventually, *heavy-heavy* bound states of quarks and antiquarks are small and compact objects, where the typical binding energies $E \sim mv^2/2$ are even smaller than the typical momenta $p \sim mv$ (with $v \ll c$). Thus, there is another layer of the hierarchy $E \sim \alpha_s/r \ll p \sim 1/r \ll m_h$, which permits the multipole expansion of such amplitudes, see Fig. 5. The EFT obtained in this manner is called potential nonrelativistic QCD (pNRQCD) [35, 36]. pNRQCD has non-local Wilson coefficients, which have the meaning of various potential or non-potential terms similar to those used in nonrelativistic quark models. In pNRQCD, such potentials can be derived from first principles. For a review of NRQCD and pNRQCD see Refs. [37, 38].

2.7 Implementation of QCD on the lattice

In lattice gauge theory, generally only the three *light* quark flavors, or additionally the charm quark, are considered as thermalized degrees of freedom. Since the up or down quark masses m_u or m_d are much smaller than the strange quark mass m_s , QCD is very often approximated in the isospin limit, where instead of up and down quarks two degenerate light quarks with an average light quark mass $m_l = (m_u + m_d)/2$ are considered. For this scenario the terms (2+1)- or (2+1+1)-flavor QCD are commonly used.

The most simple lattice action for the gauge fields is the Wilson plaquette action, i.e. a sum of the trace of all elementary 1×1 Wilson loops, which has leading discretization errors of order a^2 . The breaking of rotational symmetry is less pronounced for the improved gauge actions, namely the tree-level (or one-loop) Symanzik gauge action, which includes all elementary 1×2 (or also $1 \times 1 \times 1$) Wilson loops, too, and has discretization errors of order a^4 and $\alpha_s a^2$ (or $\alpha_s^2 a^2$).

Local link distributions in lattice simulations tend to suffer from violent UV fluctuations at short separations, which can be ameliorated through the use of a variety of iterative link smoothing techniques. Typical link smoothing algorithms are the APE smearing [39], the HYP (hypercubic) smearing [40], stout smearing [41] or the Wilson flow [42, 43]. These techniques can be applied to subsets of the links, i.e. typically only to spatial links or to all links, and with or without mixing links at different times. Any of these link smoothing techniques tend to distort the physics at small temporal and/or spatial separations, while suppressing the UV divergences of lattice operators. For this reason, the appropriate amount and type of smoothing is problem specific in lattice simulations.

Quarks on the lattice are more complicated. The naive lattice derivative of Eq. (14) has discretization errors of order a^2 , but produces 2^d degenerate lattice fermions. Hence, it is not directly suitable for QCD, since the continuum limit of such a discretization does not produce a theory with correct number of dynamical degrees of freedom. There are two commonly used approaches² to remedy this problem: Wilson and staggered.

The Wilson fermion approach [11] includes a momentum-dependent mass term at order a – the Wilson term – which breaks chiral symmetry explicitly even in the limit $m_{0f} \rightarrow 0$, and introduces the additive mass renormalization (due to the different renormalization of the two parts of the Wilson term). An improved formulation of Wilson fermions introduces the so-called Clover term to achieve discretization errors of order a^2 [46], but all individual quark bilinears using (improved) Wilson fermions require additional corrections for the order a errors.

²The more recent, overlap [44] and domain-wall [45] fermions realize an exact or almost exact chiral symmetry with the correct axial anomaly on the lattice and also have discretization errors of order a^2 , but are substantially more computationally expensive. As such, we will not discuss these formulations here.

The staggered fermion approach [47], which is derived from the naive discretization, has the same discretization errors of order a^2 . For even number of dimensions d the corresponding $2^{d/2}$ spinor components are decoupled through a unitary transform and $2^{d/2} - 1$ of these are omitted. The staggered discretization still has a reduced doubling problem with $2^{d/2}$ degenerate fermions that can only be accounted for by taking the $(2^{d/2})$ th root of the staggered quark determinant. The components of the fermions become distributed over 2^d lattice sites and the 2^d hyperquadrants of the Brillouin zone. Due to couplings between the 2^d hyperquadrants in the interacting field theory, the discretization errors are numerically large. Various formulations of improved staggered fermions have reduced discretization errors of order a^4 and $\alpha_s a^2$, and suppress the coupling between the hyperquadrants, namely, the AsqTad [48] and HISQ (highly improved staggered quarks) [49] formulations, whereas the stout formulation [41] simply reduces the a^2 and a^4 errors substantially. Staggered fermions are the most popular quark discretization for QCD at finite temperature.

In practice the evaluation of the quark determinant $\det\{D[A_\mu](m_{0f}, \mu_f)\}$ (using stochastic estimators) is the most expensive part of the Markov Chain Monte Carlo algorithm, in particular, if the sea quark masses are small. At each lattice site $\det\{D[A_\mu](m_{0f}, \mu_f)\}$ in Eq. (11) is sensitive to the gauge fields on all links of the entire lattice, whereas the gauge part of the QCD Lagrangian contains only small Wilson loops, and thus, very localized couplings. For this reason, lattice QCD simulations are often performed with a *light* quark mass that is larger than the physical value, or even without sea quarks at all, in the so-called quenched approximation, where the quark determinant is approximated by 1 and purely local updating can be used. It needs to be stressed that the Markov Chain that is generated in the quenched approximation samples the partition function of $SU(N_c)$ pure gauge theory.

3 Screening of static charges

Before introducing the observables related to the properties of the medium and screening effects in a non-Abelian gauge theory, such as QCD, let us recall some of the important features of the well-studied, both on classical and quantum level, Abelian gauge theory – Quantum Electrodynamics.

One of the simplest questions one can ask when encountering a new force of nature is what is the force between two static point-like objects capable

of interacting through that force. For macroscopic electromagnetism the answer to this question has been experimentally established in 18th century with the discovery of Coulomb's law. As is well known today, the force between two static probe charges q_1 and q_2 is long-range and falls off as $F \sim q_1 q_2 / r^2$ with the distance between the charges, which corresponds to the Coulomb-type potential $V \sim \alpha_{\text{em}} / r$. If the test charges are embedded in an electromagnetically interacting medium, such as an electromagnetic plasma, this long-range force gets *screened* and the range of interaction (excluding the van-der-Waals force that arises due to the polarization of the medium) becomes finite, governed by the screening length. The potential becomes of a Yukawa type e^{-mr} / r , where $r_D = 1/m$ – is the Debye-Hückel length [2]. Thus, studying the force between static probe charges, one learns about the properties of the medium, and the nonperturbative lattice QCD approach follows a very similar strategy as discussed in the following sections.

Another ingredient that helps to set up the stage for QCD is the Aharonov-Bohm effect [50] in electrodynamics. Namely, while propagation of a charged particle on the classical level is completely determined by the electric and magnetic fields, on the quantum level it is sensitive to the phase induced by the electromagnetic potential A_μ , even if the particle is propagating through the regions of space where the electric and magnetic fields are zero. This phase, acquired by the particle propagating in the gauge field background plays a fundamental role in the discussion of the thermodynamic properties of the strongly interacting medium.

3.1 The Polyakov loop and related quantities

3.1.1 Wilson line and the Polyakov loop

For a non-Abelian gauge theory the analog of the path-dependent phase in the Aharonov-Bohm effect is the *gauge connection* or *Wilson line*:

$$W(y, x) = P \exp \left\{ i \int_x^y A_\mu(z) dz^\mu \right\}. \quad (19)$$

where the integral is understood as a line integral along the path connecting y and x and P represents *path ordering*. The latter plays an important role for a non-Abelian case, since local A_μ fields at different points generally do not commute, as clear from Eq. (3). The discussion is still in the continuum, but one can easily recognize that the gauge link variables introduced in Eq. (13)

are the shortest possible Wilson lines that can be resolved on a lattice with spacing a .

A *Wilson loop* is a Wilson line over a closed path. Such a construction is gauge invariant, and lattice observables built of only gauge fields need to be always formulated in terms of Wilson loops traced over the color indices. A Wilson line running in the temporal direction represents the phase acquired by a static probe charge whose position in space remains fixed. A flat Wilson loop of size, *e.g.* $L_x \times L_t$ in (x, t) plane represents a static quark-antiquark pair (since the temporal Wilson lines have to run in the opposite direction when going over the loop, thus, naturally representing a particle and anti-particle). Wilson loops or correlators of spatially separated temporal Wilson lines are therefore natural objects to study the force between static probe charges.

While planar loops that do not wind around the lattice can be contracted to a point, there are also non-trivial Wilson loops that are closed paths due to the periodic boundary conditions. A special kind of a loop represented by a temporal Wilson line that forms a closed path by connecting to itself through the periodic boundary in the temporal direction is called *the Polyakov loop*:

$$L(\mathbf{r}) = \frac{1}{N_c} \text{tr} P \exp \left\{ i \int_0^\beta A_0(t, \mathbf{r}) dt \right\}. \quad (20)$$

We refer to this object as a *thermal Wilson line* if the trace is not taken. On the lattice Eq. (20) is particularly simple, it amounts to taking the trace of a product of gauge links going in the temporal direction to obtain the bare Polyakov loop:

$$L^{\text{bare}}(\mathbf{x}) = \frac{1}{N_c} \text{tr} \prod_{\tau=a}^{aN_\tau} U_{0,(\tau, \mathbf{x})}. \quad (21)$$

It is customary in lattice QCD calculations to take advantage of the translational invariance and define quantities summed over the whole lattice. This self-averaging often significantly improves the signal-to-noise ratio, even though the nearby points are strongly correlated. The lattice-averaged Polyakov loop is

$$L = \frac{1}{V} \sum_{\mathbf{x}} L(\mathbf{x}). \quad (22)$$

The expectation value of the Polyakov loop in the sense of Eq. (2) is related to the difference in free energy between the medium and the medium with a

single static charge inserted into it:

$$\langle L \rangle = \exp \left\{ -\frac{F_q}{T} \right\}. \quad (23)$$

On the one hand, in a pure gauge theory (*i.e.* with dynamical gauge fields but no dynamical fermions) the Polyakov loop is a (non-local) order parameter for the confinement-deconfinement transition, similar to the magnetization in spin systems. As discussed in Ref. [51], the Polyakov loop is associated with the center symmetry, $Z(N_c)$. In the symmetric, confined phase its expectation value is zero, which is interpreted as an infinite free energy F_q associated with insertion of a static probe color charge in the fundamental representation. This also hints that a concept of an isolated color charged object is not consistent with the confinement property of non-Abelian gauge theories. Namely, it is rigorously impossible to combine any number of gluons, which transform in the adjoint representation of the group, and one quark that transforms in the fundamental representation into an object that transforms in the trivial representation that would be allowed by the confinement. On the contrary, some higher representations of the Polyakov loop do not vanish in the confined phase, and may be related to the *glue-balls*. The Polyakov loop has been studied in higher representations in the SU(3) pure gauge theory [52] and in the (2+1)-flavor QCD [53]. Some of its higher representations can be defined (with $L_3 \equiv L$) as

$$\langle L_6 \rangle = \frac{1}{6}(\langle (3L_3)^2 \rangle - \langle 3L_3^* \rangle), \quad \langle L_8 \rangle = \frac{1}{8}(\langle |3L_3|^2 \rangle - 1), \dots, \quad (24)$$

where $\langle L_8 \rangle$ is the expectation value of the Polyakov loop in the adjoint representation. In the broken, deconfined phase $\langle L \rangle$ has a non-zero value, corresponding to finite F_q . Viewed from this perspective the high-temperature phase of a SU(N_c) pure gauge theory is a phase with spontaneously broken center symmetry, similar to e.g. a low-temperature phase of a ferromagnet. On the other hand, in a theory with dynamical fermions the quark condensate acts as a symmetry-breaking field, and the expectation value of the Polyakov loop in the fundamental representation does not go to zero in the low temperature phase.

Since the physics in the low-temperature phase of QCD and around the confinement-deconfinement transition is nonperturbative, a fully nonperturbative approach, such as lattice QCD is necessary to study the behavior of

the Polyakov loop with full theoretical control. Indeed, the Polyakov loop has been a subject of study on the lattice since the earliest days of lattice gauge theory [54, 55] until today [56].

For computational reasons simulations with dynamical fermions were hardly affordable in 1980s and 1990s and studies of the qualitative features of QCD were performed in SU(2) and SU(3) pure gauge theory. The finite temperature phase transition in SU(2) is of the second order and in SU(3) is of the first order. In the pure gauge theory the Polyakov loop susceptibility

$$\chi_L = VT^3 (\langle |L|^2 \rangle - \langle |L| \rangle^2) = VT^3 \left(\frac{1}{9} + \frac{8}{9} \langle L_8 \rangle - \langle L_3 \rangle^2 \right) \quad (25)$$

can be used to unambiguously define the transition temperature in the continuum and thermodynamic limit³. In full QCD with fermions this is not such a simple issue, since the Polyakov loop susceptibility mixes different representations.

3.1.2 The static quark potential and the renormalized Polyakov loop

While the temperature T_χ where χ_L becomes infinite defines the confinement-deconfinement phase transition temperature in pure gauge theory, in full QCD the transition is a smooth crossover and one needs to understand the quantitative behavior of the Polyakov loop and the associated free energy across the transition and in the deconfined phase.

The bare free energy as calculated on the lattice contains a linear divergence which makes the bare Polyakov loop vanish in the continuum limit. Renormalization of non-local operators such as Wilson loops was considered first in perturbation theory [57, 58] and later nonperturbatively on the lattice [59, 60]. A common procedure to renormalize the Polyakov loop is to first consider the free energy of a static quark-antiquark pair. The ultraviolet divergence in this quantity is temperature independent and is already present at zero temperature where the free energy coincides with the static quark-antiquark energy.

On the lattice the zero-temperature static quark-antiquark energy $E(r)$ can be extracted from the expectation value of the temporal Wilson loop of

³Given that numerical simulations are always done with a finite number of degrees of freedom, proper finite-size scaling techniques are employed to extrapolate to the thermodynamic limit and rigorously determine the order of the phase transition.

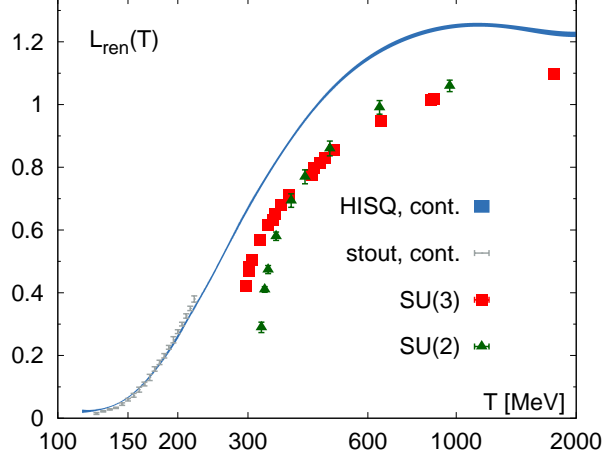


Figure 6: The renormalized Polyakov loop in SU(2) and SU(3) pure gauge theory (zero values in the confined phase are not shown) and in 2+1 flavor QCD with the HISQ and stout action. The chiral crossover temperature in QCD is $T_c = 155$ MeV.

size $r \times \tau$ or a correlator of temporal Wilson lines of length τ separated by a distance r in a fixed gauge (the Coulomb gauge is an especially convenient choice)

$$\begin{aligned}
 W^{\text{bare}}(\tau, \mathbf{r}; g_0^2) &= \frac{1}{N_c} \left\langle \sum_{\mathbf{x}} \text{tr} \left[W(\tau + \tau_0, \mathbf{x}; \tau, \mathbf{x}) W(\tau, \mathbf{x} + \mathbf{r}; \tau + \tau_0, \mathbf{x} + \mathbf{r}) \right] \right\rangle^{\text{gf}} \\
 &= \exp[-E^{\text{bare}}(r; g_0^2)\tau] \left(A_0(r) + \sum_{i=1}^{\infty} A_i(r) \exp[-\Delta_i(r)\tau] \right),
 \end{aligned} \tag{26}$$

where $\Delta_i(r) \sim \Lambda_{\overline{\text{MS}}}$ are the positive energy differences between the ground state $E^{\text{bare}}(r)$ and the excited states. The bare gauge coupling g_0 is an input parameter of lattice QCD simulations and here we explicitly emphasize that we refer to a quantity evaluated at non-zero lattice spacing. Non-perturbative renormalization of the static quark-antiquark energy then amounts to choosing a renormalization condition that the renormalized energy

$$E^{\text{ren}}(r) = E^{\text{bare}}(r; g_0^2) - C(g_0^2) \tag{27}$$

is equal to a prescribed value at some fixed distance \tilde{r} , for instance,

$$E^{\text{ren}}(\tilde{r}) = 0. \quad (28)$$

The chosen renormalization condition, e.g. Eq. (28), determines the additive shift $C(g_0^2)$, which is twice the self-energy of a static quark in the lattice scheme.

The renormalized Polyakov loop can then be defined as

$$L^{\text{ren}}(T) = L^{\text{bare}}(T; g_0^2) e^{N_\tau C(g_0^2)/2}. \quad (29)$$

An alternative renormalization procedure for the Polyakov loop is possible [53] with using recently introduced *gradient flow* [42]. In any case, the renormalized Polyakov loop has a well defined continuum limit $g_0 \rightarrow 0$, or equivalently, $a \rightarrow 0$.

The behavior of the renormalized Polyakov loop $L^{\text{ren}}(T)$ in SU(2), SU(3) pure gauge theory and in 2+1 flavor QCD is shown in Fig. 6. One can observe that in full QCD the renormalized Polyakov loop is smooth across the transition. It may be tempting [61, 17] to interpret the inflection point of the renormalized Polyakov loop as a location of the confinement-deconfinement transition, however, Eq. (29) shows that the exact details of the temperature dependence of L^{ren} depend on $C(g_0^2)$ and thus on the renormalization prescription. Such an approach typically yields a transition temperature above 170 MeV, about 15 MeV higher than the chiral crossover temperature at $T_c = 156.5$ MeV. See Sec. 2 for brief remarks on the chiral crossover.

The renormalization of the Polyakov loops in the higher representations $\langle L_{\mathbf{R}} \rangle$ is a somewhat different case. The renormalization constant can be obtained from the static energy only in the fundamental representation ($\langle L_3 \rangle \equiv \langle L \rangle$). For all other representations, one has to rely on other procedures, such as the direct renormalization [52, 56] or the gradient flow renormalization [53]. For temperatures below about twice the chiral crossover temperature, i.e. $T < T_c = 300$ MeV in (2+1)-flavor QCD, the Polyakov loop exhibits a large violation of the Casimir scaling between the different representations, which begin at the four-loop order in the weak-coupling expansion [62].

3.1.3 Static quark free energy and entropy

In contrast to the Polyakov loop, the renormalization of the static quark free energy F_q , Eq. (23), is additive like the static quark potential, and it

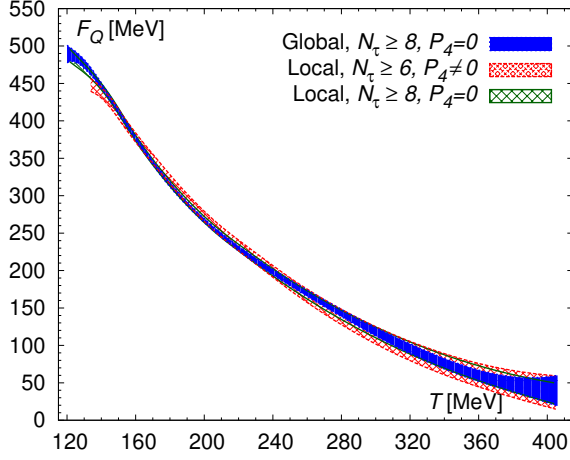


Figure 7: The renormalized static quark free energy F_q in 2+1 flavor QCD extrapolated to the continuum limit. The details of the extrapolations are given in Ref. [56].

is therefore a more robust observable to describe the transition region. The temperature dependence of the continuum extrapolated renormalized free energy in 2+1 flavor QCD is shown in Fig. 7. At the lowest temperature in the confined phase $T = 120$ MeV accessible in the lattice calculation it is about 500 MeV, rapidly decreasing to 400 MeV at the chiral crossover at the pseudo-critical temperature $T_c = 156.5$ MeV and then gradually dropping by an order of magnitude in the deconfined phase in the temperature range from 155 to 400 MeV, or $T_c - 2.5T_c$. The color screening effects of the medium in QCD kick in slowly which is quite different from the rapid drop of the static quark free energy associated with the first order phase transition in SU(3) pure gauge theory.

Nevertheless, it is still meaningful to consider the inflection point in the static quark free energy as one of the quantitative measures of the crossover into the deconfined phase. For this purpose we first define the entropy shift due adding to the medium a static quark [63, 64] as

$$S_q(T) = -\frac{\partial F_q(T)}{\partial T}. \quad (30)$$

The inflection point of $F_q(T)$ corresponds to the location of the peak in the

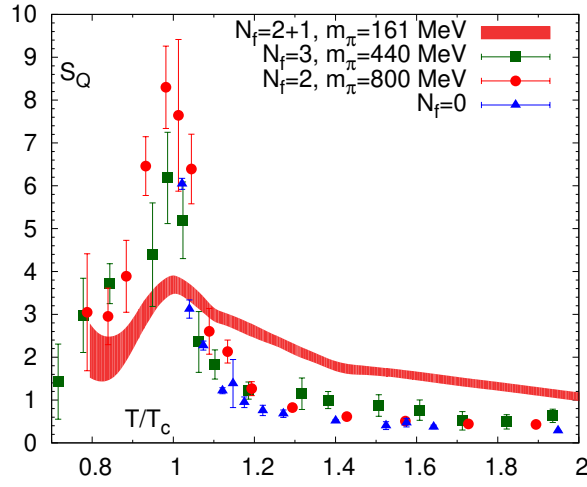


Figure 8: The static quark entropy S_q in 2+1 flavor QCD extrapolated to the continuum limit (solid red curve) compared with earlier calculations at finite cutoff and heavier than physical light quark masses and in pure gauge theory. Because of the different particle content the numerical value of the transition temperature T_c and thus the temperature scale is presented in units of T_c corresponding to $T_S = 153$ for 2+1 flavor QCD (see text), $T_\chi = 193$ MeV and $T_\chi = 200$ MeV for the $N_f = 3$ and $N_f = 2$ results and $T_L = 270$ MeV for the pure gauge ($N_f = 0$) case.

static entropy

$$\frac{\partial S_q}{\partial T} = 0. \quad (31)$$

The static quark entropy in the transition region for 2+1 flavor QCD at the almost physical light quark mass⁴ and at larger light quark masses [65, 64] is shown in Fig. 8. Again, one can observe that the temperature dependence of the static entropy in the real-world QCD is smoother in the transition region than in the theories with larger quark masses. The location of the maximum of S_q can be interpreted as the deconfinement transition temperature. The numerical result of Ref. [56] is $T_S = 153^{+6.5}_{-5}$ MeV which matches within the uncertainties the latest determination of the chiral crossover temperature $T_c = 156.5 \pm 1.5$ MeV [19, 20]. One has to bear in mind that while the latter is related to the critical behavior of QCD in the two-flavor chiral limit (masses of the up- and down-quark set to 0), the former comes from the observables that are not related to any singular behavior in the chiral limit. It may be that this agreement is incidental for the real-world QCD⁵. In the chiral limit the chiral crossover turns into an actual phase transition whose temperature $T_c^0 = 132^{+3}_{-6}$ MeV [16] is about 20 MeV below the chiral crossover temperature at the physical light quark masses. One may wonder whether or not the transition temperature defined from the static quark entropy T_S would decrease further when going towards the chiral limit, since, on the one hand, it has little obvious sensitivity to the chiral critical behavior, but, on the other hand, has been found to follow the chiral crossover temperature T_χ closely in terms of the quark mass dependence and the discretization effects. This open question however requires further theoretical investigation.

While the physics of the strongly interacting medium is nonperturbative in the vicinity of the transition, one expects that at high temperatures

⁴Although the pion mass in calculations of Ref. [56] is about 160 MeV, this deviation of about 20 MeV from the physical value plays no role within the statistical precision that can be reached on the thermodynamic observables.

⁵It is worth pointing out that ratios of properly renormalized Polyakov loop susceptibilities as suggested in Ref. [66], i.e.

$$R_T = \frac{\langle (\text{Im}L)^2 \rangle}{\langle |L|^2 \rangle - \langle L \rangle^2} \quad \text{due to} \quad \langle \text{Im}L \rangle = 0, \quad (32)$$

show smooth crossover behavior in full QCD [56]. Due to the mixing between different representations, these ratios can only be calculated with controlled uncertainties in the gradient flow renormalization at large enough flow time.

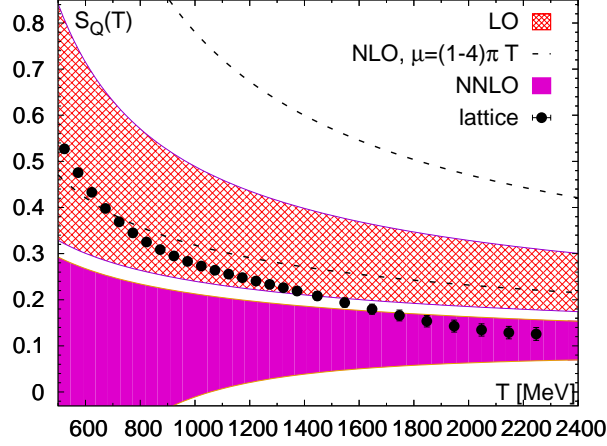


Figure 9: The static quark entropy S_q calculated on the lattice [67] and in a weak-coupling expansion [62] up to the next-to-next-to-leading order.

weak-coupling expansions may be reliable. The static quark free energy was recently calculated to next-to-next-to leading order (NNLO) in Ref. [62]. Direct comparison of free energies between the lattice and weak-coupling calculations is complicated because the calculations are performed in different renormalization schemes. They can be related by matching the temperature independent shift, e.g. $C(g_0^2)$ arising from renormalizing the static quark-antiquark energy, Eq. (27). However, the most straightforward way to perform the comparison is to consider the entropy where this shift is eliminated by the derivative with respect to temperature, Eq. (30). A challenge for lattice QCD calculations is however to reach very high temperatures, since this requires very fine lattices which are computationally expensive. Ref. [67] calculated S_q in the continuum limit up to temperature $T \sim 2.2$ GeV, shown in Fig. 9. The bands shown in the figure correspond to scale variation from $\mu = \pi T$ to $4\pi T$. At the highest temperature the lattice results and the NNLO results agree within the uncertainties. At temperatures below 1.5 GeV the lattice results are closer to the LO weak-coupling results. The rather poor convergence at the level of the NLO calculation and its apparent inconsistency with the lattice result can be understood from the observation that this is an expansion in g as required for the static Matsubara modes, which still misses the leading correction from an expansion in $\alpha_s = g^2/(4\pi)$ for the non-static Matsubara modes and the fermions.

3.2 Polyakov loop correlators

It was noted quite early in the considerations concerning thermal field theories that a single, isolated probe charge cannot be considered as a physically meaningful concept in a confining theory such as the non-Abelian $SU(N_c)$ pure gauge theory [68]. In other words the physical meaning of the Polyakov loop is not evident in the confined phase of Yang-Mills theory. In fact, only after combining the charges into even representations of the gauge group one may obtain states that are consistent with confinement. If the probe charges transform in the (anti-)fundamental representation like the static (anti-)quarks, then confinement demands that the most simple states are obtained by combining fields in the fundamental and anti-fundamental representations as $\mathbf{N}_c \times \overline{\mathbf{N}}_c = \mathbf{1} + (\mathbf{N}_c^2 - \mathbf{1})$ into states in either the trivial or the adjoint representations. Given the importance of $SU(3)$ as the gauge group of QCD, it is customary to speak of the *color singlet* and *color octet* independent of the actual N_c . Nevertheless, in the case of full QCD, a single, isolated static quark can be complemented in the confined phase by drawing an antiquark out of the vacuum and combining the two charges into an even representation.

Hence, correlation functions of paired static quarks and antiquarks were considered already in the earliest numerical studies [69, 54], i.e. in the simplest case the correlation function of a single static quark-antiquark pair in $SU(2)$ pure gauge theory. Representing each static quark by a Polyakov loop as in Eq. (20), one arrives at the Polyakov loop correlator, which is related to the difference in free energy between a system with and without the static quark-antiquark pair,

$$C_L^{\text{bare}}(T, r) = \frac{1}{N_c^2} \left\langle \sum_{\mathbf{x}} L(\mathbf{x}) L^\dagger(\mathbf{x} + \mathbf{r}) \right\rangle = \exp \left\{ -\frac{F_{q\bar{q}}^{\text{bare}}(T, r)}{T} \right\}. \quad (33)$$

For infinite separation C_L approaches the limit of $\langle L \rangle^2$, i.e. the static quark and antiquark decouple from each other, either due to the string breaking in the vacuum or due to the color screening in the high temperature phase. For this reason it is clear that the multiplicative renormalization factor of C_L^{bare} is just the square of the renormalization factor of $\langle L^{\text{bare}} \rangle$. Hence, the ratio $C_L / \langle L \rangle^2$ does not require renormalization and defines a subtracted free energy $F_{q\bar{q}}^{\text{sub}}(T, r) = F_{q\bar{q}}(T, r) - 2F_q(T)$ that vanishes for infinite separation. Results for the free energy $F_{q\bar{q}} \equiv F_{q\bar{q}}^{\text{ren}}$ with the renormalization scheme of Eq. (29) from a recent lattice calculation are shown in Fig. 10.

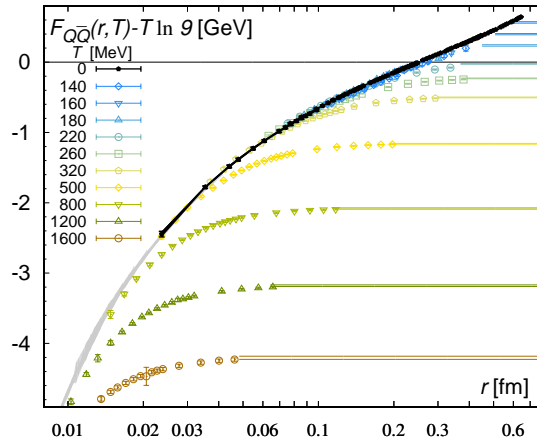


Figure 10: The continuum limit of the free energy $F_{q\bar{q}}$. The black band and symbols show the $T = 0$ QCD static energy E and the light gray band shows the singlet free energy F_S at high temperatures and very short distances, where finite temperature effects are smaller than the statistical errors. The subtraction of $T \ln 9$ is required for matching to the static energy at short distances due to the normalization convention used for $F_{q\bar{q}}$. The horizontal bands outline the $r \rightarrow \infty$ limit of $F_{q\bar{q}}$, i.e., $2F_q - T \ln 9$.

Before embarking on the further discussion of the properties of C_L in a non-Abelian gauge theory let us begin again with a brief look at the Abelian case, namely Quantum Electrodynamics. We consider the thermal correlation function of an electron-positron pair, which can only combine to a state in the trivial representation. Hence, the associated free energy and potential are both Coulomb-like. For infinite separation only two isolated charges are left due to the cluster decomposition, thus giving physical meaning to the notion of a single, isolated electron. Although the electric field between the two probe charges is screened inside of an electromagnetic plasma, there are unscreened contributions from the magnetic fields that contribute at higher loop orders and eventually lead to the takeover by a power-law falloff instead [14].

3.2.1 Singlet and octet free energies

Now let us juxtapose this to the case of the non-Abelian pure gauge theory. The $SU(N_c)$ Fierz identity permits rewriting Eq. (33) in terms of the sum of the color singlet and octet contributions

$$\begin{aligned} C_L(T, r) &= \exp \left\{ -\frac{F_{q\bar{q}}(T, r)}{T} \right\} \\ &= \frac{1}{N_c^2} \exp \left\{ -\frac{F_S(T, r)}{T} \right\} + \frac{N_c^2 - 1}{N_c^2} \exp \left\{ -\frac{F_O(T, r)}{T} \right\}. \end{aligned} \quad (34)$$

For infinite separation, both F_S and F_O share the same limit $2F_q$, since the two color charges are decoupled entirely. For this reason it is convenient to define subtracted singlet and octet free energies $F_{S,O}^{\text{sub}} \equiv F_{S,O} - 2F_q$ just as in the case for the Polyakov loop correlator.

A direct operator representation for the singlet or octet correlation functions or free energies is less straightforward than for the Polyakov loop correlator. The former two are mixed under renormalization, and only Eq. (34) or the difference

$$\exp \{-F_S/T\} - \exp \{-F_O/T\} = \frac{N_c^2}{N_c^2 - 1} (\exp \{-F_S/T\} - C_L) \quad (35)$$

are renormalized multiplicatively [71]. The difference in Eq. (35) is multiplicatively renormalizable at short distances, where the weak-coupling expansion is reliable.

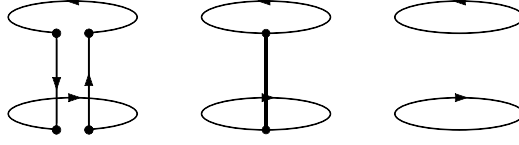


Figure 11: The thermal expectation values of cyclic Wilson loops (center) are obtained from the thermal expectation values of non-cyclic Wilson loops (left) by collapsing the two spatial Wilson lines to the same time Euclidean time across the periodic temporal boundary. Cyclic Wilson loops mix with the Polyakov loop correlator (right). From Ref. [70]).

The singlet or octet free energies require two color charges fixed with respect to each other at a finite distance between them. Any thermal correlation function $C_{S,O} \equiv \exp \{-F_{S,O}/T\}$ involving the hermitian conjugate for one of its two thermal Wilson lines defines a scheme for one among the free energies $F_{S,O}$. Its counterpart in the same scheme is automatically given by Eq. (35). We note that any choice of the scheme only reshuffles the individual contributions between the color singlet and octet configurations, but cannot modify the energies and hierarchies for any of these states.

Such a scheme may be realized in a manifestly gauge-invariant manner in the form of a single closed contour — a thermal or cyclic Wilson loop W_C , see Fig. 11 — which introduces multiple types of UV divergences that are not contained in the Polyakov loop. These divergences have to be suppressed through suitable link-smoothing techniques in lattice simulations (see Sec. 2 for details), i.e. the spatial Wilson lines \widetilde{W} making up the cyclic Wilson loops

$$W_C^{\text{bare}}(T, r) = \frac{1}{N_c} \left\langle \sum_{\mathbf{x}} \text{tr} \left[W(aN_\tau, \mathbf{x}; 0, \mathbf{x}) \widetilde{W}(aN_\tau, \mathbf{x} + \mathbf{r}; aN_\tau, \mathbf{x}) \right. \right. \\ \left. \left. W(0, \mathbf{x} + \mathbf{r}; aN_\tau, \mathbf{x} + \mathbf{r}) \widetilde{W}(0, \mathbf{x}; 0, \mathbf{x} + \mathbf{r}) \right] \right\rangle \quad (36)$$

have to be drawn from a modified thermal distribution.

Alternatively, these singlet and octet free energies may be realized in terms of thermal Wilson line correlation functions that are evaluated in a suitably fixed gauge such that the spatial Wilson lines can be omitted altogether,

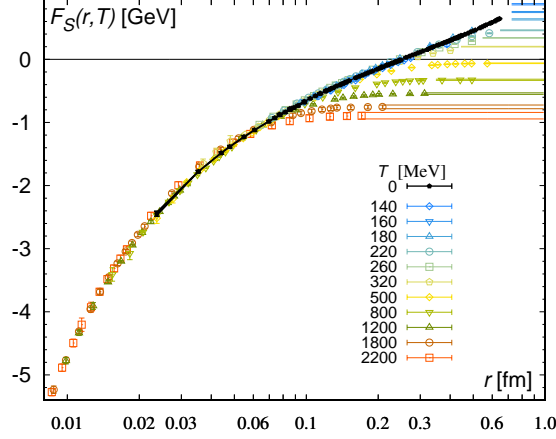


Figure 12: The continuum limit of the singlet free energy F_S defined with Wilson line correlators in Coulomb gauge. The black band and symbols show the $T = 0$ QCD static energy E . The horizontal bands outline the $r \rightarrow \infty$ limit of F_S , i.e., $2F_q$.

$$\begin{aligned}
C_S^{\text{bare}}(T, r) &= \frac{1}{N_c} \left\langle \sum_{\mathbf{x}} \text{tr} \left[W(aN_\tau, \mathbf{x}; 0, \mathbf{x}) W(0, \mathbf{x} + \mathbf{r}; aN_\tau, \mathbf{x} + \mathbf{r}) \right] \right\rangle^{\text{gf}} \\
&= \exp \{ -F_S^{\text{bare}}/T \}.
\end{aligned} \tag{37}$$

We have to stress the key difference between the thermal Wilson line correlation function and the Polyakov loop correlator. Namely, the thermal Wilson lines are traced individually in Eq. (33), while the trace of the product of two separated Wilson lines is taken in Eq. (37), which requires the fixing of a gauge. Coulomb gauge is particularly useful, since the free energies are finite in Coulomb gauge and the renormalization is particularly simple [71], see Fig. 12. While both alternative definitions of the singlet free energy exhibit different UV behavior [71], they are found to be consistent at intermediate and large distances within statistical errors in direct (2+1)-flavor QCD lattice simulations [72, 67] using staggered (HISQ) quarks, see Fig. 13.

Lastly, using the weak-coupling approach and pNRQCD it is possible to define gauge-invariant thermal singlet and octet correlators. Their expectation values are the exponentiated pNRQCD singlet or octet free energies f_s and f_o [73], whose linear combination formally recombines to C_L as in

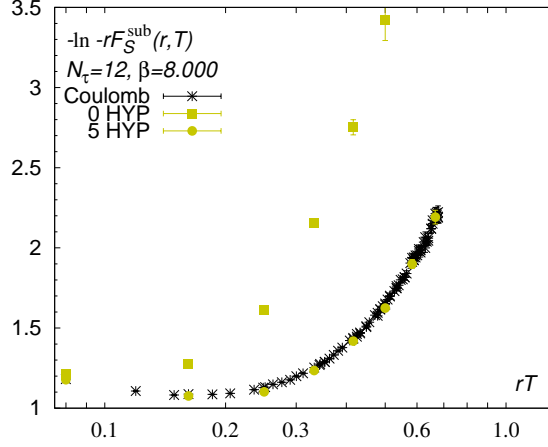


Figure 13: The logarithm of the singlet screening function $-rF_S^{\text{sub}}$ defined in terms of the Coulomb gauge Wilson line correlator or the gauge-invariant cyclic Wilson loop with appropriate amount of spatial hypercubic (HYP) link smearing show the quantitatively very similar screening behavior [67]. At shorter distances small differences can be seen.

Eq. (34). Key relations between f_s and f_o that have been tested are found to be reproduced quite well by F_S and F_O defined in terms of the Coulomb gauge Wilson line correlation function on the lattice [67].

3.2.2 Vacuum-like regime and vacuum physics

The singlet or octet free energies F_S or F_O are given to leading order g^2 by the corresponding zero temperature Coulomb-like potentials $V_{s,o} = c_{s,o} \alpha_s/r$ with $c_s = -C_F$ or $c_o = +C_F/(N_c^2 - 1)$. At very short distances $r \ll \alpha_s/T$, the running of the coupling $\alpha_s(1/r)$ is controlled by the inverse distance as in the vacuum. The two Coulomb-like potentials with opposite signs become large, and thus the repulsive octet contribution can be neglected. In other words, at such short distances, the free energy behaves in the non-Abelian case up to a temperature dependent shift $+T \ln(N_c^2)$ due to the color factors and the different running coupling (i.e. different beta function) just as in the Abelian case, namely $F_{q\bar{q}} = F_S + T \ln(N_c^2) = V_s + T \ln(N_c^2)$ at leading order. We recall that the singlet potential V_s and the static energy E coincide at leading order. The former relation (between $F_{q\bar{q}}$ and F_S or E) has been observed for nonperturbative lattice calculations in (2+1)-flavor

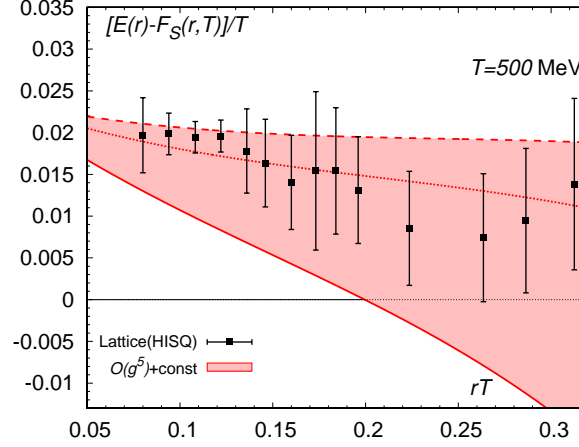


Figure 14: Lattice and weak-coupling results for $E - F_S$ [67]. The weak-coupling results are shifted by a small constant to match them to the lattice results at the shortest distance to account for a matching constant of order g^6 . The dotted line corresponds to the renormalization scale $\mu = 2\pi T$, while the band corresponds to its variation from πT (solid) to $4\pi T$ (dashed).

QCD using staggered (HISQ) quarks at shorter and shorter distances up to temperatures $T \lesssim 0.5 \text{ GeV}$ [67], while the latter relation (between F_S and E) even holds at larger distances $r \lesssim 0.3/T$ for much higher temperatures $T \lesssim 2 \text{ GeV}$ [31]. The corresponding thermal corrections are small due to a partial cancellation between the contributions from non-static gluons or sea quarks, and from the static gluons, see Fig. 14. In particular, as the contributions from the former are restricted to even powers of the gauge coupling g starting at g^4 , while the latter are restricted to odd powers of the gauge coupling g starting at g^5 , it is clear that this partial cancellation is effective only in a limited temperature window which happens to coincide with phenomenologically interesting temperatures.

In particular, the Polyakov loop correlator at distances up to $r \lesssim 0.3/T$ is determined to good accuracy in terms of the singlet and octet zero temperature potentials and the adjoint Polyakov loop as predicted in pNRQCD [73], see Fig. 15.

For all larger distances we have to distinguish between the vacuum and the thermal medium at high temperatures. Let us first take a closer look at C_L in the vacuum, i.e. in the confining phase. At larger distances $r \sim$

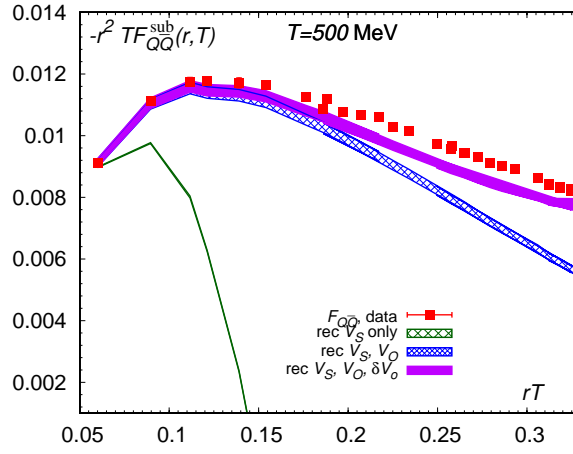


Figure 15: The subtracted free energy $F_{q\bar{q}}^{\text{sub}}$ multiplied by $-r^2 T$ calculated on an $N_\tau = 16$ lattice (squares, using 1 step of 4D hypercubic (HYP) smearing [40] for $r \geq \sqrt{6}/a \approx 0.15/T$) and compared to the reconstruction based on pNRQCD (bands) at $T = 500$ MeV (the fully reconstructed result is in magenta, while the blue band ignores the Casimir scaling violating contributions to the octet potential and the green one ignores the octet contribution).

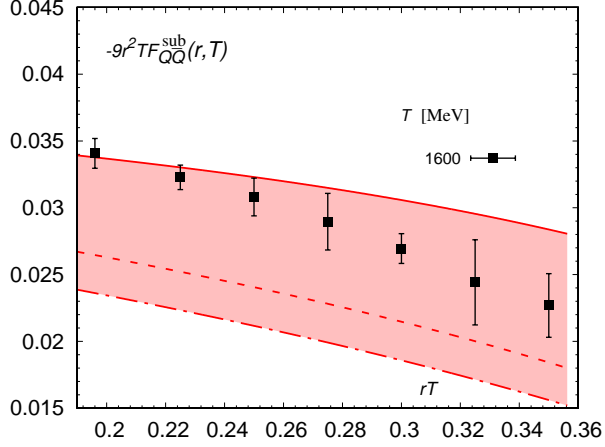


Figure 16: The subtracted free energy $F_{q\bar{q}}^{\text{sub}}$ multiplied by $-9r^2T$ evaluated for $T = 1600 \text{ MeV}$ and compared with the N^3LO weak-coupling expression (lines) [67]. The upper line corresponds to $\mu = \pi T$, the middle one to $\mu = 2\pi T$, and the lower line corresponds to $\mu = 4\pi T$.

$1/\Lambda_{\overline{\text{MS}}}$, the Coulomb-like interaction is not dominant anymore. Instead, the singlet and octet free energies are dictated to a large extent by the energies of the respective lowest states, i.e. the QCD string or the excited QCD string, which both behave as $\sim \sigma r \sim \Lambda_{\overline{\text{MS}}}$. As a consequence, the free energy behaves in pure $\text{SU}(N_c)$ gauge theory up to details of the normalization similar to the quark-antiquark static energy. This can be clearly resolved only at the shortest distances that are accessible in lattice gauge theory, see Fig. 10 for the case of full (2+1)-flavor QCD. In full QCD, the thermal Wilson lines can decouple via string breaking, since each thermal Wilson line – being a closed contour – can combine with a sea (anti-)quark into the trivial representation of the gauge group. For this reason, screening due to the string-breaking mechanism in the vacuum modifies the (singlet) free energy already in the vacuum phase of QCD. However, due to the severe signal-to-noise problem, the free energies cannot be studied in the string-breaking regime at low temperatures without extensive application of noise-reduction techniques, see Ref. [74] for preliminary work in this direction.

3.2.3 Thermal dissociation and the free energy

In the high temperature phase without confinement the free energy behaves rather differently. Let us consider distances $r \ll 1/T$, for which the running of the coupling $\alpha_s(T)$ is controlled by the temperature T , which is the lowest scale. If — on top of that — the hierarchy $\alpha_s/T \ll r \ll 1/T$ is satisfied, then thermal gluons are sufficiently energetic to overcome the spectral gap between the singlet and octet configurations and the singlet states begin to dissociate and recombine again. Whereas the dissociation and recombination are dynamical processes that cannot be resolved directly in an imaginary time approach, the thermally equilibrated distribution that is their consequence is resolved by the Polyakov loop correlator! Due to $\alpha_s/(rT) \ll 1$, the exponential functions in Eq. (34) can be expanded in the gauge coupling, and the color factors lead to a cancellation of the leading Coulomb-like terms between the singlet and octet contributions. In this hierarchy the subtracted free energy is given at leading order as

$$F_{q\bar{q}}^{\text{sub}}(T, r) = -\frac{N_c^2 - 1}{8N_c^2} \left(\frac{\alpha_s}{r}\right)^2, \quad (38)$$

with a non-Coulombic $(\alpha_s/r)^2$ behavior. This behavior clearly indicates that the leading interaction between the two Polyakov loops at such distances is the emission of two *electric* A_0 *gluons*, which have to be in a color singlet configuration. The Polyakov loop correlator has been calculated in the weak-coupling approach up to order g^7 in the small r expansion [71] and found to be compatible with the nonperturbative lattice calculation for (2+1)-flavor QCD using staggered (HISQ) quarks for $0.2/T \lesssim r \lesssim 0.3/T$ at temperatures $T \gtrsim 1.5 \text{ GeV}$ [67], see Fig. 16.

3.2.4 Chromoelectric screening

At larger distances the quark-antiquark system enters the scale hierarchy $r \sim 1/m_D$, which is associated with the electric screening that is controlled by the mass parameter of the adjoint scalar field associated with *electric* A_0 *gluons* in EQCD, which is often called the (perturbative) Debye mass. It is given to leading or next-to-leading order [23] as

$$m_D^2|_{\text{LO}}(\nu) = \frac{2N_c + N_f}{6} g^2(\nu) T^2, \quad (39)$$

$$m_D^2|_{\text{NLO}}(\nu) = m_D^2|_{\text{LO}}(\nu) \times \frac{\alpha_s(\nu)}{4\pi} \left[2\beta_0 \left(\gamma_E + \ln \frac{\nu}{4\pi T} \right) + \frac{5N_c}{3} + \frac{2N_f}{3}(1 - 4 \ln 2) \right] - C_F N_f \alpha_s^2(\nu) T^2, \quad (40)$$

where typical values of the scale ν are of the order of $2\pi T$, i.e. of the order of the lowest nonstatic Matsubara mode. The next-to-next-to-leading order contribution to the Debye mass has been calculated so far only in pure Yang-Mills theory [75]. The N²LO Debye mass lies between the central values of NLO and LO, but has a much smaller scale dependence. Since the effect of the N_f quarks on the Debye mass is rather mild $\sim 20\%$ to 30% , similar results are to be expected for the full QCD calculation. The regime of electric screening is mixed up with the previous regime of thermal dissociation, since the hierarchies are not well separated (separate regimes would require $\alpha_s(\nu)m_D(\nu) \gtrsim T$, i.e. $g(\nu) \gtrsim 2.5$). To leading order the free energy and singlet free energy are given in the regime of electric screening by

$$F_{q\bar{q}}^{\text{sub}}|_{\text{LO}}(T, r, \nu) = -\frac{N_c^2 - 1}{8N_c^2} \left(\frac{\alpha_s(\nu) e^{-m_D(\nu)r}}{r} \right)^2, \quad (41)$$

$$F_S^{\text{sub}}|_{\text{LO}}(T, r, \nu) = -C_F \frac{\alpha_s(\nu) e^{-m_D(\nu)r}}{r}. \quad (42)$$

After including the full next-to-leading order corrections [71] quantitative consistency with (2+1)-flavor QCD lattice simulations using staggered (HISQ) quarks could be shown for $T > 300$ MeV and $0.3/T \lesssim r \lesssim 0.6/T$ [67], see Fig. 17. In particular, the interaction between Polyakov loops and adjoint Polyakov loops is predominantly mediated in the electric screening regime by the emission of two *electric* A_0 *gluons* in a color singlet configuration with one unit of the perturbative Debye mass each. On the contrary, the interaction between thermal Wilson lines and adjoint thermal Wilson lines is predominantly mediated in the electric screening regime by the exchange of one *electric* A_0 *gluon* with one unit of charge in the adjoint representation and one unit of the perturbative Debye mass.

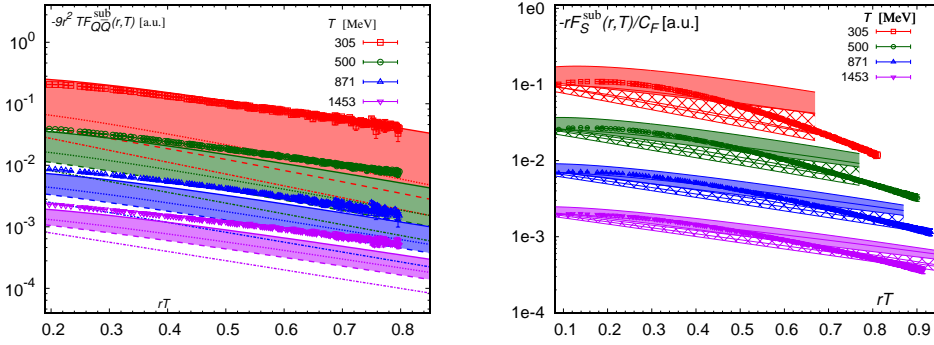


Figure 17: The screening functions of the subtracted free energy $F_{q\bar{q}}^{\text{sub}}$ or singlet free energy F_S^{sub} , i.e. $F_{q\bar{q}}^{\text{sub}}$ is multiplied by $-9r^2T$ or F_S^{sub} is multiplied by $-r/C_F$, see [67] for details of the calculation. The bands represent the NLO (solid) results, where the scale has been varied as $\mu = \pi T$, $2\pi T$, and $4\pi T$ (solid, dotted, and dashed lines). Data are calculated on an $N_\tau = 16$ lattice using 1 step of 4D hypercubic (HYP) smearing [40] for $r \geq \sqrt{6}/a \approx 0.15/T$. (Left) The separate dash-dotted lines correspond to the LO result evaluated at $\mu = 4\pi T$. (Right) The hashed bands correspond to the LO result evaluated at $\mu = \pi T$, $2\pi T$, and $4\pi T$ (solid, dotted, and dashed lines).

3.2.5 Asymptotic screening

The color screening at asymptotically large distances cannot be understood in terms of the perturbative Debye mass defined in terms of the pole position of the *electric* A_0 *gluon* propagator in EQCD. This is most easily understood in the dimensionally-reduced effective field theory (*magnetostatic QCD*) picture, where the three-dimensional $SU(N_c)$ pure gauge theory of the *magnetic gluons* gives rise to a confinement radius $r \sim 1/(g^2 T)$. At distances of the order of this magnetic confinement radius, the nonperturbative interaction between the *electric* A_0 *gluons* and the magnetic gluons becomes too strong. The *electric* A_0 *gluons* have to be dressed with compensating charges in order to obtain bound states that transform in the trivial representation of $SU(N_c)$ with binding energies $\sim g^2 T$. Thus, the *magnetic* confinement scale acts as the infrared cutoff for the *electric* A_0 *gluons*. It is not evident whether a gauge-dependent *electric* A_0 *gluon* propagator could even be employed for defining an order-by-order (odd powers of g) gauge-independent pole mass in a nonperturbative framework, or whether the notion of a single *electric* A_0 *gluon* at such scales is physically meaningful at all. On this basis the perturbative definition of the Debye mass in Eq. (40) is inadequate for describing the asymptotic screening.

Instead, the interactions between the *electric* A_0 *gluons* and the fluctuating *magnetic* fields entail the additive, nonperturbative renormalization of the leading-order Debye mass $\sim gT$ at the *magnetic* confinement scale $\sim g^2 T$, and yields the expression for the nonperturbative Debye mass

$$m_{D|\text{NP}}(\nu) = m_{D|\text{LO}}(\nu) + \frac{N_c}{4\pi} g^2(\nu) T \ln \left(\frac{m_{D|\text{LO}}(\nu)}{g^2(\nu) T} \right) + c_{N_c} g^2(\nu) T + \mathcal{O}(g^3 T). \quad (43)$$

Here, c_{N_c} is a constant that has to be determined numerically using lattice simulations⁶, while the leading logarithmic contribution can be determined in

⁶ c_{N_c} has been determined from the exponential falloff $\sim \exp[-m_W r]$ of an adjoint Wilson line in the lattice regularization (Wilson plaquette action) between a suitable discretization of the magnetic field strength tensor [76]. Matching between the lattice regularization and the continuum result in dimensional regularization yields at one loop order [14]

$$c_{N_c} = \frac{m_W}{g^2 T} + \frac{N_c}{4\pi} (\ln(g^2) - 1). \quad (44)$$

Specifically, for $SU(2)$ or $SU(3)$ the coefficients $c_2 = 1.14(4)$, or $c_3 = 1.65(6)$ were calcu-

one-loop resummed perturbation theory [77, 14]. When counting the second term into the *perturbative contribution* (i.e. that is calculable with perturbative methods), then the *nonperturbative contribution* due to c_{N_c} (only the third term) significantly exceeds the *perturbative contribution* (the first two terms) for phenomenologically interesting temperatures and remains quantitatively important even at asymptotically high temperatures.

In principle it is possible to fix an appropriate gauge and calculate the longitudinal and transverse components of the gluon propagator or form factor nonperturbatively. In the spatial gluon correlation functions access to the magnetic gluons is permitted by the transverse modes of the propagator, while access to the *electric A_0 gluons* is permitted by its longitudinal modes. The first, pioneering studies were completed for the gauge group SU(2) [78, 79, 80, 81, 82]. The functional form of the nonperturbative inverse magnetic or electric screening lengths and their ratio, i.e. $1/\lambda_M \sim g^2 T$ or $1/\lambda_E \sim gT$ and $\lambda_E/\lambda_M \sim g(T)$ respectively as predicted in the weak-coupling picture, can be verified already at temperatures as low as $T \sim 2T_c$ in SU(2) [78, 79, 80]. The *electric A_0 gluon* screening length λ_E is indeed still dominated by large nonperturbative effects at temperatures as high as $T \sim 10^4 T_c$, and the singlet free energy in Landau gauge, i.e. Eq. (37), in the SU(2) (pure gauge) Yang-Mills theory has the same asymptotic screening length, λ_E [79]. Further lattice studies comparing the four-dimensional theory and the dimensionally reduced effective field theory (EQCD) indicate that the individual gluon propagators are consistent between both formulations [82]. The propagator of *electric A_0 gluons* exhibits a strong gauge dependence in its UV part, but its decay is consistent with a gauge- and volume-independent pole mass. This is not true at all for the propagator of magnetic gluons, which is infrared suppressed and strongly volume dependent, thus excluding a pole mass as a possible cause of its exponential decay. For large momenta the magnetic gluon propagator becomes negative in Landau gauge, while being bounded in absolute value by its universally positive counterpart in maximal Abelian gauge [81]. Contrary to naive expectations from the weak-coupling picture it is the symmetric, namely, confining phase of EQCD that corresponds to the deconfined phase of the four-dimensional Yang-Mills theory [80]. There is very little sensitivity of the purely magnetic glue-balls on the adjoint scalar field representing the *electric A_0 gluons*, namely, EQCD and three-dimensional Yang-Mills theory have the same glue-

lated using three-dimensional SU(N_c) + adjoint Higgs theory [76].

ball spectrum. While the bound state masses of EQCD are compatible with a constituent model picture, there is no apparent connection between the bound states of the *electric* A_0 *gluons* and the inverse screening length $1/\lambda_E$ of the electric gluon propagator. The qualitative features carry over from SU(2) to SU(3) [83]. Whereas the transverse form factor related to the magnetic gluons remains almost featureless through the phase transition, the longitudinal form factor exhibits the features of an order parameter (using Landau gauge) in SU(3) Yang-Mills theory [84]. In particular, the overlap factor between the *electric* A_0 *gluon* state and a massive quasi-particle state as well as the infrared mass scale associated with such a state expose unambiguous critical behavior. Both gluon screening lengths in the confined and deconfined phases are consistent with a running gluon mass picture that is natural in the Dyson-Schwinger equation framework. For temperatures above $T \gtrsim 400$ MeV the *electric* A_0 *gluon* screening length is largely consistent with the weak-coupling expectation, if a temperature independent nonperturbative contribution is permitted.

The strongest correlations in the high temperature phase are not mediated by the exchange of individual gluons at asymptotic distances, but by the exchange of the lightest bound states available in each channel of EQCD, i.e. the three-dimensional SU(N_c) pure gauge theory coupled to the adjoint scalar representing the *electric* A_0 *gluons*. This is similar to the nuclear force in the vacuum, which is mediated at the largest distances by the exchange of the lightest hadrons, i.e. the pions. In the case of thermal QCD, this role is fulfilled by either the purely *magnetic glue-balls* with masses at the confinement scale $\sim g^2 T$, or by the bound states of *electric* A_0 *gluons* (with individual masses $\sim m_D$ and the binding energy at the confinement scale $\sim g^2 T$). These states are classified by their quantum numbers $J_{\mathcal{R}}^{PC}$, where J is spin, P is parity, C is charge conjugation, and \mathcal{R} is Euclidean time reflection. In particular, the even or odd sectors $\mathcal{R} = \pm 1$ under Euclidean time reflection have been referred to as *magnetic* or *electric* in an unfortunately misleading convention. The *magnetic sector* ($\mathcal{R} = +1$) includes any bound states with even numbers of *electric* A_0 *gluons* (including the purely *magnetic glue-balls*), while the *electric sector* ($\mathcal{R} = -1$) includes any bound states with odd numbers of *electric* A_0 *gluons*.

For phenomenologically interesting temperatures, the naïve hierarchy is inverted in all channels (at least for spin $J = 0$ or $J = 1$), i.e. bound states with $2n$ *electric* A_0 *gluons* are found to be systematically lighter than glue-

balls made from $2n$ *magnetic gluons* (irrespective of the quantum numbers $J_{\mathcal{R}}^{PC}$, or the numbers of the dynamical quark flavors) [26], see Fig. 3. In general, the mixing between the bound states with different *electric A_0 gluon* content is rather weak. This inverted hierarchy is not particularly surprising, since the QCD coupling $g(\nu)$ with $\nu \sim 2\pi T$ is typically larger than 1 for such temperatures. In the following we refer to the lightest bound state with given $J_{\mathcal{R}}^{PC}$ simply as $m(J_{\mathcal{R}}^{PC})$ irrespective of the hierarchy. It has been suggested to define the inverse nonperturbative Debye mass $m_D|_{\text{NP}}$ as the largest correlation length of any correlation function constructed from local, gauge-invariant operators that are odd under Euclidean time reflection [14], i.e. to define the Debye mass as $m_D|_{\text{NP}} \equiv \min(m(J_{\mathcal{R}}^{PC}))$. This resolves the issues associated with a perturbative definition of the Debye mass. The lightest bound state in the $\mathcal{R} = -1$ sector has been obtained in the dimensionally-reduced QCD for operators involving each one *electric A_0 gluon* and one *magnetic field strength* [26]⁷, the minimal field content to achieve gauge invariance in the $\mathcal{R} = -1$ sector.

The asymptotic screening masses of the Polyakov loop correlators are given in terms of the lightest bound state masses with which they mix. The Polyakov loop may be split into its real or imaginary parts $L(\vec{x}) = \text{Re } L(\vec{x}) + i \text{Im } L(\vec{x})$, which transform as even or odd under Euclidean time reflection, i.e. they correspond to quantum numbers $J_{\mathcal{R}}^{PC} = 0_+^{++}$ or $J_{\mathcal{R}}^{PC} = 0_-^{+-}$. Thus, even if the correlation function of the imaginary part is separated, this channel is not suitable for studying the nonperturbative Debye mass, because the quantum numbers of $\text{Im } L(\vec{x})$ are 0_-^{+-} instead of 0_-^{++} for the lowest state in the $\mathcal{R} = -1$ sector. On the one hand, the screening mass $m(0_+^{++})$ of the correlation function of the real part is either the mass of the lightest scalar bound state consisting of two *electric A_0 gluons*, $\sim 2m_D + E(2A_0)$ in the inverted naïve hierarchy at phenomenologically interesting temperatures (such that $g \gtrsim 1$), or the mass of the lightest magnetic glue-ball $\sim g^2 T$ in the naïve hierarchy at asymptotically high temperatures (such that $g \ll 1$). On the other hand, the screening mass $m(0_-^{+-})$ of the correlation function of the imaginary part is the mass of the lightest bound state consisting of three *electric A_0 gluons*, $\sim 3m_D + E(3A_0)$, or the mass of the bound state of one *electric A_0 gluon* and two *magnetic gluons*. Here, the binding energies

⁷In the four-dimensional QCD language this bound state has the quantum numbers $J_{\mathcal{R}}^{PC} = 0_-^{++}$. The quantum numbers $J_{\mathcal{R}}^{PC} = 0_-^{+-}$ given for this state in the dimensionally-reduced QCD make use of a redefined parity that reflects only a single spatial direction [26].

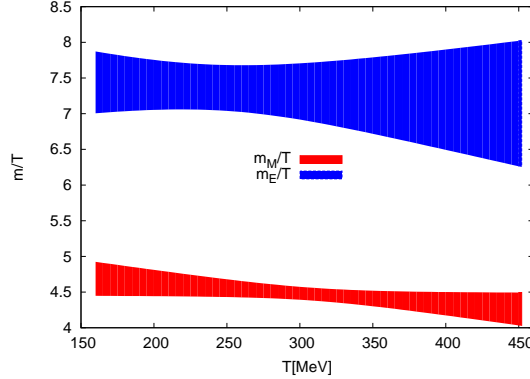


Figure 18: The continuum limit of the screening masses associated with the correlation function of the real (red) or imaginary parts (blue) of the Polyakov loops [85].

of these states $E(2A_0)$ and $E(3A_0)$ are parametrically of order $\sim g^2T$ (the confinement scale), whereas the dominant contribution to m_D is parametrically of order $\sim gT$. As the mass of the lightest ($\mathcal{R} = +1$) state is typically much smaller than the nonperturbative Debye mass or the mass of the lightest ($\mathcal{R} = -1$) state, i.e. $m(0_+^{++}) < m(0_-^{++}) \leq m(0_-^{+-})$, the free energy $F_{q\bar{q}}^{\text{sub}}$ obtained from the (full) Polyakov loop correlation function in the asymptotic screening regime is dominated by the contribution from the real parts of the Polyakov loops.

For temperatures up to $T \lesssim 3T_c$ the screening masses of the correlation functions of the real and imaginary parts of the Polyakov loop have been determined in (2+1)-flavor QCD lattice simulations at the physical point [85] using the stout-smearred staggered fermions and link smoothing techniques (4D hypercubic (HYP) smearing [40]). Previous results from 2-flavor QCD lattice simulations using improved Wilson fermions and two unphysically large values of the sea quark mass [86] are quantitatively similar, and verified, in particular, the consistency of the screening masses associated with the full Polyakov loop correlator and the real part correlator. The screening masses in the full QCD lattice calculation were found to be in fair agreement with the results obtained in the dimensionally-reduced QCD lattice simulations [26]. For $T \approx 2T_c$ the ratio between the corresponding masses is re-

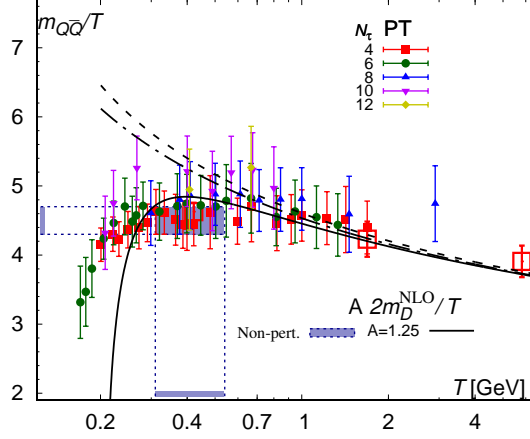


Figure 19: The screening mass associated with the free energy $F_{q\bar{q}}$ [67].

ported to be $m(0_{-}^{+-})/m(0_{+}^{++}) = 1.76(17)$ in the dimensionally-reduced QCD and $m(0_{-}^{+-})/m(0_{+}^{++}) = 1.63(8)$ in the QCD calculation [85]. The screening masses show a slightly decreasing trend for higher temperatures. (2+1)-flavor QCD lattice simulations using staggered (HISQ) quarks have shown that the asymptotic screening mass of $F_{q\bar{q}}^{\text{sub}}$ is only slightly larger than the corresponding expectation in a constituent model of two *electric* A_0 *gluons*, $2m_D|_{\text{NLO}}$ [67], suggesting that the binding energy $E(2A_0) \sim g^2T$ leads to a quantitative compensation of the nonperturbative dressing $\sim g^2T$ of the two *electric* A_0 *gluons* to a large extent.

The case of the color singlet correlation function in the asymptotic screening regime is still more intricate. First of all, the interaction that is dominant in the electric screening regime is mediated by the emission of one *electric* A_0 *gluon*, which carries one unit of charge in the adjoint representation. Hence, due to its charge this exchanged *electric* A_0 *gluon* cannot mix on its own with the bound states of the three-dimensional $\text{SU}(N_c)$ pure gauge theory, which have to transform in the trivial representation for any confining gauge theory. As a consequence, this mode of emission can only accumulate the nonperturbative dressing $\sim g^2T$, and thus one would naively suppose that it should be screened with the nonperturbative Debye mass $m_D|_{\text{NP}}$, or with some operator-dependent screening mass that receives contributions both $\sim gT$ and $\sim g^2T$ (due the definition of the nonperturbative Debye mass, operator-dependent screening masses for $R = -1$ cannot be smaller

than $m_D|_{\text{NP}}$). Whether or not this mode could propagate at asymptotically large distances may also depend on the details of the operators, i.e. the gauge-fixed thermal Wilson line correlator or the path-dependent spatially-smeared cyclic Wilson loop. In the former case, the Coulomb gauge gives rise to a *dimension-two magnetic gluon condensate* $\langle \mathbf{A}^2 \rangle$. The *electric* A_0 *gluon* may scatter on the *magnetic gluons* of this condensate and acquire contributions from the confinement scale $\sim g^2 T$ of the three-dimensional $\text{SU}(N_c)$ pure gauge theory. In the latter case, the spatial Wilson lines involve spatially-extended operators, by which the emitted *electric* A_0 *gluon* may couple to *magnetic gluons* in a gauge-invariant multi-particle state of the three-dimensional $\text{SU}(N_c)$ pure gauge theory. For either correlation function, such states must have the quantum numbers $\mathcal{R} = -1$ and $P = +1$. Calling the energy of the lowest accessible state $m(X_-^+)$, we note that it cannot have a lower energy than the lowest bound state with the same quantum numbers, namely $m(X_-^+) \gtrsim m_D|_{\text{NP}}$. Arguing from the rationale of the quantitative similarity between the cyclic Wilson loops with spatial smearing and the Wilson line correlators in Coulomb gauge in the asymptotic screening regime, see Fig. 13, it appears as if these two operator-dependent singlet correlation functions may have access to the same set of screening lengths, which would suggest that the state X_-^+ could be in fact operator independent.

Yet this is not the whole story. The nonperturbative Debye mass is larger than $m(0_+^{++})$, i.e. the mass of the lightest bound state with $\mathcal{R} = +1$ (whether this is a bound state of two *electric* A_0 *gluons* or a *magnetic glue-ball* is irrelevant in this regard). Just like the Polyakov loops, the untraced Wilson line operators in the singlet correlators making up Eqs. (36) or (37) have separable real or imaginary parts, too, that each have well-defined behavior under Euclidean time reflection. In fact, the thermal Wilson lines also couple directly to two or three *electric* A_0 *gluons* through their real or imaginary parts, respectively, although these couplings are formally suppressed by two or four powers of the coupling g . On the one hand, the singlet correlation function of the real parts of the thermal Wilson lines receives contributions from the $\mathcal{R} = +1$ bound states of the three-dimensional $\text{SU}(N_c)$ pure gauge theory. The contribution from the emission of one *electric* A_0 *gluon* is screened in the asymptotic regime with $m(X_-^+) \gtrsim m_D|_{\text{NP}}$, while the contribution from the emission of two *electric* A_0 *gluons* in a color singlet configuration mixes with the lightest bound state of the three-dimensional $\text{SU}(N_c)$ pure gauge theory with mass $m(0_+^{++})$ satisfying $m(0_+^{++}) < m_D|_{\text{NP}}$ for all thermal hier-

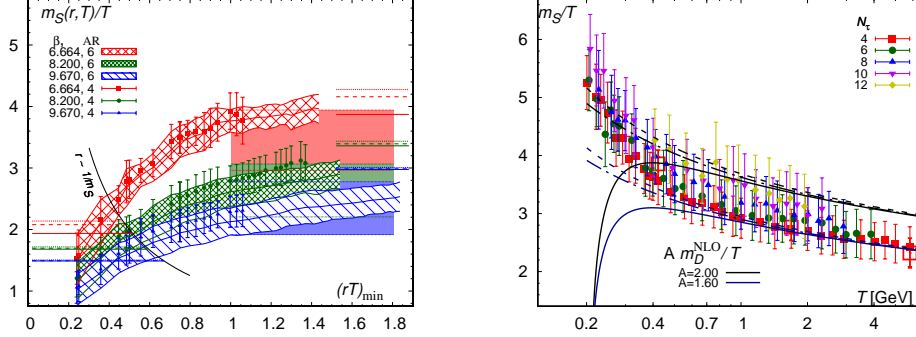


Figure 20: The screening mass associated with the singlet free energy F_S [67]. (Left) The local screening mass associated with the singlet free energy defined in Eq. (37) increases at larger distances. The horizontal lines to the left indicate the perturbative Debye mass $m_D|_{\text{NLO}}$, and the horizontal lines to the right indicate twice the perturbative Debye mass, $2m_D|_{\text{NLO}}$. Available results are obtained with $N_\tau = 4$ and may be affected by substantial discretization effects. (Right) The screening mass associated with the singlet free energy has a similar temperature dependence than the perturbative Debye mass $m_D|_{\text{NLO}}$.

archies. Hence, the latter contribution with screening length $1/m(0^{++})$ has to dominate the singlet correlation function of the real parts eventually. On the other hand, the singlet correlation function of the imaginary parts of the thermal Wilson lines, however, mixes the contribution from the emission of one *electric* A_0 *gluon* with the contribution from the emission of three *electric* A_0 *gluons*. Although the latter mixes with the 0^{+-} bound states of the three-dimensional $\text{SU}(N_c)$ pure gauge theory, all of these masses are larger than the nonperturbative Debye mass $m_D|_{\text{NP}}$. Hence, in the end, either the potentially operator-dependent screening mass $m(X^\pm) \gtrsim m_D|_{\text{NP}}$ or the mass of the lightest scalar bound state consisting of three *electric* A_0 *gluons* in the three-dimensional $\text{SU}(N_c)$ pure gauge theory, $\sim 3m_D + E(3A_0)$, may be the smallest inverse correlation length for the correlation function of the imaginary parts of the Wilson lines. Since the latter exchange mode is suppressed by four powers of g , this channel may actually be well-suited to a determination of the operator-dependent screening mass $m(X^\pm) \gtrsim m_D|_{\text{NP}}$ even with a possibly small mass difference between the X^\pm and 0^{+-} screening masses.

(2+1)-flavor QCD lattice simulations using staggered (HISQ) quarks show

that the local screening mass associated with F_S^{sub} defined in terms of Wilson line correlation functions in Coulomb gauge, see Eq. (37), is only slightly larger than $m_D|_{\text{NLO}}$ for $r \sim 1/m_D|_{\text{NLO}}$ [67]. This screening mass becomes systematically larger with increasing distances, and seems to saturate quite close to $2m_D|_{\text{NLO}}$ for $r \gg 1/T$, see Fig. 20 as in the case of the correlator of the real parts of two Polyakov loops.

This screening mass also exhibits a similar temperature dependence as $m_D|_{\text{NLO}}$ for temperatures $T > 300 \text{ MeV}$. The unambiguous, quantitative analysis of the asymptotic screening of the singlet correlation function is still lacking and requires the use of link-smoothing techniques to overcome the severe signal-to-noise problem of static quark correlation functions, see e.g. Ref. [74] for preliminary results of ongoing work along these lines.

At temperatures that correspond to the vacuum phase, the asymptotic screening mass $m(0_{++}^+)$ due to the lowest $J_R^{PC} = 0_{++}^+$ bound state of the dimensionally-reduced QCD smoothly connects to the screening mass due to the string breaking in the vacuum phase of QCD, i.e. the energy difference between the static quark-antiquark energy and the mass of two static-light mesons.

3.2.6 Screening in different representations

In the deconfined phase of $\text{SU}(N_c)$ gauge theory (with or without quarks) the notion of diquarks, which transform non-trivially under the gauge group, appears to be quite natural. In the vacuum, heavy-heavy diquarks seem to play an important role for the formation of heavy-light tetraquark systems, see e.g. Ref. [87]. In particular, it must be expected that – if diquarks exist at all as individual objects – heavy-heavy diquarks are still quite strongly bound at temperatures slightly above T_c . In the following we apply again the terminology for $N_c = 3$, i.e. use anti-triplet ($\bar{\mathbf{3}}$) for the *anti-fundamental* representation and sextet ($\mathbf{6}$) for the $(\mathbf{N}_c^2 - \mathbf{N}_c)$ -dimensional representation arising from $\mathbf{N}_c \times \mathbf{N}_c = \bar{\mathbf{N}}_c + (\mathbf{N}_c^2 - \mathbf{N}_c)$. The most simple objects related to the screening of the static diquarks are the Polyakov loops in other representations, which have been studied in the $\text{SU}(3)$ pure gauge theory [52] and in the (2+1)-flavor QCD [53, 56]. Key results for single Polyakov loops in different representations are briefly discussed in Sec. 3.1. Correlation functions of Polyakov loops and thermal Wilson lines in suitable representations correspond to spatially extended diquarks.

Thus, correlation functions of diquarks transforming in the anti-triplet

or sextet representations can be studied with the lattice approach, e.g. after fixing Coulomb gauge through

$$C_3(T, r) = \frac{1}{2N_c} \left\{ \left\langle \sum_{\mathbf{x}} L(\mathbf{x}) L(\mathbf{x} + \mathbf{r}) \right\rangle - \left\langle \sum_{\mathbf{x}} \text{tr} W(aN_\tau, \mathbf{x}; 0\mathbf{x}) W(aN_\tau, \mathbf{x} + \mathbf{r}; 0\mathbf{x} + \mathbf{r}) \right\rangle^{\text{gf}} \right\}, \quad (45)$$

$$C_6(T, r) = \frac{1}{4N_c} \left\{ \left\langle \sum_{\mathbf{x}} L(\mathbf{x}) L(\mathbf{x} + \mathbf{r}) \right\rangle + \left\langle \sum_{\mathbf{x}} \text{tr} W(aN_\tau, \mathbf{x}; 0\mathbf{x}) W(aN_\tau, \mathbf{x} + \mathbf{r}; 0\mathbf{x} + \mathbf{r}) \right\rangle^{\text{gf}} \right\}. \quad (46)$$

In particular, $\text{SU}(N_c)$ pure gauge theory, or 2-, or (2+1)-flavor QCD lattice studies using improved Wilson fermions [88, 89, 90] found that the different channels with two thermal Wilson lines in the singlet, octet, anti-triplet and sextet representation satisfy the naive Casimir scaling with the Casimir factors $C_{\mathbf{R}} = \langle \sum_{c=1}^{N_c^2-1} t^c(\mathbf{x}) t^c(\mathbf{x} + \mathbf{r}) \rangle_{\mathbf{R}}$ for representations \mathbf{R} as

$$C_1 = -\frac{N_c^2 - 1}{2N_c}, \quad C_8 = \frac{1}{2N_c}, \quad C_3 = \frac{1}{N_c}, \quad C_6 = \frac{1 - N_c}{N_c} \quad (47)$$

in the asymptotic regime to a good approximation for temperatures higher than $T \gtrsim 300 \text{ MeV}$. 2-flavor QCD lattice simulations [91] with improved staggered fermions indicate consistent results. On the basis of the preceding discussion that the asymptotic screening length is determined in all of these cases by the inverse mass $1/m(0_+^{++})$ of the same lightest scalar state, to which the real parts of the Wilson lines couple through the emission/absorption of two *electric* A_0 *gluons* this is hardly surprising.

3.2.7 Screening at finite chemical potential

Nonperturbative studies at finite chemical potential are challenging due to the sign problem associated with quark or baryon chemical potential in the lattice approach. One has to resort to either reweighting methods, or to the Taylor expansion in μ/T , or to analytical continuation of results obtained at

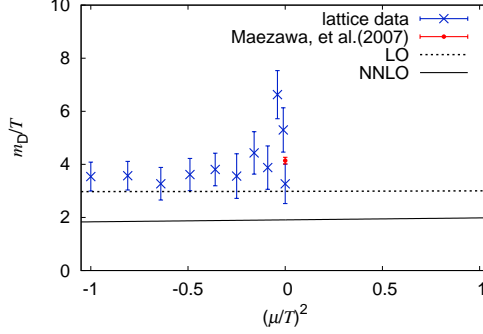


Figure 21: The screening mass associated with the singlet free energy F_S at imaginary chemical potential [92]. Available results are obtained with $N_\tau = 4$.

imaginary chemical potential $\mu_I = i\mu$. Within their limited radii of applicability these approaches yield consistent results for the dependence of the free energies on the chemical potential [92]. Available results are obtained with $N_\tau = 4$ and may be affected by significant discretization effects.

On the one hand, the singlet or octet correlation functions (as well as C_L , see Eq. (34)) are even functions of μ/T , while, on the other hand, the anti-triplet and sextet correlation functions, Eqs. (45) and (46) contain the nontrivial odd contributions in the expansion in μ/T [89]. The coefficients at higher orders in the Taylor expansion are suppressed by an order of magnitude against the $\mu = 0$ result. The Taylor expansion coefficients associated with even powers $(\mu/T)^{2n}$ in the expansion of the asymptotic screening mass (i.e. the mass of the lightest scalar $m(0_+^{++})$) are found to be positive, and about 10% of the $\mu = 0$ result for temperatures $T \approx 2T_c$, see Fig. 21.

At finite chemical potential charge conjugation and Euclidean time reflection \mathcal{R} cease to be good quantum numbers, since the number density operator in Eq. (9) breaks the symmetries under charge conjugation and Euclidean time reflection. Hence, mixing between the bound states with even or odd numbers of *electric* A_0 *gluons* may eventually become quite strong in the medium at finite density, which implies that the real or imaginary parts of the Polyakov loop cannot fluctuate independently. Yet the mass $m(0_+^+)$ of the lightest scalar state has been found to be still significantly smaller than the masses of all other states in dimensionally-reduced QCD lattice simula-

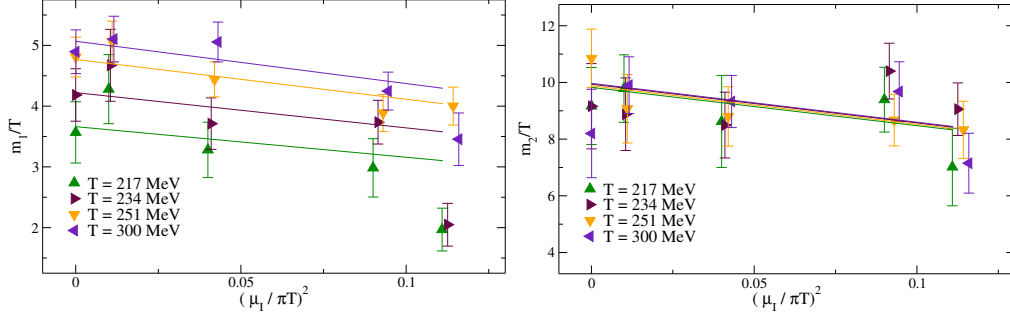


Figure 22: The screening masses m_1/T and m_2/T associated with the diagonalized components of the correlation matrix of the real and imaginary parts of the Polyakov loop at imaginary chemical potential [93]. Available results are obtained with $N_\tau = 8$.

tions [26] with an increase of only about 10% at $\mu/T = 1$ and about 20% at $\mu/T = 2$. For this reason, the correlation functions that primarily couple to this state are expected to be only mildly affected. On the contrary, however, the screening lengths in the $\mathcal{R} = -1$ channels such $J_{\mathcal{R}}^P = 0_-^+$ are expected to increase quite dramatically towards the screening lengths associated with some scalar $J_{\mathcal{R}}^P = 0_+^+$ channel.

The correlation functions of real and imaginary parts of the Polyakov loops are indeed mixed, i.e. there is a nontrivial cross-correlator, and the 2×2 correlation matrix has to be diagonalized. (2+1)-flavor QCD lattice simulations at imaginary chemical potential [93] have verified this behavior. On the one hand, the smaller screening mass m_1/T in the diagonalized basis is found to be only marginally ($\sim 10\%$) larger than for the correlation function of the real part, whereas, on the other hand, the larger screening mass m_2/T in the diagonalized basis increases by about 20% compared to the $\mu = 0$ result for temperatures sufficiently above the Roberge-Weiss transition up to $T \lesssim 2T_c$. Note that the behavior in Fig. 22 is the opposite, since the horizontal axis represents squared imaginary chemical potential.

3.2.8 Screening in external magnetic fields

It has been known for some time that external magnetic fields modify the properties of the QCD crossover transition. In particular, the presence of the magnetic fields leads to the anisotropy of the quark-antiquark interaction

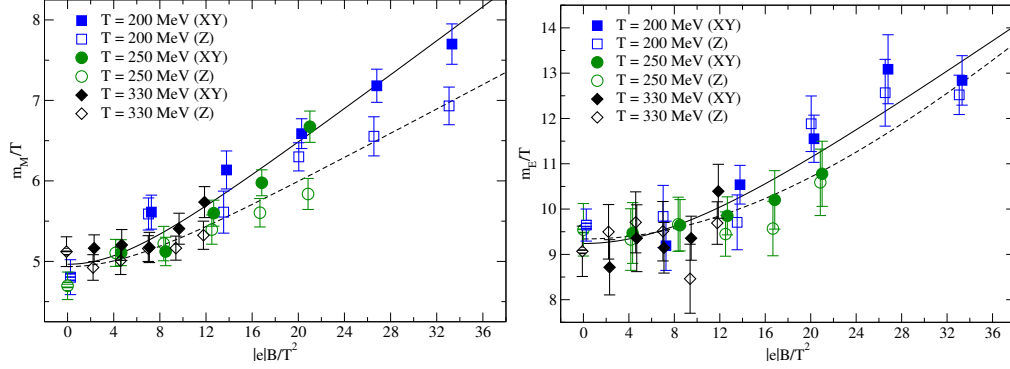


Figure 23: The screening masses m_m/T ($J_{\mathcal{R}}^{PC} = 0_{+}^{++}$) and m_E/T ($J_{\mathcal{R}}^{PC} = 0_{-}^{+-}$) associated with the correlation function of the real or imaginary parts of the Polyakov loops in an external magnetic field [95]. Available results are obtained with $N_{\tau} = 8$.

for different orientations with respect to the magnetic field. For vanishing magnetic field the free energy $F_{q\bar{q}}$ is for temperatures well below T_c and $r \lesssim 1/\Lambda_{\overline{\text{MS}}}$ or for distances much smaller than the inverse temperature ($r \ll 1/T$) up to the trivial change of normalization $+T \ln(N_c^2)$ almost indistinguishable from the quark-antiquark static energy. In an external magnetic field the screening behavior of $F_{q\bar{q}}$ is evident for temperatures much lower than T_c , whereas the chiral condensate still does not show signs of inverse magnetic catalysis [94].

For this reason an influence of the magnetic fields on the thermal screening masses has to be expected. A calculation in (2+1)-flavor QCD lattice simulations [95] indicated that the screening masses of the correlation function of the real and imaginary parts of the Polyakov loops are increased in strong magnetic fields. While the ratio between the screening masses in the $J_{\mathcal{R}}^{PC} = 0_{-}^{+-}$ and $J_{\mathcal{R}}^{PC} = 0_{+}^{++}$ is rather mildly affected, the individual masses increase quite strongly for a rising external magnetic field. The modified screening masses scale with $|e|B/T^2$, see Fig. 23. Whereas the 0_{-}^{+-} channel is similarly affected for both alignments with regard to the external magnetic field, the 0_{+}^{++} channel has to be aligned perpendicular to the external magnetic field for the largest modification.

4 Interplay between screening and dissociation

Shortly after the first conjectures of quark-gluon plasma as the state of nuclear matter at high temperature and the beginning of the era of heavy-ion collision experiments as tools for studies of the QCD phase diagram, the idea was brought up in Ref. [96] that color screening causes rearrangements of the in-medium bound states leading to the sequential melting of quarkonia. The relative yields from the various in-medium quarkonia produced in heavy-ion collisions would then serve the role of an experimentally accessible probe for the temperature of the plasma. However, over the years this static picture has been replaced by a dynamical picture, in which both dissociation and recombination take place inside of the plasma, too. See e.g. Ref. [97] for a discussion of this paradigm change. These processes may be too rapid for permitting the restructuring of the bound states as demanded in the static picture and may even regenerate already depleted bound states. In this case, the in-medium quarkonia have to be considered as an open quantum system and treated in a real-time approach. While there are indeed indications that this is the case, the questions of color screening and dissociation in a realistic scenario cannot be treated separately. In the following, we will discuss the interplay between both for the static quarks that we have discussed so far and relax the infinite mass limit taking a look at relativistic heavy and light quarks as well.

We discuss the basic ideas about extracting real-time information from Euclidean lattice correlators through the spectral functions in subsection 4.1. We outline the key differences between how temporal and spatial meson correlators can provide information. After discussing the relatively simpler case of the real-time dynamics of static quark-antiquark pairs in subsection 4.2, we turn our attention to heavy-heavy or heavy-light systems beyond the static limit in subsection 4.3. We close this discussion after comparing these results to the case of light-light systems in subsection 4.4.

4.1 Euclidean correlation functions and spectral functions

Earlier we discussed how screening properties of the deconfined medium can be studied theoretically by looking at the response of the medium to insertion

of static probe charges. We now turn to the discussion on screening properties of systems with dynamical quarks. Ultimately, we are interested in how the deconfined medium affects the QCD spectrum, *i.e.* various bound states and resonances composed of light (u, d, s) and heavy (c, b) dynamical quarks. We focus our discussion on mesons – hadrons composed of quark and antiquark.

4.1.1 Temporal correlation functions

The information on how the thermal medium, quark-gluon plasma modifies hadrons and eventually leads to the their dissolution at high temperatures is encoded in spectral functions. The latter are Fourier transforms of the real-time correlation functions which are, however, not directly accessible in lattice QCD. Instead, one can compute the Euclidean correlation functions. A Euclidean temporal meson correlation function projected to a given spatial momentum \mathbf{p} has the following form:

$$G(\tau, \mathbf{p}, T) = \int d^3x e^{i\mathbf{p}\cdot\mathbf{x}} \langle J_H(\tau, \mathbf{x}) J_H(0, \mathbf{0}) \rangle, \quad (48)$$

where $J_H = \bar{q}\Gamma_H q$ is a meson operator and $\Gamma_H = 1, \gamma_5, \gamma_\mu, \gamma_5\gamma_\mu, \gamma_\mu\gamma_\nu$ projects onto a channel with given quantum numbers.

Taking into account the periodicity in the temporal direction one can relate the Euclidean correlation functions to the spectral functions $\rho(\omega, \mathbf{p}, T)$:

$$G(\tau, \mathbf{p}, T) = \int_0^\infty d\omega \rho(\omega, \mathbf{p}, T) K(\omega, \tau, T), \quad (49)$$

$$K(\omega, \tau, T) = \frac{\cosh(\omega(\tau - 1/(2T)))}{\sinh(\omega/(2T))}. \quad (50)$$

The temperature dependence of $\rho(\omega, \mathbf{p}, T)$ shows how the deconfined medium screens the interactions and at what temperatures the mesons dissolve.

Ideally, one would like to calculate the spectral functions nonperturbatively in lattice QCD. However, in the Euclidean lattice formalism Eq. (49) has then to be considered as an integral equation from which the spectral function $\rho(\omega, \mathbf{p}, T)$ needs to be *reconstructed*. Eq. (49) poses a very ill-defined inverse problem. There are several fundamental features that make it particularly hard in practice. First, the temporal extents of finite-temperature lattices, where $G(\tau, \mathbf{p}, T)$ is evaluated, are of $\mathcal{O}(10)$ data points. while the spectral function $\rho(\omega, \mathbf{p}, T)$ has typically a rich structure, requiring hundreds

of frequency points to be resolved. Right from the start the problem is very underdetermined. Second, the kernel of the transformation $K(\omega, \tau, T)$ falls off exponentially with the frequency ω , suppressing the features of the spectral function. This exponential loss of information leads to very little sensitivity of $G(\tau, \mathbf{p}, T)$ to thermal modification of the spectral function. And, third, all correlation functions are determined from Monte Carlo sampling and, thus, feature significant statistical fluctuations.

If we restrict ourselves to a static quark-antiquark pair instead of a relativistic quark-antiquark pair, as we will be doing in subsection 4.2, we will encounter a milder version of this inverse problem. In this case, the transformation kernel $K(\omega, \tau, T)$ simplifies to the Laplace kernel $\exp(-\omega\tau)$ and sheds its explicit temperature dependence. Moreover, the Laplace kernel is not symmetric under $\tau \rightarrow 1/T - \tau$, such that the full range of the correlation function provides useful information.

To deal with the inverse problem (49) Bayesian methods, such as the Maximum Entropy Method, are often employed [98]. Despite almost two decades of effort in the lattice QCD community starting with the pioneering work of Refs. [99, 100, 101], determination of spectral functions with fully quantified uncertainties remains an open problem. A recent comprehensive review on the status of the field of calculating spectral functions in perturbative approaches and lattice QCD for heavy quarkonia can be found in [97].

4.1.2 Spatial correlation functions

Given all the complications of extracting the information from the temporal correlation functions, one could consider mesonic *spatial* correlation functions, as was first pointed out in Refs. [102, 103]:

$$G(z, T) = \int_0^{1/T} d\tau \int dxdy \langle J_H(\tau, x, y, z) J_H(0, 0, 0, 0) \rangle. \quad (51)$$

They are related to the same spectral function as the temporal correlation functions but in a slightly more involved way:

$$G(z, T) = \int_0^\infty \frac{2d\omega}{\omega} \int_{-\infty}^\infty dp_z e^{ip_z z} \rho(\omega, p_z, T). \quad (52)$$

However, unlike for the temporal direction, the separation is not limited to inverse temperature. Thus, the spatial correlation functions are more sensitive to the in-medium modification effects, since they can be studied at

larger quark–antiquark separation. Moreover, absence of the temperature-dependent kernel, as apparent from comparing Eq. (52) with (49), means that the temperature dependence of the spatial correlation function comes entirely from the spectral function. Thus, one can directly study the temperature dependence of $G(z, T)$ without the need of reconstructing $\rho(\omega, p_z, T)$. Deviations of the spatial correlation function at finite temperature from its vacuum form directly signal in-medium modification of the corresponding hadronic state.

At large distances the spatial correlation functions decay exponentially

$$G(z, T) \sim \exp(-M(T)z), \quad (53)$$

where the fall-off is governed by the temperature-dependent *screening mass*, or inverse screening length, $M(T)$. At small enough temperatures where a well-defined mesonic bound state exists, the spectral function has a δ -like peak

$$\rho(\omega, p_z, T) \sim \delta(\omega^2 - p_z^2 - M_0^2) \quad (54)$$

and $M(T)$ coincides with the propagator pole mass M_0 .

At high enough temperatures where the mesonic state is dissociated, the spatial correlation function describes propagation of a free quark-antiquark pair. In this case the screening mass is [104]

$$M_{\text{free}} = \sqrt{m_{q_1}^2 + (\pi T)^2} + \sqrt{m_{q_2}^2 + (\pi T)^2}, \quad (55)$$

where m_{q_1} and m_{q_2} are the pole masses of the quark and antiquark that form the meson. As was shown in Ref. [104], and was also argued earlier in Ref. [105] for the case of massless quarks, the appearance of the lowest fermionic Matsubara frequency mode πT in the meson screening mass is a direct consequence of the anti-periodic temporal boundary conditions for fermions. Thus, a crossover from one limiting behavior, Eq. (54) to the other, Eq. (55), would indicate that the mesonic state dissociates in the plasma and the lowest-order contribution to the screening mass comes from two independently propagating fermionic degrees of freedom.

4.2 The complex static energy

The quark-antiquark static energy $E(T, r)$ in the thermal medium is modified, too. In particular, in the deconfined phase $E(T, r)$ acquires a nonzero

imaginary part and exhibits the color screening. However, contrary to the $T = 0$ situation, lattice studies of the complex in-medium static energy $E(T, r)$ are fraught with profound difficulties that we can illustrate only briefly in this review.

In the following, we begin by juxtaposing the zero and finite temperature cases, beginning with the more simple situation at $T = 0$. In the vacuum the static energy $E(r)$ can be defined in terms of the infinite time limit of the logarithm of the real-time Wilson loop $W(t, r)$, i.e.

$$E(r) = \lim_{t \rightarrow \infty} \frac{i}{t} \ln W(t, r), \quad W(t, r) = \left\langle P \exp \left\{ i \oint_{W(t, r)} dz^\mu A_\mu \right\} \right\rangle, \quad (56)$$

or similarly in Euclidean space-time after $t \rightarrow -i\tau$. As before, P represents the path ordering. The Wilson loops have a spectral decomposition in the vacuum (using Euclidean space-time)

$$W(\tau, r) = \int_0^\infty d\omega \rho_{W(r)}(\omega) e^{-\omega\tau}, \quad \rho_{W(r)}(\omega) = \sum_{n=0}^\infty A_n \delta(E_n(r) - \omega), \quad (57)$$

where the spectral function $\rho_{W(r)}(\omega)$ is a weighted sum of delta functions that gives rise to the weighted sum of exponentials mentioned in Eq. (26).

Eq. (56) can be directly evaluated on the lattice in the vacuum phase, see Eq. (26), since the length of the Euclidean time direction can be as large as technically affordable such that only the first delta function in the sum in Eq. (57) that is associated with the ground state contributes. If the Euclidean time direction is periodic with period aN_τ , then the Wilson loop must be evaluated at sufficiently large values of $\tau < aN_\tau$ such that excited state contributions are quantitatively irrelevant or can be included in a robust fit.

In the perturbative expansion $E(r)$ and $F(r) = \partial_r E(r)$ are known analytically to next-to-next-to-next-to-leading order, and at next-to-next-to-next-to-leading logarithmic accuracy [106]. To leading order the static energy is given by the leading order singlet potential

$$E(r) = -C_F \frac{\alpha_s}{r} = V_s(r). \quad (58)$$

Higher order contributions are proportional to the LO result and involve higher powers of α_s , and — starting at three loops — $\ln(\alpha_s)$. The latter

are due to an interplay between the contribution from the singlet potential and from the ultrasoft contribution. The latter is due to transitions between color-singlet and -octet configurations on internal lines, starts at N³LO, and includes contributions from coupling to the nonperturbative QCD condensates. With the exceptions of the ultrasoft contribution that is absent in Abelian gauge theories, this result is in all respects formally quite similar to the QED result. Comparison to lattice simulations shows that the N³LO result describes the static energy very well up to $r \lesssim 0.15$ fm [31].

Since there is no closed loop in the time direction, there cannot be any overlap with states involving (static) D mesons, and thus the screening of the static energy due to the string breaking in the vacuum cannot be resolved without explicitly including other operators that overlap with the pair of (static) D mesons and solving a generalized eigenvalue problem, see Ref. [32] for a recent calculation. This is evidently different from the free energy in the vacuum, where the string breaking explicitly contributes.

On the contrary, the spectral function of the finite temperature Wilson loops representing a static quark-antiquark pair in the thermal medium,

$$W(\tau, T, r) = \int_0^\infty d\omega \rho_{W(T,r)}(\omega) e^{-\omega\tau}, \quad (59)$$

is a sum of smeared delta peaks that may be shifted away from their zero temperature frequencies and a high frequency continuum that is due to the fully dissociated states. If there is a well-defined lowest peak that is clearly separable from the rest of the spectral function, then one can interpret its position as the real part of $E(T, r)$ and its width as the imaginary part of $E(T, r)$. However, as different peaks may merge with each other or into the encroaching high frequency continuum for increasing temperature, it is not completely obvious whether there actually are well defined peaks at all and if the notion of a finite temperature static energy $E(T, r)$ is physically appropriate at all. Moreover, the time direction is physically fixed to the inverse temperature $aN_\tau = 1/T$ in a lattice setup at finite temperature, and thus the limit $\tau \rightarrow \infty$ in which the ground state could be isolated is completely out of reach in practical lattice simulations. For this reason, one has to deal with the excited state contamination, the early-time dynamics, and the bound state formation. It follows from very general considerations that the contribution from the complex static energy $E(T, r)$ to the spectral

function takes the form of a skewed Breit-Wigner peak, where the skewing is due to the early time dynamics of the bound state formation [107]. However, it is not a priori clear how much this spectral feature is distorted by the rest of the spectral function. The real-time static energy at finite temperature has been calculated to next-to-leading order [108, 109] using the HTL approach. $E(T, r)$ has been found to exhibit an imaginary part in the electric screening regime $r \sim 1/m_D$,

$$E(T, r) = -C_F \alpha_s(\nu) \left\{ \frac{e^{-m_D(\nu)r}}{r} + m_D(\nu) + iT\phi(rm_D(\nu)) \right\}, \quad (60)$$

$$\phi(x) = 2 \int_0^\infty \frac{dz}{(z^2 + 1)^2} z \left\{ 1 - \frac{\sin(zx)}{zx} \right\}, \quad (61)$$

where $\phi(x)$ is a strictly monotonically increasing function. While the imaginary term appears already in the vacuum-like regime $r \ll 1/T$ [109], the result is parametrically quite different as

$$E(T, r) = -C_F \alpha_s(1/r) + \left[\left\{ \#_1 \frac{\Delta V}{T} + \#_2 \frac{m_D^2}{T^2} + \#_3 \frac{m_D^3}{T^3} \right\} + i \left\{ \#_4 \frac{\Delta V^2}{T^2} + \#_5 \frac{m_D^2}{T^2} \right\} \right] g^2 r^2 T^3, \quad (62)$$

with coefficients $\#_i$, $i = 1, \dots, 5$ given in Ref. [109]. It is understood that the origin of the imaginary part (in both regimes) is in part due to the dissipative scattering (Landau damping) of the emitted gluons with the various degrees of freedom in the thermal medium, and in part due to transitions between the color-singlet and -octet configurations of the static quark-antiquark pair. Beyond NLO these two dynamical processes cannot be separated anymore. These weak-coupling results for two different regimes indicate that the notion of the finite temperature static energy $E(T, r)$ is at least justified for sufficiently small distances and sufficiently high temperatures such that the weak-coupling approach applies. Whether or not this concept is suitable at phenomenologically interesting temperatures and at distances relevant to the melting or survival of in-medium quarkonium bound states must be addressed using nonperturbative methods. Whereas the real part $\text{Re } E(T, r)$ agrees with the singlet free energy $F_S(T, r)$ at order g^3 both in the vacuum-like regime $r \ll 1/T$ and in the electric screening regime $r \sim 1/m_D$, they differ at order g^4 due to different UV contributions. However, $F_S(T, r)$ is screened

already in the vacuum of full QCD (with sea quarks) due to the string breaking, whereas $E(T, r)$ defined in terms of the large time limit of the Wilson loop cannot couple directly to states involving static D mesons⁸. Hence, any screening mass associated with a nonperturbative analog of Eqs. (60) or (62) must necessarily vanish in the vacuum phase at $T < T_c$.

These different sources of information, i.e. the dissociative imaginary part from the perturbative HTL result in Eq. (60), and the real part from the zero temperature lattice calculation were used to construct a maximally binding, minimally dissociative model potential with ad-hoc exponential screening in Ref. [110]. It could be shown that the dominant source for in-medium quarkonium melting is the dissociation even in such a simplistic model.

In order to calculate $E(T, r)$ directly, the real-time formalism is required, since the imaginary part arises due to dynamical real-time processes. However, the real-time formalism introduces a sign problem in the QCD path integral, and thus prevents the application of the importance sampling in the Markov Chain Monte Carlo algorithm employed in lattice simulations. Nevertheless, both the real-time and the imaginary-time Wilson loops are related to the same underlying spectral function $\rho_{W(T,r)}(\omega)$ through analyticity,

$$W(t, T, r) = \int_{-\infty}^{+\infty} d\omega e^{-i\omega t} \rho_{W(T,r)}(\omega) \quad \text{real time,} \quad (63)$$

$$W(\tau, T, r) = \int_{-\infty}^{+\infty} d\omega e^{-\omega\tau} \rho_{W(T,r)}(\omega) \quad \text{imaginary time,} \quad (64)$$

where $W(\tau, T, r)$ is directly calculable on the lattice, at most with $\mathcal{O}(10)$ data points for a thermal correlation function. However, any reliable reconstruction of narrow spectral features and some continuum requires covering hundreds of frequency values. This makes the inverse problem of reconstructing $\rho_{W(T,r)}(\omega)$ from the imaginary-time Wilson loop $W(\tau, T, r)$ ill-posed, and solutions to it are beyond the scope of this review. One has to resort to model assumptions on the form of the spectral function, or Bayesian analysis that incorporates prior knowledge. Even a brief discussion of the various Bayesian

⁸This applies to a definition in terms of the large time limit of Wilson line correlators in Coulomb gauge as well.

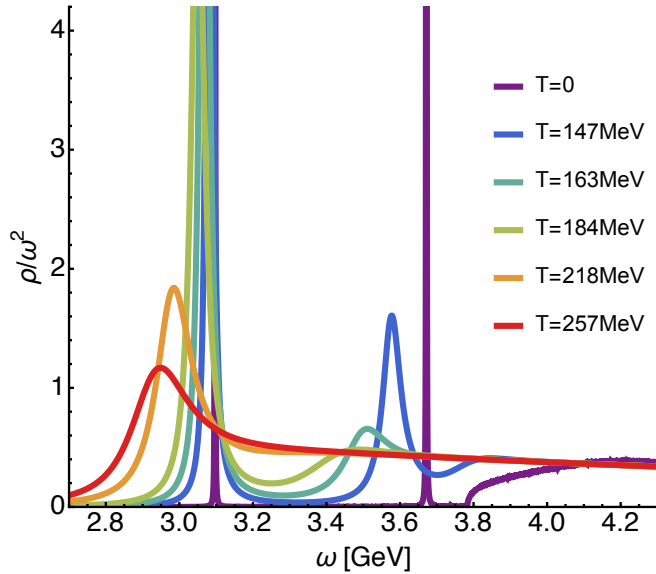


Figure 24: Charmonium in-medium spectral functions from a continuum corrected in-medium heavy quark potential with AsqTad action [113].

techniques that have been developed for solving this problems exceeds the scope of this review, see [111, 112, 97] for an overview of the current state of the art. Upon assuming that the spectral function $\rho_{W(T,r)}(\omega)$ has been determined using a nonperturbative lattice simulation, i.e. see Fig. 24 for results obtained from (2+1)-flavor lattice simulations using the AsqTad action, the complex, real-time static energy follows from its lowest peak structure.

SU(3) pure gauge theory [115] or (2+1)-flavor QCD lattice simulations using the AsqTad action [116] have been employed to calculate Eq. (64), while tackling the inverse problem through the Bayesian reconstruction method [111]. The solution of the inverse problem in the analysis of more precise correlators from (2+1)-flavor QCD lattice simulations using the HISQ action proved to be more difficult due to the smaller statistical errors, and has led to somewhat unclear, preliminary results so far, whether by using rescaled results from HTL calculations [117], fits to the moments of the lattice correlators [118], or by using the analytic continuation of Padé fits or the BR method [114], see Fig. 25 for the current state of the art result from (2+1)-flavor QCD lattice simulations with the HISQ action. In particular, a reliable determination of $\text{Im } E(T, r)$ in QCD has proved elusive so far. Very recently exciting new

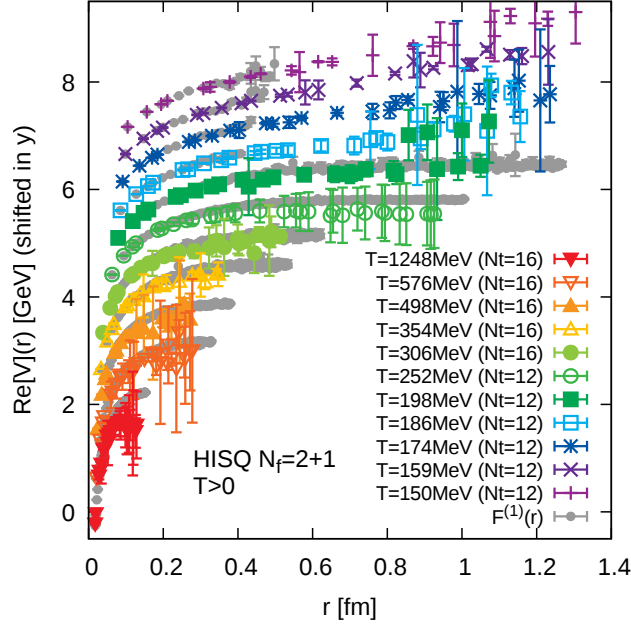


Figure 25: The real part of the potential obtained from Padé reconstructed spectral functions of the Wilson line correlation function in Coulomb gauge on $48^3 \times 12$, and $64^3 \times 16$ lattices in (2+1)-flavor QCD with HISQ action [114]. The values are shifted by hand in y-direction for better readability from the lowest temperature $T = 151$ MeV on top to the highest temperature $T = 1248$ MeV at the bottom. The gray data represent the color singlet free energy in Coulomb gauge calculated on the same lattices.

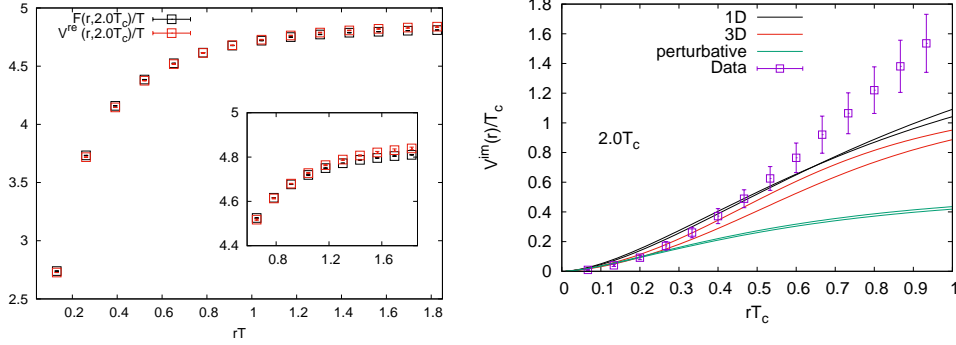


Figure 26: (Left) Detailed comparison of $\text{Re } E(T, r)$ and F_S in SU(3) pure gauge theory indicate small differences between the quantities that become larger in the asymptotic screening regime. (Right) $\text{Im } E(T, r)$ obtained in SU(3) pure gauge theory lattice simulations increases faster than the HTL result, and also faster than the imaginary parts obtained with various forms of medium permittivity, see [119] for details.

results in SU(N_c) pure gauge theory indicate that an elegant solution to the inverse problem may have finally been identified [119], see Fig. 26.

All present results indicate that at the level of the somewhat large systematic uncertainties the relation between $\text{Re } E(T, r)$ and $F_S(T, r)$ at order g^3 seems to be approximately realized in the nonperturbative calculation with relatively mild differences. Furthermore, the screening mass parameter that has been extracted from the real part of the static energy $\text{Re } E(T, R)$ seems to be consistent with going to zero at T_c and in the vacuum. For this reason, an increase of the difference at larger distances has to be expected even at the lowest temperatures.

4.3 Meson screening masses for heavy and heavy-light mesons

To illustrate the utility of Eq. (52) we start the discussion with the spatial Euclidean correlation functions as calculated on the lattice. A ratio of the Euclidean correlation function at non-zero temperature to its zero-temperature counterpart directly probes thermal modification of the spectral function. Ref. [120] calculated the correlation functions in various channels using stag-

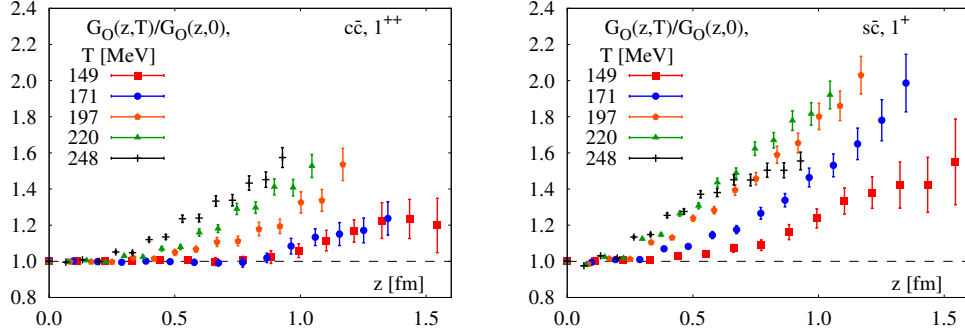


Figure 27: The oscillating (positive parity) parts of the axial-vector (1^{++} or 1^+) correlation functions for the $c\bar{c}$ (left) and $s\bar{c}$ (right) sectors at different temperatures normalized by the zero-temperature results.

gered fermions up to temperature of 250 MeV which is about $1.6T_c$ in 2+1 flavor QCD with the physical light quark masses.

A complication with staggered fermions is that mesonic correlation functions contain contributions from excitations with opposite parity eigenvalues, where one causes a non-oscillating and the other causes an oscillating contribution:

$$G(z) = A_{NO}^2 (e^{-M_{NO}z} + e^{-M_{NO}(N_\sigma - z)}) - (-1)^z A_O^2 (e^{-M_O z} + e^{-M_O(N_\sigma - z)}). \quad (65)$$

These contributions need to be separated before comparing to zero-temperature results. This is possible by constructing effective mass correlators as described in Ref. [120].

From the point of view of the static picture of color screening it is to be expected that axial-vector mesons — being in a P-wave, and thus being larger — are dissociated already at lower temperatures than the corresponding vector mesons. The tightly bound pseudoscalars are expected to behave similarly to the vector mesons, whereas the scalar mesons ought to exhibit a pattern more akin to the axial-vector states. Moreover, due to the smaller quark masses involved in open heavy-flavor mesons leading to a larger size of the bound states, the thermal modification is expected to be more pronounced and at lower temperatures even in the static picture. Since dynamical processes certainly enhance these trends, any observation of these patterns does not lead to a statement whether the static color screening or the dynamic dissociation and recombination is the dominant cause of the

thermal modification.

On the one hand, the ratio of the positive parity contribution to the spatial Euclidean axial-vector correlation function at finite temperature to the one at zero temperature is shown in Fig. 27 (left) for $c\bar{c}$ and Fig. 27 (right) for $s\bar{c}$ mesons. At zero temperature the ground states in these channels are, respectively, χ_{c1} or D_{s1} mesons. For the ratios in the χ_{c1} channel significant thermal modifications of the ground state are seen at temperatures below $T \sim 200$ MeV only at large distances $z \gtrsim 1$ fm, while these modifications occur at much smaller distances for temperatures above $T \sim 200$ MeV. This is consistent with the analyses attempting to reconstruct the spectral functions from the temporal correlation by solving the inverse problem, Eq. (49) [97]. In contrast, the temperature dependence resolved in these ratios is more complicated for the open-charm state D_{s1} , with a deviation of about 20% from the zero-temperature value already in the crossover region, i.e. at $T \sim 150$ MeV. At even higher temperatures, the increase of the ratio stalls below $T \sim 250$ MeV. The case of the scalar channels — the respective zero temperature ground states being χ_{c0} or D_{s0}^* mesons — is quantitatively similar. On the other hand, the vector meson channels with J/ψ or D_s^* mesons, or the pseudoscalar meson channels with η_c or D_s mesons as the respective ground states, exhibit less pronounced features. For both $c\bar{c}$ channels significant thermal modifications of the ground states are seen at temperatures above $T \sim 200$ MeV with a decreasing slope in z , but do not show any clearly non-monotonic z - or temperature-dependence. For both open-charm channels, a deviation of about 15 to 20% from the zero-temperature value is present already at $T \sim 170$ MeV. Therefore, these ratios confirm the intuition of sequential melting based on the static picture of color screening. A recent analysis of the charm-quark susceptibilities [121] is also consistent with this observation suggesting that open-charm states start to melt at temperatures around the chiral crossover temperature $T_c = 156.5$ MeV.

To further assess thermal modification effects, one can extract the screening masses in the corresponding channels by fitting the long-distance behavior of the correlation functions, Eq. (65). The temperature dependence of the screening masses for all four (axial vector, scalar, vector and pseudo-scalar) channels for the $c\bar{c}$ and $s\bar{c}$ mesons is shown in Fig. 28. Three qualitatively distinct regions can be identified: the low temperature region, where the screening masses are close to the corresponding vacuum masses (horizontal solid lines), the intermediate temperature region, where there are about 10–15% changes in the values of the screening masses with respect to the

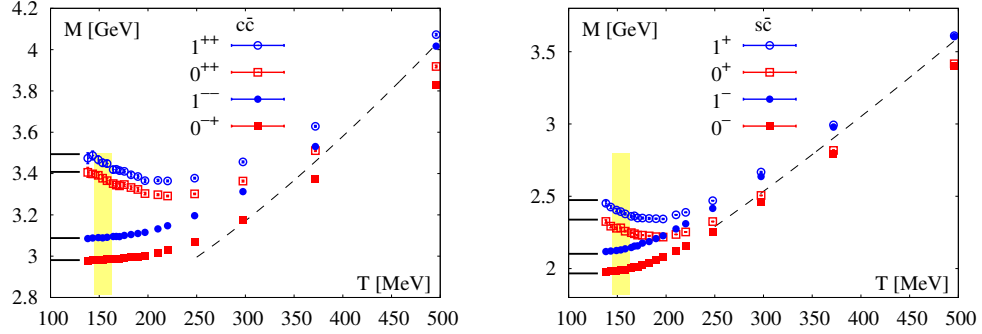


Figure 28: The screening masses for different channels in the $c\bar{c}$ (left) and $s\bar{c}$ (right) sectors as functions of temperature. The solid horizontal lines are the zero-temperature masses of the corresponding ground-state mesons and the dashed lines indicate the free theory result.

corresponding vacuum masses and the high temperature region, where the screening masses approach the free theory result (dashed lines). The onset of the high temperature behavior in the $c\bar{c}$ sector starts at $T > 300$ MeV, and in the $s\bar{c}$ sector earlier, at about $T = 250$ MeV. This matches the previous observation in the ratios of the correlation functions that thermal modifications depend on the quark content of the states and appear earlier for the states containing quarks with lower masses.

The behavior of the screening masses corresponding to the negative and positive parity states in the low and intermediate temperature regions is qualitatively different. The screening masses of the negative parity states increase with temperature from their vacuum values monotonically. Those of the positive parity states first decrease, with the decrease beginning close to the chiral crossover region. In the intermediate temperature region the trend reverses and the masses increase to eventually follow the high-temperature asymptotics. Moreover, in the intermediate region the ordering of the screening masses changes and the masses of the opposite parity partners approach each other to become degenerate at sufficiently high temperatures. While this is less apparent in the $c\bar{c}$ sector, since it requires temperatures on the order of the charm mass, it is evident in the $s\bar{c}$ sector, where the masses of the pseudoscalar and scalar or vector and axial-vector states become degenerate above 350 MeV. In the high temperature region the pseudoscalar screening masses stay below the vector screening masses, as was observed in earlier

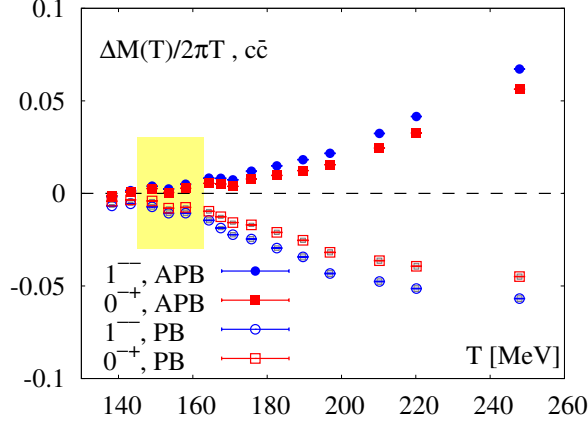


Figure 29: The differences in the screening masses for the pseudoscalar and vector charmonia states and the vacuum masses, Eq. (66), for anti-periodic (filled symbols) and periodic (open symbols) temporal boundary conditions for fermions.

lattice [122] and Dyson-Schwinger formalism calculations [123].

Following earlier work [124, 125, 126] Ref. [120] also considered sensitivity of the charmonia screening masses to the temporal boundary conditions. At finite temperature the boundary conditions in the temporal direction must be periodic for the bosonic and anti-periodic for the fermionic fields. However, on the lattice the Euclidean correlation functions, Eq. (48), can be also measured with artificially imposed periodic temporal boundary conditions for fermions. The vacuum masses of stable mesons are insensitive to the boundary conditions. At very high temperatures where the bound states dissolve and the two quarks propagate independently, the mesonic screening masses approach twice the value of the lowest Matsubara frequency, as evident from Eq. (55), which is $2\pi T$ due to the anti-periodic boundary conditions on fermions. In contrast, if periodic temporal boundary conditions for fermions are imposed, the screening masses should become vanishingly small at very high temperatures. Thus sensitivity of correlation functions and in turn the screening masses to the boundary conditions helps one to judge if at a given temperature quarks still constitute a bosonic bound state, or if thermal modifications uncover its fermionic structure.

The charmonium screening masses in the pseudo-scalar and vector channels calculated using anti-periodic and periodic boundary conditions are

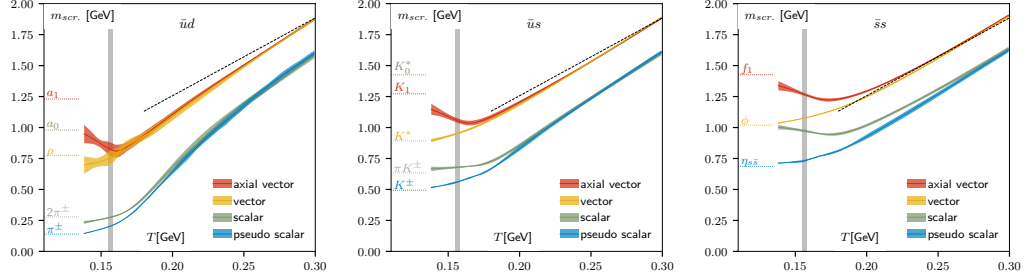


Figure 30: The continuum extrapolated mesonic screening masses for different channels in the $\bar{u}d$ (left), $\bar{u}s$ (middle) and $\bar{s}s$ (right) sectors as functions of temperature. The solid horizontal lines are the zero-temperature masses of the corresponding ground-state mesons or two-particle states (see text) and the dashed lines indicate the free theory result.

shown in Fig. 29. The difference between the screening mass $M(T)$ and its vacuum value M_0

$$\Delta M(T) = M(T) - M_0 \quad (66)$$

is normalized with $2\pi T$, since one expects that at asymptotically high temperature the quadratic difference between the screening masses with the two types of boundary conditions approaches $(2\pi T)^2$. Although the screening masses become sensitive to the modification of the boundary conditions already in the chiral crossover region, the sensitivity is small up to about 170 MeV. The difference gets larger with increasing temperature and the overall picture supports melting of the η_c and J/ψ states above 200 MeV.

4.4 Meson screening masses for light mesons

The observables that we discussed in the previous sections, related to static or heavy quarks act as external probes of the deconfined medium since their mass scales are well separated from the temperature scales of the transition. It is natural to ask how the color screening properties of quark-gluon plasma affect the states in the QCD spectrum composed of light and strange quarks such as π , K , ρ , etc. The situation there is more complicated since the dynamics of the transition is driven by the dynamics of the light quarks and their composites. For instance, the Hadron Resonance Gas (HRG) model [127, 128, 129, 130, 131] approximates the partition function of QCD

by an ideal gas of stable particles and resonances. This approximation works surprisingly well up to temperatures of about 140–150 MeV, and, of course, breaks down close to the chiral crossover. The dominant contribution into the HRG partition function comes from the lightest states, *e.g.* the expansion for observables with zero strangeness and baryon number starts with the pion, for non-zero strangeness with kaon and so on. Light degrees of freedom are also closely related to the fundamental symmetries of QCD such as the $SU_L(2) \times SU_R(2)$ chiral symmetry and the anomalous axial $U_A(1)$ symmetry. While the chiral symmetry is completely restored at the chiral phase transition temperature T_c^0 (in the chiral limit) and is smoothly restored within a narrow temperature range around the chiral crossover temperature T_c in QCD with physical light quark masses as indicated by the melting of the chiral condensate, the fate of the $U_A(1)$ is not completely clear at present. Most studies agree that it gets effectively restored in the high temperature phase in QCD. However, some differ in if it happens at the same temperature as the chiral symmetry restoration or at some higher temperature.

The large distance behavior of the spatial correlation functions defined in Eq. (52) is sensitive to various patterns of chiral symmetry restoration [102, 103]. A recent analysis of the screening masses for mesons composed of light and strange quarks was performed in Ref. [132] with the HISQ action. The continuum extrapolated mesonic screening masses for the four channels are shown in Fig. 30 for the light-light, light-strange and strange-strange mesons. We should first note that extraction of the scalar state poses difficulties with staggered fermions when the quark masses are light. Due to the taste exchange interactions there are unphysical contributions in the scalar channel that allow the scalar state composed of u and d quarks decay into two pions at finite lattice spacing [133], while this decay does not occur in nature due to parity, isospin and G -parity conservation. For this reason the scalar screening mass in the left panel of Fig. 30 approaches the energy of the two-pion state instead of the true scalar ground state ($a_0(980)$ or $a_0(1450)$) or the allowed $\pi\eta$ two-particle state. This problem could be resolved if the continuum limit is taken for the spatial correlation function (65) first and then the screening mass is extracted from the continuum correlator. This approach is however difficult due to the oscillating terms in Eq. (65), and Ref. [132] resorted to extracting the screening masses from correlators at finite lattice spacing and then taking the continuum limit for the screening masses. In the $\bar{u}s$ channel the situation is better since the decay to $K\pi$ occurs in nature. The continuum limit of the scalar screening mass extracted from the $\bar{u}s$ correlator

at finite lattice spacing approaches the $K\pi$ state as indicated in the middle panel of Fig. 30.

The overall trends in Fig. 30 are similar to the ones observed for heavy-heavy and heavy-light states discussed in Sec. 4.3. Thermal modifications happen at lower temperatures for the states with lower quark masses. Due to the restoration of chiral symmetry one expects that the vector (ρ) and axial vector (a_1) screening masses become degenerate. As can be seen from the left panel of Fig. 30, the axial vector screening mass decreases significantly (it is already about 20% below the vacuum value at the lowest temperature available in the calculation) while the vector mass slightly increases and the two indeed become degenerate at the chiral crossover temperature. For the states involving the strange quark in the middle and right panel of Fig. 30 the degeneracy of the axial vector and vector screening masses happens at higher temperature.

Restoration of the $U_A(1)$ symmetry is signaled by degeneracy of the scalar and pseudoscalar screening masses. In the $\bar{u}d$ sector it is observed at temperature about 200 MeV, however, one has to be careful with its interpretation due to the unphysical effects in the scalar channel. Discussion of the technical subtleties is beyond the scope of this review and we refer the reader to [132] where another measure such as a difference of continuum extrapolated integrated scalar and pseudoscalar correlators was constructed to estimate the temperature of the $U_A(1)$ symmetry restoration. The numerical evidence points out to the restoration temperature $T \sim 200$ MeV, in general, consistent with the degeneracy of the screening masses observed in the left panel of Fig. 30.

The temperature dependence of the screening masses becomes qualitatively consistent with the free theory behavior at temperatures above 300 MeV. Around that temperature the vector and axial vector masses are numerically consistent with the free theory behavior, the scalar and pseudoscalar masses are below by 10-20%. As full degeneracy of the screening masses is expected at infinite temperature, Ref. [132] followed the temperature dependence of the screening masses up to $T \sim 2.5$ GeV. The screening masses normalized by the temperature in the high temperature region are shown in Fig. 31. It is argued that above $T \sim 1$ GeV the cutoff effects are small and the calculation is performed only on $N_\tau = 8$ lattices above that temperature.

Perturbatively the correction to the free theory screening mass can be calculated in electrostatic QCD (EQCQ) [23]. Ref. [134] evaluated this correction which turns out to be independent of the spin. Its value is positive

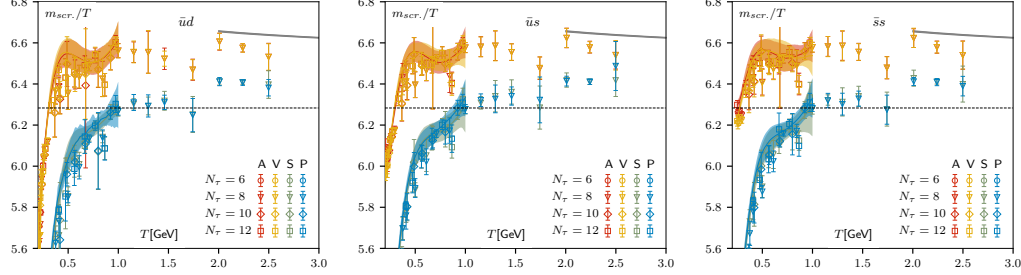


Figure 31: The mesonic screening masses normalized by the temperature for different channels in the $\bar{u}d$ (left), $\bar{u}s$ (middle) and $\bar{s}s$ (right) sectors as functions of temperature shown for higher temperatures in the deconfined phase, compare with Fig. 30. The dashed horizontal line indicates the free theory result, 2π , and the solid line the EQCD correction (see text).

and is qualitatively consistent with the lattice results, as shown by the solid lines in Fig. 31. As can be seen from the figure, the vector and axial vector screening masses overshoot the free theory result at $T \sim 400$ MeV and stay approximately constant reasonably close to the weak-coupling EQCD result. The scalar and pseudoscalar screening masses increase past the free theory value at $T \sim 1$ GeV and in the observed temperature range stay significantly below the weak-coupling result. It hints that higher-order, spin-dependent corrections [135, 136] may be important since the EQCD coupling g_E^2 is not small in this temperature range. Moreover, since it decreases logarithmically, only at significantly higher temperatures (by orders of magnitude) one may expect the screening masses to approach the free theory value $2\pi T$.

5 Summary

In this review paper we discussed the color screening in the quark-gluon plasma as it is studied using lattice QCD. We presented a brief overview of the field-theoretical foundations and summarically contrasted specific phenomena associated with the color screening in QCD with their counterparts in QED or cold nuclear matter. We reviewed in pure gauge theory and in full QCD the Polyakov loop and its various correlation functions, which are the primary observables by which color screening is still being studied on the lattice and in other approaches. Going beyond static limit we reviewed the

status of dynamic, spatial meson screening correlation functions for heavy-heavy, heavy-light, and light-light flavors and spin 0 or 1 states. In particular, we reviewed the behavior and phenomena from the upper end of the confined phase at low temperature all the way up to phenomena in the weakly-coupled quark-gluon plasma at high temperature. To date, all known color screening phenomena tend to become fairly compatible with the weak-coupling picture for $T \gtrsim 300$ MeV, which largely coincides with the QCD scale $\Lambda_{\overline{\text{MS}}}$.

We highlighted the role of the Polyakov loop in pure gauge theory as the order parameter of the deconfinement transition and its continued relevance in full QCD, where its renormalization is required. In full QCD the renormalization scheme independent static quark entropy shift that signals deconfinement helps with better understanding of the transition regime at $T \sim T_c$ (with $T_c = 156.5(1.5)$ MeV). Whether the coincidence of chiral symmetry restoration and deconfinement, which has been observed down to almost physical quark masses, holds even in the chiral limit is one of the open questions regarding the Polyakov loop.

We scrutinized the different regimes of static, spatial screening correlation functions in various channels, and how the corresponding screening behavior changes with the separation of the quark and antiquark, relating these to the picture sketched by the dimensionally-reduced QCD and the hard thermal loop QCD. In particular, we juxtaposed direct lattice QCD calculations with results from the weak-coupling approach, where those were available and applicable. Eventually, direct lattice QCD simulations quantitatively confirm these ideas, establish the existence of a vacuum-like regime, a dissociation regime, an electric screening regime, and an asymptotic screening regime, where finally the nonperturbative physics becomes dominant, and in part explain the success of weak-coupling descriptions of color screening phenomena. We reviewed the existence of the qualitatively different screening patterns at different values of the external control parameters temperature T , chemical potential μ/T and magnetic field $|eB|/T$. We indicated open issues regarding these static screening correlation functions.

Lastly, we addressed the interplay of the real-time dynamical processes and the color screening in quark-gluon plasma, as it plays out in the complex static energy at finite temperature, which has to be obtained from lattice QCD after solving the inverse problem of reconstructing the spectral function from the Euclidean correlation functions. Finally passing on from the static limit to the dynamical heavy and light quarks, we discussed meson correlation functions and repeated the arguments for using spatial meson

screening correlation functions. We reviewed studies of these with a wide variety of flavor contents down from the charm- to the average light-quark considering hidden and open flavor. The naive expectation of the earlier modification of correlation functions involving lower quark masses is quantitatively confirmed and the weak-coupling like behavior is postponed to higher temperatures for larger quark masses, while the approximate degeneracy between parity partners sets in a bit later. Indications of the degeneracy of scalar and pseudoscalar states that signals the effective $U_A(1)$ restoration is consistent with about $T \sim 200$ MeV. Open heavy flavor mesons are generally modified already slightly above the QCD crossover transition.

Taken together, all of these observations largely support the sequential melting picture and suggest that in-medium quark-antiquark systems can be understood in terms of the weak-coupling picture for $T \gtrsim 300$ MeV.

Acknowledgments

We would like to thank the HotQCD and TUMQCD collaborations for the productive work, and F. Karsch, A. Lahiri and P. Petreczky for valuable discussions, a careful reading and comments on the manuscript. This work was in part supported by the U.S. Department of Energy, Office of Science, Office of Nuclear Physics and Office of Advanced Scientific Computing Research within the framework of Scientific Discovery through Advance Computing (SciDAC) award “Computing the Properties of Matter with Leadership Computing Resources” and the U.S. National Science Foundation under the award PHY-1812332.

References

- [1] Hideki Yukawa. On the interaction of elementary particles. *Proc.Phys.Math.Soc.Jap.*, 17:48–57, 1935.
- [2] P Debye and E Hueckel. Zur Theorie der Elektrolyte. *Physikalische Zeitschrift*, 24:185–206, 1923.
- [3] F.J. Dyson. The Radiation theories of Tomonaga, Schwinger, and Feynman. *Phys. Rev.*, 75:486–502, 1949.

- [4] Julian Schwinger. On gauge invariance and vacuum polarization. *Phys. Rev.*, 82:664–679, Jun 1951.
- [5] E. A. Uehling. Polarization effects in the positron theory. *Phys. Rev.*, 48:55–63, Jul 1935.
- [6] M.B. Kislinger and P.D. Morley. Collective Phenomena in Gauge Theories. 1. The Plasmon Effect for Yang-Mills Fields. *Phys. Rev. D*, 13:2765, 1976.
- [7] David J. Gross, Robert D. Pisarski, and Laurence G. Yaffe. QCD and Instantons at Finite Temperature. *Rev. Mod. Phys.*, 53:43, 1981.
- [8] D.J. Gross and Frank Wilczek. Asymptotically Free Gauge Theories - I. *Phys. Rev. D*, 8:3633–3652, 1973.
- [9] H.David Politzer. Reliable Perturbative Results for Strong Interactions? *Phys. Rev. Lett.*, 30:1346–1349, 1973.
- [10] Thomas Appelquist, Michael Dine, and I.J. Muzinich. The Static Potential in Quantum Chromodynamics. *Phys. Lett. B*, 69:231–236, 1977.
- [11] Kenneth G. Wilson. Confinement of Quarks. pages 45–59, 2 1974.
- [12] I.T. Drummond. Strong coupling model for string breaking on the lattice. *Phys. Lett. B*, 434:92–98, 1998.
- [13] Owe Philipsen and Hartmut Wittig. String breaking in nonAbelian gauge theories with fundamental matter fields. *Phys. Rev. Lett.*, 81:4056–4059, 1998. [Erratum: *Phys.Rev.Lett.* 83, 2684 (1999)].
- [14] Peter Brockway Arnold and Laurence G. Yaffe. The NonAbelian Debye screening length beyond leading order. *Phys. Rev.*, D52:7208–7219, 1995.
- [15] Sudhir Nadkarni. Nonabelian Debye Screening. 1. The Color Averaged Potential. *Phys. Rev. D*, 33:3738, 1986.
- [16] H. T. Ding et al. Chiral Phase Transition Temperature in (2+1)-Flavor QCD. *Phys. Rev. Lett.*, 123(6):062002, 2019.

- [17] Y. Aoki, Szabolcs Borsanyi, Stephan Durr, Zoltan Fodor, Sandor D. Katz, Stefan Krieg, and Kalman K. Szabo. The QCD transition temperature: results with physical masses in the continuum limit II. *JHEP*, 06:088, 2009.
- [18] A. Bazavov et al. The chiral and deconfinement aspects of the QCD transition. *Phys. Rev. D*, 85:054503, 2012.
- [19] A. Bazavov et al. Chiral crossover in QCD at zero and non-zero chemical potentials. *Phys. Lett.*, B795:15–21, 2019.
- [20] Szabolcs Borsanyi, Zoltan Fodor, Jana N. Guenther, Ruben Kara, Sandor D. Katz, Paolo Parotto, Attila Pasztor, Claudia Ratti, and Kalman K. Szabo. The QCD crossover at finite chemical potential from lattice simulations. 2020.
- [21] C. Rohrhofer, Y. Aoki, G. Cossu, H. Fukaya, C. Gatttringer, L.Ya. Glozman, S. Hashimoto, C.B. Lang, and S. Prelovsek. Symmetries of spatial meson correlators in high temperature QCD. *Phys. Rev. D*, 100(1):014502, 2019.
- [22] Eric Braaten and Agustin Nieto. Effective field theory approach to high temperature thermodynamics. *Phys. Rev.*, D51:6990–7006, 1995.
- [23] Eric Braaten and Agustin Nieto. Free energy of QCD at high temperature. *Phys. Rev.*, D53:3421–3437, 1996.
- [24] Jan Moller and York Schroder. Dimensionally reduced QCD at high temperature. *Prog. Part. Nucl. Phys.*, 67:168–172, 2012.
- [25] Andrei D. Linde. Infrared Problem in Thermodynamics of the Yang-Mills Gas. *Phys. Lett.*, 96B:289–292, 1980.
- [26] A. Hart, M. Laine, and O. Philipsen. Static correlation lengths in QCD at high temperatures and finite densities. *Nucl. Phys.*, B586:443–474, 2000.
- [27] Stefan Scherer. Introduction to chiral perturbation theory. *Adv. Nucl. Phys.*, 27:277, 2003.
- [28] Stefan Scherer and Matthias R. Schindler. *A Primer for Chiral Perturbation Theory*, volume 830. 2012.

- [29] Evgeny Epelbaum, Hans-Werner Hammer, and Ulf-G. Meissner. Modern Theory of Nuclear Forces. *Rev. Mod. Phys.*, 81:1773–1825, 2009.
- [30] R. Machleidt and D.R. Entem. Chiral effective field theory and nuclear forces. *Phys. Rept.*, 503:1–75, 2011.
- [31] Alexei Bazavov, Nora Brambilla, Xavier Garcia Tormo, I, Péter Petreczky, Joan Soto, Antonio Vairo, and Johannes Heinrich Weber. Determination of the QCD coupling from the static energy and the free energy. 2019.
- [32] John Bulava, Ben Horz, Francesco Knechtli, Vanessa Koch, Graham Moir, Colin Morningstar, and Mike Peardon. String breaking by light and strange quarks in QCD. *Phys. Lett. B*, 793:493–498, 2019.
- [33] W.E. Caswell and G.P. Lepage. Effective Lagrangians for Bound State Problems in QED, QCD, and Other Field Theories. *Phys. Lett. B*, 167:437–442, 1986.
- [34] Geoffrey T. Bodwin, Eric Braaten, and G.Peter Lepage. Rigorous QCD analysis of inclusive annihilation and production of heavy quarkonium. *Phys. Rev. D*, 51:1125–1171, 1995. [Erratum: *Phys.Rev.D* 55, 5853 (1997)].
- [35] Nora Brambilla, Antonio Pineda, Joan Soto, and Antonio Vairo. The Infrared behavior of the static potential in perturbative QCD. *Phys. Rev. D*, 60:091502, 1999.
- [36] Nora Brambilla, Antonio Pineda, Joan Soto, and Antonio Vairo. Potential NRQCD: An Effective theory for heavy quarkonium. *Nucl. Phys. B*, 566:275, 2000.
- [37] Nora Brambilla, Antonio Pineda, Joan Soto, and Antonio Vairo. Effective field theories for heavy quarkonium. *Rev. Mod. Phys.*, 77:1423, 2005.
- [38] Antonio Pineda. Review of Heavy Quarkonium at weak coupling. *Prog. Part. Nucl. Phys.*, 67:735–785, 2012.
- [39] M. Albanese et al. Glueball Masses and String Tension in Lattice QCD. *Phys. Lett.*, B192:163–169, 1987.

- [40] Anna Hasenfratz and Francesco Knechtli. Flavor symmetry and the static potential with hypercubic blocking. *Phys. Rev.*, D64:034504, 2001.
- [41] Colin Morningstar and Mike J. Peardon. Analytic smearing of SU(3) link variables in lattice QCD. *Phys. Rev. D*, 69:054501, 2004.
- [42] Martin Luescher. Properties and uses of the Wilson flow in lattice QCD. *JHEP*, 08:071, 2010. [Erratum: JHEP03,092(2014)].
- [43] Martin Lüscher and Peter Weisz. Perturbative analysis of the gradient flow in non-abelian gauge theories. *JHEP*, 02:051, 2011.
- [44] Herbert Neuberger. Exactly massless quarks on the lattice. *Phys. Lett. B*, 417:141–144, 1998.
- [45] David B. Kaplan. A Method for simulating chiral fermions on the lattice. *Phys. Lett.*, B288:342–347, 1992.
- [46] B. Sheikholeslami and R. Wohlert. Improved Continuum Limit Lattice Action for QCD with Wilson Fermions. *Nucl. Phys. B*, 259:572, 1985.
- [47] John B. Kogut and Leonard Susskind. Hamiltonian Formulation of Wilson’s Lattice Gauge Theories. *Phys. Rev. D*, 11:395–408, 1975.
- [48] Kostas Orginos, Doug Toussaint, and R. L. Sugar. Variants of fattening and flavor symmetry restoration. *Phys. Rev.*, D60:054503, 1999.
- [49] E. Follana et al. Highly improved staggered quarks on the lattice, with applications to charm physics. *Phys. Rev.*, D75:054502, 2007.
- [50] Y. Aharonov and D. Bohm. Significance of Electromagnetic Potentials in the Quantum Theory. *Physical Review*, 115(3):485–491, August 1959.
- [51] Benjamin Svetitsky and Laurence G. Yaffe. Critical Behavior at Finite Temperature Confinement Transitions. *Nucl. Phys.*, B210:423–447, 1982.
- [52] Sourendu Gupta, Kay Huebner, and Olaf Kaczmarek. Renormalized Polyakov loops in many representations. *Phys. Rev.*, D77:034503, 2008.

- [53] P. Petreczky and H. P. Schadler. Renormalization of the Polyakov loop with gradient flow. *Phys. Rev.*, D92(9):094517, 2015.
- [54] Larry D. McLerran and Benjamin Svetitsky. Quark Liberation at High Temperature: A Monte Carlo Study of SU(2) Gauge Theory. *Phys. Rev.*, D24:450, 1981.
- [55] J. Engels, F. Karsch, H. Satz, and I. Montvay. Gauge Field Thermodynamics for the SU(2) Yang-Mills System. *Nucl. Phys.*, B205:545–577, 1982.
- [56] A. Bazavov, N. Brambilla, H. T. Ding, P. Petreczky, H. P. Schadler, A. Vairo, and J. H. Weber. Polyakov loop in 2+1 flavor QCD from low to high temperatures. *Phys. Rev.*, D93(11):114502, 2016.
- [57] Jean-Loup Gervais and A. Neveu. The Slope of the Leading Regge Trajectory in Quantum Chromodynamics. *Nucl. Phys.*, B163:189–216, 1980.
- [58] Alexander M. Polyakov. Gauge Fields as Rings of Glue. *Nucl. Phys.*, B164:171–188, 1980.
- [59] O. Kaczmarek, F. Karsch, P. Petreczky, and F. Zantow. Heavy quark anti-quark free energy and the renormalized Polyakov loop. *Phys. Lett.*, B543:41–47, 2002.
- [60] Adrian Dumitru, Yoshitaka Hatta, Jonathan Lenaghan, Kostas Orginos, and Robert D. Pisarski. Deconfining phase transition as a matrix model of renormalized Polyakov loops. *Phys. Rev.*, D70:034511, 2004.
- [61] Y. Aoki, G. Endrodi, Z. Fodor, S. D. Katz, and K. K. Szabo. The Order of the quantum chromodynamics transition predicted by the standard model of particle physics. *Nature*, 443:675–678, 2006.
- [62] Matthias Berwein, Nora Brambilla, Peter Petreczky, and Antonio Vairo. Polyakov loop at next-to-next-to-leading order. *Phys. Rev.*, D93(3):034010, 2016.
- [63] Olaf Kaczmarek and Felix Zantow. Static quark anti-quark interactions in zero and finite temperature QCD. I. Heavy quark free energies, running coupling and quarkonium binding. *Phys. Rev.*, D71:114510, 2005.

- [64] Olaf Kaczmarek and Felix Zantow. Static quark anti-quark interactions at zero and finite temperature QCD. II. Quark anti-quark internal energy and entropy. 2005.
- [65] P. Petreczky and K. Petrov. Free energy of a static quark anti-quark pair and the renormalized Polyakov loop in three flavor QCD. *Phys. Rev.*, D70:054503, 2004.
- [66] Pok Man Lo, Bengt Friman, Olaf Kaczmarek, Krzysztof Redlich, and Chihiro Sasaki. Probing Deconfinement with Polyakov Loop Susceptibilities. *Phys. Rev.*, D88(1):014506, 2013.
- [67] Alexei Bazavov, Nora Brambilla, Peter Petreczky, Antonio Vairo, and Johannes Heinrich Weber. Color screening in (2+1)-flavor QCD. *Phys. Rev.*, D98(5):054511, 2018.
- [68] Alexander M. Polyakov. Thermal Properties of Gauge Fields and Quark Liberation. *Phys. Lett.*, 72B:477–480, 1978.
- [69] J. Kuti, J. Polonyi, and K. Szlachanyi. Monte Carlo Study of SU(2) Gauge Theory at Finite Temperature. *Phys. Lett.*, 98B:199, 1981. [287(1980)].
- [70] Matthias Berwein, Nora Brambilla, Jacopo Ghiglieri, and Antonio Vairo. Renormalization of the cyclic Wilson loop. *JHEP*, 03:069, 2013.
- [71] Matthias Berwein, Nora Brambilla, Peter Petreczky, and Antonio Vairo. Polyakov loop correlator in perturbation theory. *Phys. Rev.*, D96(1):014025, 2017.
- [72] Johannes Heinrich Weber, Peter Petreczky, and Alexei Bazavov. Polyakov loop correlators and cyclic Wilson loop from lattice QCD. *PoS, LATTICE2015*:177, 2016.
- [73] Nora Brambilla, Jacopo Ghiglieri, Peter Petreczky, and Antonio Vairo. The Polyakov loop and correlator of Polyakov loops at next-to-next-to-leading order. *Phys. Rev.*, D82:074019, 2010.
- [74] Sebastian Steinberger and Johannes Heinrich Weber. Color screening in 2 + 1 flavor QCD at large distances. 2018.

- [75] Ioan Ghisoiu, Jan Moller, and York Schroder. Debye screening mass of hot Yang-Mills theory to three-loop order. *JHEP*, 11:121, 2015.
- [76] M. Laine and O. Philipsen. The Nonperturbative QCD Debye mass from a Wilson line operator. *Phys. Lett. B*, B459:259–264, 1999.
- [77] Anton K. Rebhan. NonAbelian Debye screening in one loop resummed perturbation theory. *Nucl. Phys. B*, 430:319–344, 1994.
- [78] Urs M. Heller, F. Karsch, and J. Rank. The Gluon propagator at high temperature. *Phys. Lett. B*, 355:511–517, 1995.
- [79] Urs M. Heller, F. Karsch, and J. Rank. The Gluon propagator at high temperature: Screening, improvement and nonzero momenta. *Phys. Rev. D*, 57:1438–1448, 1998.
- [80] F. Karsch, M. Oevers, and P. Petreczky. Screening masses of hot SU(2) gauge theory from the 3-d adjoint Higgs model. *Phys. Lett. B*, 442:291–299, 1998.
- [81] A. Cucchieri, F. Karsch, and P. Petreczky. Magnetic screening in hot nonAbelian gauge theory. *Phys. Lett. B*, 497:80–84, 2001.
- [82] A. Cucchieri, F. Karsch, and P. Petreczky. Propagators and dimensional reduction of hot SU(2) gauge theory. *Phys. Rev. D*, 64:036001, 2001.
- [83] A. Nakamura, T. Saito, and S. Sakai. Lattice calculation of gluon screening masses. *Phys. Rev. D*, 69:014506, 2004.
- [84] P. J. Silva, O. Oliveira, P. Bicudo, and N. Cardoso. Gluon screening mass at finite temperature from the Landau gauge gluon propagator in lattice QCD. *Phys. Rev.*, D89(7):074503, 2014.
- [85] Szabolcs Borsányi, Zoltán Fodor, Sándor D. Katz, Attila Pásztor, Kálmán K. Szabó, and Csaba Török. Static $\bar{Q}Q$ pair free energy and screening masses from correlators of Polyakov loops: continuum extrapolated lattice results at the QCD physical point. *JHEP*, 04:138, 2015.

- [86] Y. Maezawa, S. Aoki, S. Ejiri, T. Hatsuda, N. Ishii, K. Kanaya, N. Ukita, and T. Umeda. Electric and Magnetic Screening Masses at Finite Temperature from Generalized Polyakov-Line Correlations in Two-flavor Lattice QCD. *Phys. Rev.*, D81:091501, 2010.
- [87] Anthony Francis, Renwick J. Hudspith, Randy Lewis, and Kim Maltman. Lattice Prediction for Deeply Bound Doubly Heavy Tetraquarks. *Phys. Rev. Lett.*, 118(14):142001, 2017.
- [88] Yu Maezawa, Takashi Umeda, Sinya Aoki, Shinji Ejiri, Tetsuo Hatsuda, Kazuyuki Kanaya, and Hiroshi Ohno. Application of fixed scale approach to static quark free energies in quenched and 2+1 flavor lattice QCD with improved Wilson quark action. *Prog. Theor. Phys.*, 128:955–970, 2012.
- [89] S. Ejiri, Y. Maezawa, N. Ukita, S. Aoki, T. Hatsuda, N. Ishii, K. Kanaya, and T. Umeda. Equation of State and Heavy-Quark Free Energy at Finite Temperature and Density in Two Flavor Lattice QCD with Wilson Quark Action. *Phys. Rev.*, D82:014508, 2010.
- [90] Y. Maezawa, N. Ukita, S. Aoki, S. Ejiri, T. Hatsuda, N. Ishii, and K. Kanaya. Heavy-quark free energy, debye mass, and spatial string tension at finite temperature in two flavor lattice QCD with Wilson quark action. *Phys. Rev.*, D75:074501, 2007.
- [91] Matthias Doring, Kay Huebner, Olaf Kaczmarek, and Frithjof Karsch. Color Screening and Quark-Quark Interactions in Finite Temperature QCD. *Phys. Rev.*, D75:054504, 2007.
- [92] Junichi Takahashi, Keitaro Nagata, Takuya Saito, Atsushi Nakamura, Takahiro Sasaki, Hiroaki Kouno, and Masanobu Yahiro. Color screening potential at finite density in two-flavor lattice QCD with Wilson fermions. *Phys. Rev.*, D88:114504, 2013.
- [93] Michele Andreoli, Claudio Bonati, Massimo D’Elia, Michele Mesiti, Francesco Negro, Andrea Rucci, and Francesco Sanfilippo. Gauge-invariant screening masses and static quark free energies in $N_f = 2 + 1$ QCD at nonzero baryon density. *Phys. Rev.*, D97(5):054515, 2018.
- [94] Claudio Bonati, Massimo D’Elia, Marco Mariti, Michele Mesiti, Francesco Negro, Andrea Rucci, and Francesco Sanfilippo. Magnetic

field effects on the static quark potential at zero and finite temperature. *Phys. Rev.*, D94(9):094007, 2016.

- [95] Claudio Bonati, Massimo D’Elia, Marco Mariti, Michele Mesiti, Francesco Negro, Andrea Rucci, and Francesco Sanfilippo. Screening masses in strong external magnetic fields. *Phys. Rev.*, D95(7):074515, 2017.
- [96] T. Matsui and H. Satz. J/ψ Suppression by Quark-Gluon Plasma Formation. *Phys. Lett. B*, 178:416–422, 1986.
- [97] Alexander Rothkopf. Heavy Quarkonium in Extreme Conditions. 2019.
- [98] Mark Jarrell and J. E. Gubernatis. Bayesian inference and the analytic continuation of imaginary-time quantum Monte Carlo data. *Phys. Rept.*, 269:133–195, 1996.
- [99] M. Asakawa, T. Hatsuda, and Y. Nakahara. Maximum entropy analysis of the spectral functions in lattice QCD. *Prog. Part. Nucl. Phys.*, 46:459–508, 2001.
- [100] M. Asakawa and T. Hatsuda. J/ψ and $\eta(c)$ in the deconfined plasma from lattice QCD. *Phys. Rev. Lett.*, 92:012001, 2004.
- [101] Saumen Datta, Frithjof Karsch, Peter Petreczky, and Ines Wetzorke. Behavior of charmonium systems after deconfinement. *Phys. Rev. D*, 69:094507, 2004.
- [102] Carleton E. Detar and John B. Kogut. The Hadronic Spectrum of the Quark Plasma. *Phys. Rev. Lett.*, 59:399, 1987.
- [103] Carleton E. Detar and John B. Kogut. Measuring the Hadronic Spectrum of the Quark Plasma. *Phys. Rev.*, D36:2828, 1987.
- [104] Wojciech Florkowski and Bengt L. Friman. Spatial dependence of the finite temperature meson correlation function. *Z. Phys.*, A347:271–276, 1994.
- [105] V. L. Eletsky and B. L. Ioffe. On Temperature Dependence of Correlators of Hadronic Currents. *Sov. J. Nucl. Phys.*, 48:384, 1988. [*Yad. Fiz.*48,661(1988)].

- [106] Nora Brambilla, Antonio Vairo, Xavier Garcia i Tormo, and Joan Soto. The QCD static energy at NNNLL. *Phys. Rev.*, D80:034016, 2009.
- [107] Yannis Burnier and Alexander Rothkopf. Disentangling the timescales behind the non-perturbative heavy quark potential. *Phys. Rev.*, D86:051503, 2012.
- [108] M. Laine, O. Philipsen, P. Romatschke, and M. Tassler. Real-time static potential in hot QCD. *JHEP*, 03:054, 2007.
- [109] Nora Brambilla, Jacopo Ghiglieri, Antonio Vairo, and Peter Petreczky. Static quark-antiquark pairs at finite temperature. *Phys. Rev.*, D78:014017, 2008.
- [110] Peter Petreczky, Chuan Miao, and Agnes Mocsy. Quarkonium spectral functions with complex potential. *Nucl. Phys.*, A855:125–132, 2011.
- [111] Yannis Burnier and Alexander Rothkopf. Bayesian Approach to Spectral Function Reconstruction for Euclidean Quantum Field Theories. *Phys. Rev. Lett.*, 111:182003, 2013.
- [112] Alexander Rothkopf. Bayesian techniques and applications to QCD. *PoS, Confinement2018*:026, 2018.
- [113] Yannis Burnier, Olaf Kaczmarek, and Alexander Rothkopf. Quarkonium at finite temperature: Towards realistic phenomenology from first principles. *JHEP*, 12:101, 2015.
- [114] Peter Petreczky, Alexander Rothkopf, and Johannes Weber. Realistic in-medium heavy-quark potential from high statistics lattice QCD simulations. *Nucl. Phys.*, A982:735–738, 2019.
- [115] Yannis Burnier and Alexander Rothkopf. A gauge invariant Debye mass and the complex heavy-quark potential. *Phys. Lett.*, B753:232–236, 2016.
- [116] Yannis Burnier, Olaf Kaczmarek, and Alexander Rothkopf. Static quark-antiquark potential in the quark-gluon plasma from lattice QCD. *Phys. Rev. Lett.*, 114(8):082001, 2015.

- [117] A. Bazavov, Y. Burnier, and P. Petreczky. Lattice calculation of the heavy quark potential at non-zero temperature. *Nucl. Phys.*, A932:117–121, 2014.
- [118] P. Petreczky and J. Weber. Lattice Calculations of Heavy Quark Potential at Finite Temperature. *Nucl. Phys.*, A967:592–595, 2017.
- [119] Dibyendu Bala and Saumen Datta. Nonperturbative potential for study of quarkonia in QGP. 2019.
- [120] Alexei Bazavov, Frithjof Karsch, Yu Maezawa, Swagato Mukherjee, and Peter Petreczky. In-medium modifications of open and hidden strange-charm mesons from spatial correlation functions. *Phys. Rev.*, D91(5):054503, 2015.
- [121] A. Bazavov et al. The melting and abundance of open charm hadrons. *Phys. Lett.*, B737:210–215, 2014.
- [122] M. Cheng et al. Meson screening masses from lattice QCD with two light and the strange quark. *Eur. Phys. J.*, C71:1564, 2011.
- [123] Kun-lun Wang, Yu-xin Liu, Lei Chang, Craig D. Roberts, and Sebastian M. Schmidt. Baryon and meson screening masses. *Phys. Rev.*, D87(7):074038, 2013.
- [124] G. Boyd, Sourendu Gupta, F. Karsch, and E. Laermann. Spatial and temporal hadron correlators below and above the chiral phase transition. *Z. Phys.*, C64:331–338, 1994.
- [125] Swagato Mukherjee. Screening of light mesons and charmonia at high temperature. *Nucl. Phys.*, A820:283C–286C, 2009.
- [126] F. Karsch, E. Laermann, Swagato Mukherjee, and P. Petreczky. Signatures of charmonium modification in spatial correlation functions. *Phys. Rev.*, D85:114501, 2012.
- [127] Roger Dashen, Shang-Keng Ma, and Herbert J. Bernstein. S Matrix formulation of statistical mechanics. *Phys. Rev.*, 187:345–370, 1969.
- [128] R. Venugopalan and M. Prakash. Thermal properties of interacting hadrons. *Nucl. Phys.*, A546:718–760, 1992.

- [129] Rolf Hagedorn. Multiplicities, p_T Distributions and the Expected Hadron \rightarrow Quark - Gluon Phase Transition. *Riv. Nuovo Cim.*, 6N10:1–50, 1983.
- [130] R. Fiore, R. Hagedorn, and F. d’Isep. Statistical Bootstrap Model and Phase Transition From Hadron Matter to Quark Gluon Plasma. *Nuovo Cim.*, A88:301, 1985.
- [131] R. Hagedorn. How We Got to QCD Matter from the Hadron Side: 1984. *Lect. Notes Phys.*, 221:53–76, 1985.
- [132] Alexei Bazavov et al. Meson screening masses in (2+1)-flavor QCD. *Phys. Rev.*, D100(9):094510, 2019.
- [133] Sasa Prelovsek. Effects of staggered fermions and mixed actions on the scalar correlator. *Phys. Rev.*, D73:014506, 2006.
- [134] M. Laine and M. Vepsalainen. Mesonic correlation lengths in high temperature QCD. *JHEP*, 02:004, 2004.
- [135] V. Koch, Edward V. Shuryak, G. E. Brown, and A. D. Jackson. The Propagation of quarks in the spatial direction in hot QCD. *Phys. Rev.*, D46:3169, 1992. [Erratum: *Phys. Rev.*D47,2157(1993)].
- [136] Edward V. Shuryak. Correlation functions in the QCD vacuum. *Rev. Mod. Phys.*, 65:1–46, 1993.